BULLETIN OF RUSSIAN STATE MEDICAL UNIVERSITY

BIOMEDICAL JOURNAL OF PIROGOV RUSSIAN NATIONAL RESEARCH MEDICAL UNIVERSITY

SUBMISSION http://vestnikrgmu.ru/login?lang=en
CORRESPONDENCE editor@vestnikrgmu.ru
COLLABORATION manager@vestnikrgmu.ru
ADDRESS ul. Ostrovityanova, d. 1, Moscow, Russia, 117997

Indexed in Scopus. CiteScore 2023: 0,8

Indexed in WoS. JCR 2021: 0.5

Five-year h-index is 10

SCImago Journal & Country Rank 2020: 0.14

Listed in HAC 31.01.2020 (№ 507)

Open access to archive

Issue DOI: 10.24075/brsmu.2025-03
The mass media registration certificate № 012769 issued on July 29, 1994
Founder and publisher is Pirogov Russian National Research Medical University (Moscow, Russia)

Approved for print 30.06.2025
Circulation: 100 copies. Printed by Print.Formula
www.print-formula.ru

ВЕСТНИК РОССИЙСКОГО ГОСУДАРСТВЕННОГО МЕДИЦИНСКОГО УНИВЕРСИТЕТА

НАУЧНЫЙ МЕДИЦИНСКИЙ ЖУРНАЛ РНИМУ ИМ. Н. И. ПИРОГОВА

ГЛАВНЫЙ РЕДАКТОР Денис Ребриков, д. б. н., профессор

ЗАМЕСТИТЕЛЬ ГЛАВНОГО РЕДАКТОРА Александр Эттингер, д. м. н., профессор

РЕДАКТОРЫ Валентина Гейдебрехт, к. б. н.; Надежда Тихомирова

ТЕХНИЧЕСКИЙ РЕДАКТОР Евгений Лукьянов

ПЕРЕВОДЧИКИ Надежда Тихомирова, Вячеслав Витюк

ДИЗАЙН И ВЕРСТКА Марины Дорониной

ПОДАЧА РУКОПИСЕЙ http://vestnikrgmu.ru/login
ПЕРЕПИСКА С РЕДАКЦИЕЙ editor@vestnikrgmu.ru
СОТРУДНИЧЕСТВО manager@vestnikrgmu.ru
АДРЕС РЕДАКЦИИ ул. Островитянова, д. 1, г. Москва, 117997

Журнал включен в Scopus. CiteScore 2023: 0,8

Журнал включен в WoS. JCR 2021: 0,5

Индекс Хирша (h⁵) журнала по оценке Google Scholar: 10

SCImago Journal & Country Rank 2020: 0,14

Журнал включен в Перечень 31.01.2020 (№ 507)

Здесь находится открытый архив журнала

DOI выпуска: 10.24075/vrgmu.2025-03
Свидетельство о регистрации средства массовой информации № 012769 от 29 июля 1994 г.
Учредитель и издатель — Российский национальный исследовательский медицинский университет имени Н. И. Пирогова (Москва, Россия)

Подписано в печать 30.06.2025
Тираж 100 экз. Отпечатано в типографии Print.Formula
www.print-formula.ru

BULLETIN OF RSMU **3, 2025**
ВЕСТНИК РГМУ

Contents
Содержание

INTRAVITAL MICROSCOPY FOR ASSESSMENT OF ANTI-TUMOR NANOTHERAPEUTIC DELIVERY

Ivanova EV[1]✉, Naumenko VA[2], Garanina AS[1], Abakumov MA[3]

[1] National University of Science and Technology MISIS, Moscow, Russia

[2] Serbsky National Medical Research Centre for Psychiatry and Narcology, Moscow, Russia

[3] Pirogov Russian National Research Medical University, Moscow, Russia

The development of effective relief for cancer is one of the most urgent tasks of biomedicine. Despite the success of anti-tumor nanotherapeutics, low targeted delivery effectiveness remains a major limiting factor for widespread introduction of those into clinical practice. Tumor microenvironment is a complex, multicomponent system, the dynamic interaction of which with nanoparticles requires adequate analysis methods. Intravital microscopy presents a unique opportunity for *in vivo* assessment of drugs and body's cells in the real-time mode. The review describes the possibilities and prospects of using intravital microscopy to study the nanotherapeutic biodistribution and delivery to tumor cells in preclinical animal models.

Keywords: intravital microscopy, preclinical tumor model, nanotherapeutics

Funding: the study was supported by the Russian Science Foundation grant (project No. 21-74-20077).

Author contribution: Ivanova EV, Naumenko VA — manuscript writing, design of the figures; Garanina AS, Abakumov MA — manuscript editing.

✉ **Correspondence should be addressed:** Elizaveta V. Ivanova
Leninsky Prospect, 4, str. 1, 119049, Moscow, Russia; m1803014@edu.misis.ru

Received: 17.06.2025 **Accepted:** 29.06.2025 **Published online:** 30.06.2025

DOI: 10.24075/brsmu.2025.033

ИНТРАВИТАЛЬНАЯ КОНФОКАЛЬНАЯ МИКРОСКОПИЯ В ИЗУЧЕНИИ ДОСТАВКИ ПРОТИВООПУХОЛЕВЫХ НАНОПРЕПАРАТОВ

Е. В. Иванова[1]✉, В. А. Науменко[2], А. С. Гаранина[1], М. А. Абакумов[3]

[1] Национальный исследовательский технологический университет «МИСИС», Москва, Россия

[2] Национальный медицинский исследовательский центр психиатрии и наркологии имени В. П. Сербского, Москва, Россия

[3] Российский национальный исследовательский медицинский университет имени Н. И. Пирогова, Москва, Россия

Разработка эффективных средств борьбы с онкологическими заболеваниями — одна из актуальнейших задач биомедицины. Несмотря на успех противоопухолевых нанопрепаратов, низкая эффективность целевой доставки остается основным лимитирующим фактором для их широкого внедрения в клиническую практику. Опухолевое микроокружение — сложная, многокомпонентная система, динамическое взаимодействие которой с наночастицами требует адекватных методов анализа. Интравитальная микроскопия представляет уникальную возможность для изучения препаратов и клеток организма *in vivo* в режиме реального времени. В обзоре описаны возможности и перспективы использования интравитальной микроскопии в изучении биораспределения и доставки нанопрепаратов к опухолевым клеткам на доклинических моделях на животных.

Ключевые слова: интравитальная конфокальная микроскопия, экспериментальная опухолевая модель, нанопрепараты

Финансирование: исследование выполнено за счет гранта Российского научного фонда (проект № 21-74-20077).

Вклад авторов: Е. В. Иванова, В. А. Науменко — написание текста, подготовка иллюстраций; А. С. Гаранина, М. А. Абакумов — редактирование текста.

✉ **Для корреспонденции:** Елизавета Викторовна Иванова
Ленинский проспект, д. 4, стр. 1, 119049; Москва, Россия; m1803014@edu.misis.ru

Статья получена: 17.06.2025 **Статья принята к печати:** 29.06.2025 **Опубликована онлайн:** 30.06.2025

DOI: 10.24075/vrgmu.2025.033

Progress and challenges of anti-tumor nanotherapeutic delivery

Nanoparticles (NPs) are increasingly used in medicine, including such fields, as chemotherapy, antimicrobial therapy, radiotherapy, diagnostics (magnetic resonance imaging (MRI), computed tomography), regenerative medicine, hyperthermia [1]. In the context of fight against cancer, three major NP applications can be distinguished. First, nanoformulations of chemotherapy drugs (Doxil, Caelyx, Onivid), the use of which makes it possible to increase drug delivery specificity and reduce accumulation of drugs in healthy tissues, have been introduced into clinical practice. Second, ferumoxytol and other metal NPs are successfully used for noninvasive detection of tumor foci by MRI. Third, nanoparticles with radionuclide components have a great potential for teranostics. In this field, the most common are polymeric NPs, liposomal carriers, dendrimers, iron oxide NPs, silicon dioxide NPs, as well as carbon nanotubes.

Efficacy of all the above diagnosis and treatment methods depends directly on NP accumulation in the tissues. It is clear that an administration route plays an extremely important role in biodistribution of the drug. In both most experimental studies and clinical practice, NPs are used in the form of intratumor (local) or intravenous (systemic) injections. In the first case, high concentration of the drug in the tumor focus is achieved, and it is possible to significantly reduce accumulation of the drug in healthy tissues. Unfortunately, this administration route can be used in specific clinical situations only, specifically when there is an easily accessible and clearly visualized primary tumor focus without metastasis. In contrast, systemic administration theoretically allows nanotherapeutics to reach tumors of any localization and size with the bloodstream; however, low delivery

effectiveness associated with the existence of several biological barriers represents a major flaw of this strategy. Thus, NPs have to escape capture by organs of the reticulo-endothelial system, flow out of the bloodstream (extravasate) in the neoplastic area, and penetrate through the dense connective tissue on their way to tumor cells. It should be noted that, despite the above challenges, it is systemic administration of the drug that represents the most promising method of combating a variety of neoplasms.

For more than 30 years it has been considered that specific NP accumulation in the tumor after systemic administration results from the so-called EPR (enhanced permeability and retention) effect, i.e. from the increased permeability of blood vessels and the decreased lymphatic drainage [2, 3]. However, in recent years, the concept of the EPR effect causes sharp criticism due to the series of failed clinical trials of nanopharmaceuticals [4, 5]. There is an opinion that this passive delivery mechanism is more typical for animal models, but it does not function in humans. In this regard, the possibility of active NP delivery, including that involving cellular carriers, attracts increasing attention of researchers [6, 7]. Neutrophils [8–11], monocytes [12,13], macrophages [14], and stem cells [15] have been proposed as potential candidates for nanopharmaceutical delivery to cancer cells.

The development of new anti-tumor therapy strategies requires thorough analysis of the processes occurring in the tumor microenvironment during carcinogenesis and in response to treatment. Tumor microenvironment is a complex system comprising both malignant and normal cells enclosed in the dense matrix of extracellular protein, as well as the chaotic blood vessel network. Due to its unique properties, tumor microenvironment can be considered a distinct tissue type. The features of the immune cell behavior in this tissue allow us to speak about tumor microenvironment as one of the cancer hallmarks [16]. More attention has been paid to new treatment methods targeting non-tumor cells of the tumor microenvironment, such as anti-angiogenic therapy and immunotherapy. However, in-depth understanding of the interplay between cells of the tumor microenvironment and nanopharmaceuticals is necessary to improve effectiveness of the above therapeutic approaches.

Exploration of the mechanisms underlying the NP delivery and antitumor activity was challenging for a long time due to the lack of adequate methods to assess the dynamic interaction between nano-objects and body's cells in situ. Until recently, the range of available tumor assessment methods was limited to microscopy of fixed specimens and biochemistry analysis, i.e. the methods not allowing one to study behavior of nanopharmaceuticals in the body in the real-time mode. The situation changed dramatically with the emergence of intravital microscopy (IVM) enabling investigation of dynamic processes in living tissues at the cellular and subcellular levels [17, 18]. This method that has proven successful in assessment of various biological processes [19–21] can be used to study the mechanisms underlying delivery and anti-tumor activity of nanopharmaceuticals at a deeper level [22].

In Russia, the use of IVM for assessment of the NP biodistribution and delivery into a tumor was embedded in pre-clinical trials of candidate anti-tumor drugs. This review presents the pilot results and prospects of using IVM to develop innovative anti-tumor therapy methods.

Intravital microscopy in studying the anti-tumor pharmaceutical delivery pathways

Interaction between NPs and cells of the immune system can have both negative and positive effects on the efficacy of therapy with nanopharmaceuticals. Thus, sequestration of NPs in resident macrophages of the liver and spleen reduces effectiveness of the therapeutic agent targeted delivery to tumors [23, 24]. In contrast, the firmly adherent leukocytes that capture NPs in the tumor microenvironment can function as a depot of the drug, the long-term gradual release of which into the tissues improves the anti-tumor response [25]. Finally, preservation of mobility by blood leukocytes after binding to NPs allows these to transport the drug over long distances and break through physiological barriers [26], which provides the basis for the concept of cell-mediated delivery. It has just recently been proposed to use neutrophils for intratumor delivery of nanopharmaceuticals; in contrast to the passive accumulation mechanism, the factors that contribute to or prevent active NP delivery are poorly understood.

The IVM method allowed us to monitor behavior of NPs of various types in the tumor. The study involved magnetite nanoparticles (MNPs) covalently bound to the Cy5 cyanine dye and liposomes, into which a lipophilic dye (DiD) was incorporated. It was shown that MNPs could break through the vascular barrier via both passive transport and the use of neutrophils as a "Trojan horse". The latter mechanism was first recorded in the real-time mode: NPs were adsorbed on the surface of the neutrophil, which, going beyond the vessel, carried these to the tumor tissue (Fig. 1A). It is interesting that transient elimination of neutrophils from the bloodstream resulted in the decreased accumulation of MNPs in the tumors. These findings confirm neutrophil involvement in delivery of MNPs to tumor cells [27].

The mechanisms underlying the intratumor delivery of liposomes were dramatically different from that underlying the delivery of MNPs [28]. Local leaks into the perivascular space (microleaks) were most often detected (Fig. 1B). This extravasation type is characterized by the limited area of the leak and penetration depth not exceeding 20 μm from the vessel. Fluorescence intensity was even inside the microleak and considerably exceeded that in the blood vessel lumen. Microleaks usually occurred rapidly (within minutes), and later the microleak zone remained almost unchanged.

Another, less frequent type of the leak (Fig. 1B) covered a vast area of the interstitium penetrating the tissues to the depth of several hundred microns. Such macroleaks were spatially and temporally unstable showing the diffusion gradient and dynamic changes in signal intensity, which, however, never exceeded fluorescence intensity of the circulating liposomes. Furthermore, we observed repeated waves of liposome extravasation from the same macroleak site. In contrast to microleaks, this extravasation type is likely to reflect NP diffusion in the interstitial space. The liposome diffusion waves always spread from the center of the tumor to the periphery, probably due to higher intra-tissue pressure inside the tumor.

As with MNPs, newtrophils also contributed to the release of liposomes from the vascular bed. When assessing the dynamics of microleak occurrence in the real-time mode, it was reported that in some cases these occurred in the neutrophil extravasation sites. Likewise, microleaks were reported occurring after the neutropil release from the blood vessel (Fig. 1B).

It should be noted that, in contrast to MNPs, liposomes were not captured by neutrophils, so the reported examples of the neutropil-mediated leaks represent a fundamentally new mechanism underlying NP delivery: liposomes exit the blood vessel not on the neutrophil, but through the vascular barrier pores opening temporarily at the time of cell transmigration. As a result, we can speak about four mechanisms of liposome delivery into the tumor: spontaneously occurring and

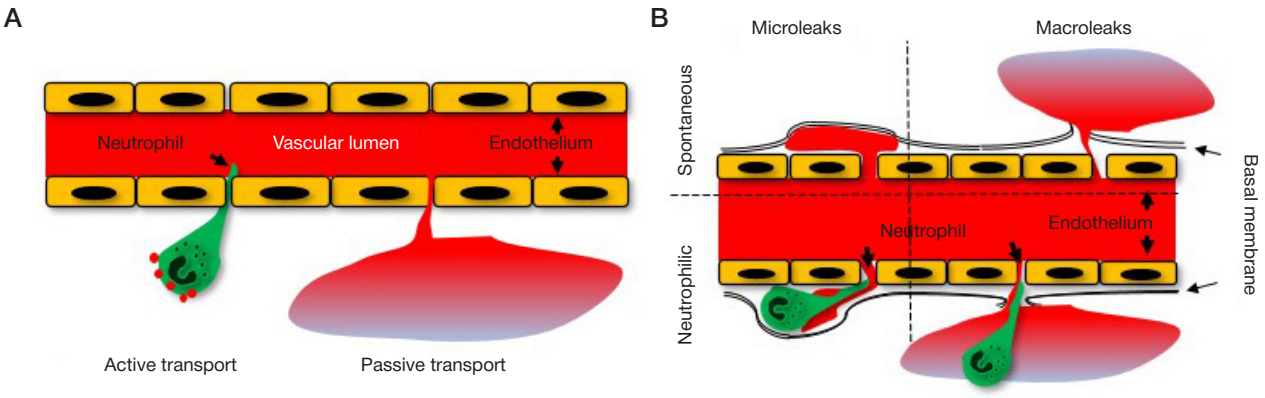

Fig. 1. Role of leukocytes in delivery of anti-tumor nanopharmaceuticals. **A**. Mechanisms underlying extravasation of magnetite nanoparticles in the tumor microvascular bed. **B**. Mechanisms underlying extravasation of liposomes in the tumor microvascular bed

neutrophil-dependent micro- and macroleaks (Fig. 1B). In the context of neutrophil depletion the effectiveness of liposome accumulation in the tumor decreased by 20–30%, which allows for a rough estimation of the contribution of neutropils to delivery of liposomal drugs to the tumor focus.

It was impossible to differentiate between the interendothelial and transendothelial pathways of liposome extravasation in thetumor vessels due to limited IVM resolving power [29]. However, *in vivo* monitoring of neutropils and liposomes in the tumor can shed light on the fundamental mechanisms underlying the NP transport from the blood vessel lumen to the tissues. Despite obvious differences, it can be assumed that there are some similarities in the extravasation behavior of neutropils and liposomes. Thus, after crossing the layer of endothelial cells, neutropils show adhesion or crawling behavior in the confined subendothelial space [30], and accumulation of neutropils in the perivascular compartment resembles the liposomal microleak. Then neutropils migrate through the non-dense areas of the basal membrane and are released from the perivascular space, similar to the NP breakthrough and diffusion in the macroleak site. It is noteworthy that some macroleaks emerge from the pre-existing microleaks, which further supports the idea that two patterns of liposome accumulation represent the consecutive stages of extravasation corresponding to transport of liposomes through the endothelial and subendothelial barriers.

It can be assumed that the described extravasation patterns play unequal parts in delivery of anti-tumor drugs. First, microleaks are found not only in tumors, but also in healthy tissues, which can explain the liposomal doxorubicin skin toxicity. Second, despite the fact that microleaks contribute to accumulation of liposomes around the tumor vessels, these do not provide access to tumor cells for nanopharmaceuticals. In contrast, macroleaks allow liposomes to penetrate deep into tumor tissues, promoting the therapeutic agent delivery to the target cells. This extravasation type that is specific for tumors shows differences depending on the tumor type. This suggests that passive delivery of liposomes to tumor cells is mediated primarily by macroleaks. Third, it is well known that, despite the fact that liposomal doxorubicin is better accumulated in the tumors, than free doxorubicin, there is little improvement of the anti-tumor response. Insufficient therapeutic efficacy can partially result from predominance of microleaks over macroleaks, which leads to the increased accumulation of liposomes at the macroscopic level, but in fact does not provide access to cancer cells for drugs.

Intravital microscopy in studying renal NP excretion

Assessment of biodistribution represents an essential phase of pre-clinical trials of pharmaceuticals. It allows one to determine such important parameters, as the drug excretion rate, accumulation dynamics, and preferential target organs.

According to modern concepts, the NP capability of being excreted by the kidneys is determined by the glomerular filter pore size, which is about 6 nm. Particles with the diameter above the specified threshold value cannot be released into urine. However, in recent years, more and more evidence has accumulated in the literature on the paradoxical renal filtration of large NPs. We observed a similar pattern when assessing biodistribution of the MNPs with the size (140 nm) significantly above the renal filtration threshold [31]. The transient increase in renal iron levels accompanied by negative contrast in the renal parenchyma on MRI was reported 2 h after intravenous administration of MNPs. These unexpected results were confirmed by confocal microscopy using the fluorescence-labeled MNPs. Furthermore, MNP administration was associated with the increased urinary iron levels, and ultrastructural analysis revealed intact NPs in the urine sediment.

In order to understand the cause of renal excretion of the NPs more than 20-fold exceeding the glomerular filter threshold, we performed IVM of superficial renal cortex at the time of MNP-Cy5 administration. Contrast enhancement of peritubular capillaries with the particles was observed immediately after the injection, and as early as 25 min later the fluorescence signal was localized mainly in the renal tubules. It is noteworthy that at the early stages after administration of the drug, accumulation occurred not in the lumen, but in the basal compartment of the tubular epithelium, indicating that MNPs were not filtered through the glomeruli, but reached the epithelium from the tubular interstitium. Further monitoring of the fate of MNP-Cy5 in the kidneys revealed the transient increase in fluorescence signal intensity in the renal tubular lumen.

Considering the results obtained, it can be assumed that translocation from blood to urine via peritubular endothelial and renal epithelial cells represents an alternative excretion pathway for synthetic NPs with the size above the glomerular filtration threshold (Fig. 2). It can be assumed that this is an underestimated mechanism that can explain some previously reported examples of paradoxical renal excretion of large NPs.

Actually, renal clearance of large NPs usually explained by the NP degradation is often reported in the literature [32–39]. At the same time, there is growing evidence for urinary excretion of intact NPs, which has remained unexplained until now. Thus, the recent study revealed renal clearance of the 20 nm pegylated magnetic NPs [40]. The authors explained this phenomenon by potential flexibility of NPs allowing these to pass through the glomerular filter membrane. One more case of unexpected renal filtration was reported for carbon nanotubes [41]. The authors assumed that certain orientation of the nanorods sized

200–300 nm with the aspect ratio between 100:1 and 500:1 within the flow makes these capable of passing through the pores. As in our experiments, both studies cited report peak excretion 30–60 min after administration and accumulation of NPs in the proximal tubules. Despite the fact that the authors explain this by NP re-absorption from the tubular lumen by the epithelial cells, an alternative hypothesis is that NPs penetrate into the renal epithelium through peritubular capillaries. In some studies, renal filtration of graphene oxide nanosheets (1 × 1000 nm, 5 × 200 nm) was explained by morphological deformation of particles (sliding, squeezing or folding) [42, 43], while the other group assumed that urinary excretion of intact silicate NPs (sized 22 × 185 nm and 65 × 720 nm) was caused by the glomerular filter membrane barrier function impairment [44].

Significant accumulation in the proximal tubules was unexpectedly reported for ferumoxytol, the FDA-approved preparation of iron oxide NPs covered with dextran (size 17–30 nm), while the dextran NPs sized 13 nm were found mostly in the glomeruli [45]. The authors assumed that this was due to the broad range of ferumoxytol diameters, such that a certain share of NPs was below the threshold glomerular filter membrane size. In this case, one would expect that the majority of NPs would still accumulate in the glomeruli, but this was not reported. Despite the fact that ferumoxytol localization in the tubules was similar to the distribution of the 5 nm dextran NPs excreted with urine, in contrast to the latter, ferumoxytol distribution had no effect on albumin endocytosis, as well as on the expression of megalin and clathrin in the proximal tubules. These data are indirect evidence suggesting that ferumoxytol gets into the epithelium from the basolateral side without involvement of absorption mechanisms in the tubules. Although the glomerular filter membrane morphological deformation and dysfunction for each distinct type of NPs cannot be ruled out, we assume that translocation through the endothelium and tubular epithelium is a more common phenomenon that can at least partially explain the earlier reported data on paradoxical filtration.

Disclosure of the alternative mechanism underlying NP translocation in the peritubular capillaries represents a paradigm shift in bio-nanotechnology, since it allows one to assume the existence of new criteria for renal clearance. Perhaps, this fact will have important clinical implications in nephrology and oncology.

Prospects of using intravital microscopy in clinical practice

In clinical practice, anti-tumor therapy with nanopharmaceuticals usually represents a series of consecutive systemic injections. In this regard, the question arises, whether the behavior of the second and subsequent doses would be different from the behavior of the first dose. Potential effect of the first NP dose on the subsequent doses can be associated with both systemic factors (change in the extent of NP capture by cells of the reticulo-endothelial system) and the tumor microenvironment modulation.

To answer these questions, specifics of biodistribution of the repeated dose of liposomes was assessed by IVM [46]. The non-labeled liposomes were administered as the first dose; the fluorescence-labeled liposomes were administered 24 h later. It was shown that the half-life and accumulation profiles of the first and second doses of liposomes in organs and tumors were the same. Quantitative analysis revealed no differences in the rate of liposome capture by blood leukocytes: both the first and second liposome doses bound mainly to monocytes, less often to neutrophils and CD4 lymphocytes, but showed almost no interaction with CD8 lymphocytes and B cells. The pattern of capture of two doses by cells of the tumor microenvironment was also the same: in both cases, the association of liposomes

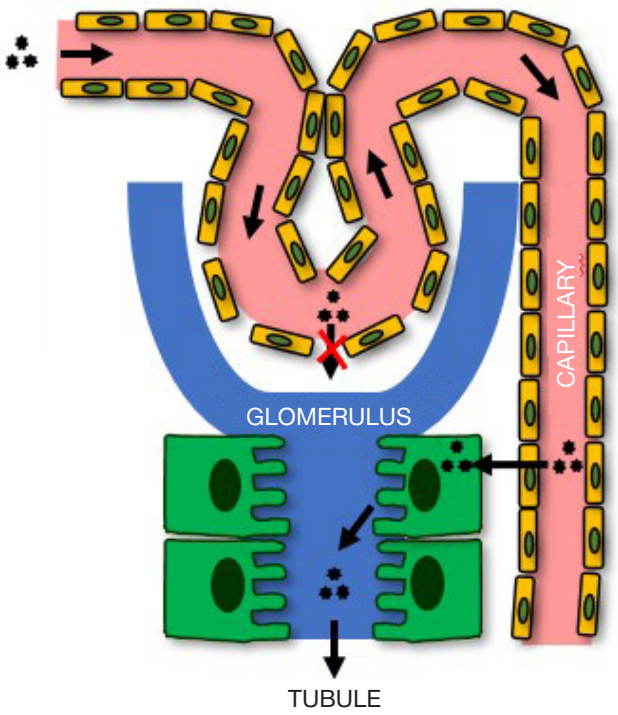

Fig. 2. Mechanism underlying renal excretion of nanoparticles with the size above the glomerular filtration threshold

with neutrophils and macrophages, and less often with other leukocytes and tumor cells was revealed. Interaction of NPs with immune cells can in some cases alter the composition of white blood cell population, which results in the fact that the subsequent drug dose faces potentially different microenvironment. However, the quantitative composition of blood and tumor leukocytes remained the same at the time of administration of the first and second doses.

As with single administration of the drug, the second dose of liposomes got into the tumor due to micro- and macroleaks. To directly assess spatial accumulation of two doses in the tumor, the experiments were conducted, in which the first and second doses of liposomes were bound to different dyes. High degree of co-localization of two fluorescence signals was reported 48 h/24 h after administration of the first/second dose of liposomes.

No difference in behavior of two liposome doses in the body opens up the possibility of using the first dose as the diagnostic one for targeted selection of the tumors showing good NP uptake, which shall also accumulate well the second (therapeutic) dose of liposomes. To test the hypothesis, the liposomes were used comprising maghemite NPs sized 5 nm that could be detected in the tumor by MRI; liposomal doxorubicin (Caelyx) was used as a therapeutic agent. IVM showed that neither loading magnetic contrast diagnostic agents into liposomes, nor the presence of the therapeutic agent in the liposomes does not disrupt the high degree of co-localization of two liposome doses in the tumor.

Validation of the algorithm for personalized diagnosis and treatment of tumors was performed in the pre-clinical model. The animals intravenously administered the dose of diagnostic liposomes were divided into groups with high and low accumulation of the drug using MRI. Then each group was divided into two subgroups, in which the animals received either Caelyx, or free doxorubicin. It was found that in the group with high accumulation of diagnostic liposomes a more pronounced decrease in the tumor growth rate and an increase in survival rate were observed compared to animals with low diagnostic

agent accumulation. It should be noted that no differences in the rate of tumor progression between groups with high and low accumulation of magnetic liposomes were revealed during treatment with free doxorubicin.

These findings suggest that estimation of accumulation of magnetic liposomes in the tumor makes it possible to predict therapeutic efficacy of liposomal drugs, but not of their free analogues.

It should be noted that the IVM technique not only allows us to solve fundamental medical and biological problems, but also has potential for practical application. Thus, in 2016, the first report was published showing the possibility of conducting IVM of tumors in patients [47].

CONCLUSION

Introduction of the IVM technique makes it possible to study biodistribution of nanopharmaceuticals and the mechanisms underlying delivery of those to tumor cells in preclinical animal models at a deeper level. Currently, the use of IVM in clinical practice is limited inter alia by the narrow range of fluorescence dyes approved for use in humans. However, the vector of development of modern microscopy methods is aimed at using the cell autofluorescence spectra for visualization of cells without any additional dyes. The emergence of commercially available microscopes using this detection principle will significantly expand the IVM diagnostic capabilities.

References

1. Ahlawat J, et al. Nanoparticles in Biomedical Applications. In: Green Nanoparticles. Springer, Cham, 2020; p. 227–250.
2. Nakamura Y, et al. Nanodrug Delivery: Is the Enhanced Permeability and Retention Effect Sufficient for Curing Cancer? Bioconjug Chem. 2016; 27 (10): 2225–38.
3. Bertrand N, et al. Cancer nanotechnology: the impact of passive and active targeting in the era of modern cancer biology. Adv Drug Deliv Rev. 2014; 66: 2–25.
4. Wilhelm S, et al. Analysis of nanoparticle delivery to tumours. Nat Rev Mater. 2016; 1 (5): 16014.
5. Danhier F. To exploit the tumor microenvironment: Since the EPR effect fails in the clinic, what is the future of nanomedicine? J Control Release. 2016; 244 (Pt A): 108–21.
6. Mitchell MJ, King MR. Leukocytes as carriers for targeted cancer drug delivery. Expert Opin Drug Deliv. 2015; 12 (3): 375–92.
7. Tiet P, Berlin JM. Exploiting homing abilities of cell carriers: Targeted delivery of nanoparticles for cancer therapy. Biochem Pharmacol. 2017; 145: 18–26.
8. Xue J, et al. Neutrophil-mediated anticancer drug delivery for suppression of postoperative malignant glioma recurrence. Nat Nanotechnol. 2017; 12 (7): 692–700.
9. Chu D, et al. Photosensitization Priming of Tumor Microenvironments Improves Delivery of Nanotherapeutics via Neutrophil Infiltration. Adv Mater. 2017; 29 (27): 1701021.
10. Chu D, et al. Nanoparticle Targeting of Neutrophils for Improved Cancer Immunotherapy. Adv Healthc Mater. 2016; 5 (9): 1088–93.
11. Luo X, et al. Neutrophil-mediated delivery of pixantrone-loaded liposomes decorated with poly(sialic acid)–octadecylamine conjugate for lung cancer treatment. Drug Deliv. 2018; 25 (1): 1200–12.
12. Smith BR, et al. High-resolution, serial intravital microscopic imaging of nanoparticle delivery and targeting in a small animal tumor model. Nano Today. 2013; 8 (2): 126–37.
13. Smith BR. et al. Selective uptake of single-walled carbon nanotubes by circulating monocytes for enhanced tumour delivery. Nat Nanotechnol. 2014; 9 (6): 481–7.
14. Qiang L, et al. A novel macrophage-mediated biomimetic delivery system with NIR-triggered release for prostate cancer therapy. J Nanobiotechnology. BioMed Central. 2019; 17 (1): 83.
15. Chen K, et al. A TRAIL-Delivered Lipoprotein-Bioinspired Nanovector Engineering Stem Cell-Based Platform for Inhibition of Lung Metastasis of Melanoma. Theranostics. 2019; 9 (10): 2984–98.
16. Hanahan D, Weinberg RA. Hallmarks of cancer: The next generation. Cell. 2011; 144 (5): 646–74.
17. Schießl IM, Castrop H. Deep insights: intravital imaging with two-photon microscopy // Pflugers Archiv European Journal of Physiology. Springer Verlag. 2016; 468 (9): 1505–16.
18. Naumenko V, Jenne C, Mahoney DJ. Intravital microscopy for imaging the tumor microenvironment in live mice. Methods Mol Biol. 2016; 1458: 217–30.
19. Li JL, et al. Intravital multiphoton imaging of immune responses in the mouse ear skin. Nat Protoc. 2012; 7 (2): 221–34.
20. Ritsma L, et al. Surgical implantation of an abdominal imaging window for intravital microscopy. Nat Protoc. 2013; 8 (3): 583–94.
21. Stolp B, Melican K. Microbial pathogenesis revealed by intravital microscopy: pros, cons and cautions. FEBS Lett. 2016; 590 (13): 2014–26.
22. Miller MA, Weissleder R. Imaging the pharmacology of nanomaterials by intravital microscopy: Toward understanding their biological behavior. Adv Drug Deliv Rev. 2017; 113: 61–86.
23. Inturi S, et al. Modulatory Role of Surface Coating of Superparamagnetic Iron Oxide Nanoworms in Complement Opsonization and Leukocyte Uptake. ACS Nano. 2015; 9 (11): 10758–68.
24. Arami H, et al. In vivo delivery, pharmacokinetics, biodistribution and toxicity of iron oxide nanoparticles. Chem Soc Rev. 2015; 44 (23): 8576–607.
25. Miller MA, et al. Tumour-associated macrophages act as a slow-release reservoir of nano-therapeutic Pt(IV) pro-drug. Nat Commun. 2015; 6: 8692.
26. Naumenko V, et al. Neutrophils in viral infection. Cell Tissue Res. 2018; 371 (3): 505–16.
27. Naumenko V, et al. Neutrophil-mediated transport is crucial for delivery of short-circulating magnetic nanoparticles to tumors. Acta Biomater. 2020; 104: 176–87.
28. Naumenko VA, et al. Extravasating Neutrophils Open Vascular Barrier and Improve Liposomes Delivery to Tumors. ACS Nano. 2019; 13 (11).
29. Moghimi SM, Simberg D. Nanoparticle transport pathways into tumors. J Nanoparticle Res. 2018; 20 (6): 169.
30. Park SA, Hyun Y-M. Neutrophil Extravasation Cascade: What Can We Learn from Two-photon Intravital Imaging? Immune Netw. 2016; 16 (6): 317–21.
31. Naumenko V, et al. Intravital microscopy reveals a novel mechanism of nanoparticles excretion in kidney. J Control Release. 2019; 307: 368–78.
32. Yang K, et al. Graphene in Mice: Ultrahigh In Vivo Tumor Uptake and Efficient Photothermal Therapy. Nano Lett. 2010; 10 (9): 3318–23.
33. Yang K, et al. In Vivo Pharmacokinetics, Long-Term Biodistribution, and Toxicology of PEGylated Graphene in Mice. ACS Nano. 2011; 5 (1): 516–22.
34. Gary-Bobo M, et al. Mannose-Functionalized Mesoporous Silica Nanoparticles for Efficient Two-Photon Photodynamic Therapy of Solid Tumors. Angew Chemie Int Ed. 2011; 50 (48): 11425–9.
35. Lu J. et al. Biocompatibility, biodistribution, and drug-delivery efficiency of mesoporous silica nanoparticles for cancer therapy in animals. Small. NIH Public Access. 2010; 6 (16): 1794–805.
36. Fischer NO, et al. Evaluation of nanolipoprotein particles (NLPs) as an in vivo delivery platform. PLoS One. 2014; 9 (3): e93342.
37. He Q, et al. In vivo Biodistribution and Urinary Excretion of Mesoporous Silica Nanoparticles: Effects of Particle Size and PEGylation. Small. 2011; 7 (2): 271–80.
38. He X, et al. In vivo study of biodistribution and urinary excretion of

surface-modified silica nanoparticles. Anal Chem. 2008; 80 (24): 9597–603.
39. Fu C, et al. The absorption, distribution, excretion and toxicity of mesoporous silica nanoparticles in mice following different exposure routes. Biomaterials. 2013; 34 (10): 2565–75.
40. Gómez-Vallejo V, et al. PEG-copolymer-coated iron oxide nanoparticles that avoid the reticuloendothelial system and act as kidney MRI contrast agents. Nanoscale. 2018; 10 (29): 14153–64.
41. Ruggiero A, et al. Paradoxical glomerular filtration of carbon nanotubes. Proc Natl Acad Sci U. S. A. 2010; 107 (27): 12369–74.
42. Jasim DA, et al. Tissue distribution and urinary excretion of intravenously administered chemically functionalized graphene oxide sheets. Chem Sci. 2015; 6 (7): 3952–64.
43. Jasim DA, et al. The Effects of Extensive Glomerular Filtration of Thin Graphene Oxide Sheets on Kidney Physiology. ACS Nano. 2016; 10 (12): 10753–67.
44. Huang X, et al. The shape effect of mesoporous silica nanoparticles on biodistribution, clearance, and biocompatibility in vivo. ACS Nano. 2011; 5 (7): 5390–9.
45. Nair AV, et al. Characterizing the interactions of organic nanoparticles with renal epithelial cells in vivo. ACS Nano. 2015; 9 (4): 3641–53.
46. Naumenko VA, et al. Intravital imaging of liposome behavior upon repeated administration: A step towards the development of liposomal companion diagnostic for cancer nanotherapy. J Control Release. 2021; 330: 244–56.
47. Fisher DT, et al. Intraoperative intravital microscopy permits the study of human tumour vessels. Nat Commun Nature Publishing Group. 2016; 7 (1): 1–9.

Литература

1. Ahlawat J, et al. Nanoparticles in Biomedical Applications. In: Green Nanoparticles. Springer, Cham, 2020; p. 227–250.
2. Nakamura Y, et al. Nanodrug Delivery: Is the Enhanced Permeability and Retention Effect Sufficient for Curing Cancer? Bioconjug Chem. 2016; 27 (10): 2225–38.
3. Bertrand N, et al. Cancer nanotechnology: the impact of passive and active targeting in the era of modern cancer biology. Adv Drug Deliv Rev. 2014; 66: 2–25.
4. Wilhelm S, et al. Analysis of nanoparticle delivery to tumours. Nat Rev Mater. 2016; 1 (5): 16014.
5. Danhier F. To exploit the tumor microenvironment: Since the EPR effect fails in the clinic, what is the future of nanomedicine? J Control Release. 2016; 244 (Pt A): 108–21.
6. Mitchell MJ, King MR. Leukocytes as carriers for targeted cancer drug delivery. Expert Opin Drug Deliv. 2015; 12 (3): 375–92.
7. Tiet P, Berlin JM. Exploiting homing abilities of cell carriers: Targeted delivery of nanoparticles for cancer therapy. Biochem Pharmacol. 2017; 145: 18–26.
8. Xue J, et al. Neutrophil-mediated anticancer drug delivery for suppression of postoperative malignant glioma recurrence. Nat Nanotechnol. 2017; 12 (7): 692–700.
9. Chu D, et al. Photosensitization Priming of Tumor Microenvironments Improves Delivery of Nanotherapeutics via Neutrophil Infiltration. Adv Mater. 2017; 29 (27): 1701021.
10. Chu D, et al. Nanoparticle Targeting of Neutrophils for Improved Cancer Immunotherapy. Adv Healthc Mater. 2016; 5 (9): 1088–93.
11. Luo X, et al. Neutrophil-mediated delivery of pixantrone-loaded liposomes decorated with poly(sialic acid)–octadecylamine conjugate for lung cancer treatment. Drug Deliv. 2018; 25 (1): 1200–12.
12. Smith BR, et al. High-resolution, serial intravital microscopic imaging of nanoparticle delivery and targeting in a small animal tumor model. Nano Today. 2013; 8 (2): 126–37.
13. Smith BR. et al. Selective uptake of single-walled carbon nanotubes by circulating monocytes for enhanced tumour delivery. Nat Nanotechnol. 2014; 9 (6): 481–7.
14. Qiang L, et al. A novel macrophage-mediated biomimetic delivery system with NIR-triggered release for prostate cancer therapy. J Nanobiotechnology. BioMed Central. 2019; 17 (1): 83.
15. Chen K, et al. A TRAIL-Delivered Lipoprotein-Bioinspired Nanovector Engineering Stem Cell-Based Platform for Inhibition of Lung Metastasis of Melanoma. Theranostics. 2019; 9 (10): 2984–98.
16. Hanahan D, Weinberg RA. Hallmarks of cancer: The next generation. Cell. 2011; 144 (5): 646–74.
17. Schießl IM, Castrop H. Deep insights: intravital imaging with two-photon microscopy // Pflugers Archiv European Journal of Physiology. Springer Verlag. 2016; 468 (9): 1505–16.
18. Naumenko V, Jenne C, Mahoney DJ. Intravital microscopy for imaging the tumor microenvironment in live mice. Methods Mol Biol. 2016; 1458: 217–30.
19. Li JL, et al. Intravital multiphoton imaging of immune responses in the mouse ear skin. Nat Protoc. 2012; 7 (2): 221–34.
20. Ritsma L, et al. Surgical implantation of an abdominal imaging window for intravital microscopy. Nat Protoc. 2013; 8 (3): 583–94.
21. Stolp B, Melican K. Microbial pathogenesis revealed by intravital microscopy: pros, cons and cautions. FEBS Lett. 2016; 590 (13): 2014–26.
22. Miller MA, Weissleder R. Imaging the pharmacology of nanomaterials by intravital microscopy: Toward understanding their biological behavior. Adv Drug Deliv Rev. 2017; 113: 61–86.
23. Inturi S, et al. Modulatory Role of Surface Coating of Superparamagnetic Iron Oxide Nanoworms in Complement Opsonization and Leukocyte Uptake. ACS Nano. 2015; 9 (11): 10758–68.
24. Arami H, et al. In vivo delivery, pharmacokinetics, biodistribution and toxicity of iron oxide nanoparticles. Chem Soc Rev. 2015; 44 (23): 8576–607.
25. Miller MA, et al. Tumour-associated macrophages act as a slow-release reservoir of nano-therapeutic Pt(IV) pro-drug. Nat Commun. 2015; 6: 8692.
26. Naumenko V, et al. Neutrophils in viral infection. Cell Tissue Res. 2018; 371 (3): 505–16.
27. Naumenko V, et al. Neutrophil-mediated transport is crucial for delivery of short-circulating magnetic nanoparticles to tumors. Acta Biomater. 2020; 104: 176–87.
28. Naumenko VA, et al. Extravasating Neutrophils Open Vascular Barrier and Improve Liposomes Delivery to Tumors. ACS Nano. 2019; 13 (11).
29. Moghimi SM, Simberg D. Nanoparticle transport pathways into tumors. J Nanoparticle Res. 2018; 20 (6): 169.
30. Park SA, Hyun Y-M. Neutrophil Extravasation Cascade: What Can We Learn from Two-photon Intravital Imaging? Immune Netw. 2016; 16 (6): 317–21.
31. Naumenko V, et al. Intravital microscopy reveals a novel mechanism of nanoparticles excretion in kidney. J Control Release. 2019; 307: 368–78.
32. Yang K, et al. Graphene in Mice: Ultrahigh In Vivo Tumor Uptake and Efficient Photothermal Therapy. Nano Lett. 2010; 10 (9): 3318–23.
33. Yang K, et al. In Vivo Pharmacokinetics, Long-Term Biodistribution, and Toxicology of PEGylated Graphene in Mice. ACS Nano. 2011; 5 (1): 516–22.
34. Gary-Bobo M, et al. Mannose-Functionalized Mesoporous Silica Nanoparticles for Efficient Two-Photon Photodynamic Therapy of Solid Tumors. Angew Chemie Int Ed. 2011; 50 (48): 11425–9.
35. Lu J. et al. Biocompatibility, biodistribution, and drug-delivery efficiency of mesoporous silica nanoparticles for cancer therapy in animals. Small. NIH Public Access. 2010; 6 (16): 1794–805.
36. Fischer NO, et al. Evaluation of nanolipoprotein particles (NLPs) as an in vivo delivery platform. PLoS One. 2014; 9 (3): e93342.
37. He Q, et al. In vivo Biodistribution and Urinary Excretion of Mesoporous Silica Nanoparticles: Effects of Particle Size and PEGylation. Small. 2011; 7 (2): 271–80.
38. He X, et al. In vivo study of biodistribution and urinary excretion of surface-modified silica nanoparticles. Anal Chem. 2008; 80 (24): 9597–603.
39. Fu C, et al. The absorption, distribution, excretion and toxicity of mesoporous silica nanoparticles in mice following different exposure routes. Biomaterials. 2013; 34 (10): 2565–75.
40. Gómez-Vallejo V, et al. PEG-copolymer-coated iron oxide

nanoparticles that avoid the reticuloendothelial system and act as kidney MRI contrast agents. Nanoscale. 2018; 10 (29): 14153–64.
41. Ruggiero A, et al. Paradoxical glomerular filtration of carbon nanotubes. Proc Natl Acad Sci U. S. A. 2010; 107 (27): 12369–74.
42. Jasim DA, et al. Tissue distribution and urinary excretion of intravenously administered chemically functionalized graphene oxide sheets. Chem Sci. 2015; 6 (7): 3952–64.
43. Jasim DA, et al. The Effects of Extensive Glomerular Filtration of Thin Graphene Oxide Sheets on Kidney Physiology. ACS Nano. 2016; 10 (12): 10753–67.
44. Huang X, et al. The shape effect of mesoporous silica nanoparticles on biodistribution, clearance, and biocompatibility in vivo. ACS Nano. 2011; 5 (7): 5390–9.
45. Nair AV, et al. Characterizing the interactions of organic nanoparticles with renal epithelial cells in vivo. ACS Nano. 2015; 9 (4): 3641–53.
46. Naumenko VA, et al. Intravital imaging of liposome behavior upon repeated administration: A step towards the development of liposomal companion diagnostic for cancer nanotherapy. J Control Release. 2021; 330: 244–56.
47. Fisher DT, et al. Intraoperative intravital microscopy permits the study of human tumour vessels. Nat Commun Nature Publishing Group. 2016; 7 (1): 1–9.

APPLICATION OF QUANTITATIVE LIGHT-INDUCED FLUORESCENCE TECHNIQUE TO DETERMINE INDIVIDUAL ORAL HYGIENE LEVELS

Kopetskiy IS, Pobozhieva LV ✉, Kopetskaya AI

Pirogov Russian National Research Medical University, Moscow, Russia

Indices that reflect individual oral hygiene levels are widely used to determine microbial plaque of the tooth surface. When teaching patients how to take care about the oral cavity, dentists use visual demonstration of the dental plaque localization. The quantitative light-induced fluorescence (QLF) technique represents a modern method to diagnose individual oral hygiene, in which even minimal microbial plaque buildup shows up as red fluorescence. The study aimed to assess the oral hygiene status using the quantitative light-induced fluorescence technique. Dental deposits were detected using QLF; the Quigley Hein, Green-Vermillion, DMF indices were detected clinically. The findings show that Simple Hygiene Scores do not exceed 2, when the caries intensity is very low or low ($p < 0.05$). In these groups, the Green-Vermillion and Quigley Hein index values reach 0.5 ± 0.23 and 0.2 ± 0.14, respectively. When the caries intensity is medium, Simple Hygiene Scores vary between 1–5 points. Very high caries intensity is characterized by the Simple Hygiene Score between 3 and 5 points (maximum Green-Vermillion and Quigley Hein index values reach 2.3 ± 0.43 and 2.1 ± 0.35) ($p < 0.05$). Thus, the quantitative light-induced fluorescence technique can be used in clinical trials for objective oral hygiene assessment, visual demonstration of dental plaque buildup to patients, and assessment of the dynamic changes in these indicators.

Keywords: dental plaque, oral hygiene, quantitative light-induced fluorescence

Author contribution: Pobozhieva LV — research procedure, data analysis, manuscript writing; Kopetskiy IS — manuscript editing; Kopetskaya AI — data analysis, manuscript writing.

Compliance with ethical standards: the study was approved by the Ethics Committee of the Pirogov Russian National Research Medical University (protocol No. 238 dated 19 March 2024). All the subjects submitted the informed consent to participation in the study.

✉ **Correspondence should be addressed:** Ludmila V. Pobozhieva
Ostrovityanova, 1, str. 7, Moscow, 117997; ludmila-stomatolog@mail.ru

Received: 23.04.2025 **Accepted:** 23.05.2025 **Published online:** 06.06.2025

DOI: 10.24075/brsmu.2025.030

ПРИМЕНЕНИЕ МЕТОДА КОЛИЧЕСТВЕННОЙ СВЕТОИНДУЦИРОВАННОЙ ФЛУОРЕСЦЕНЦИИ В ОПРЕДЕЛЕНИИ УРОВНЯ ИНДИВИДУАЛЬНОЙ ГИГИЕНЫ ПОЛОСТИ РТА

И. С. Копецкий, Л. В. Побожьева ✉, А. И. Копецкая

Российский национальный исследовательский медицинский университет имени Н. И. Пирогова (Пироговский Университет), Москва, Россия

Для определения микробного налета на поверхности зубов широко применяют индексы, которые отражают уровень гигиены полости рта. При обучении пациентов уходу за ротовой полостью врачи-стоматологи используют визуальную демонстрацию локализации зубного налета. Метод количественной светоиндуцированной флуоресценции (QLF) является современным методом диагностики индивидуальной гигиены полости рта, при использовании которого даже минимальное скопление микробного налета проявляется в виде красной флуоресценции. Целью исследования было изучить гигиеническое состояние полости рта с применением метода количественной светоиндуцированной флуоресценции. Выявление зубных отложений проводили с использованием QLF, клинически определяли индексы Quigley и Hein, Green-Vermillion, КПУ. Результаты исследования показали, что при очень низком и низком уровнях интенсивности кариозного процесса показатели Simple Hygiene Score не превышают 2 балла ($p < 0,05$). В данных группах значения индексов Green-Vermillion и Quigley, Hein достигали значений 0,5 ± 0,23 и 0,2 ± 0,14 соответственно. При среднем уровне интенсивности кариозного процесса показатели Simple Hygiene Score варьируют от 1 до 5 баллов. Очень высокий уровень кариозного процесса характеризуется значениями Simple Hygiene Score от 3 до 5 баллов (максимальные показатели индексов Green-Vermillion и Quigley, Hein достигали 2,3 ± 0,43 и 2,1 ± 0,35) ($p < 0,05$). Таким образом, метод количественной светоиндуцированной флуоресценции может быть использован в клинических исследованиях для объективной оценки гигиены полости рта, наглядной демонстрации скопления зубного налета пациентам и изучения данных показателей в динамике.

Ключевые слова: зубной налет, гигиена полости рта, количественная светоиндуцированная флуоресценция

Вклад авторов: Л. В. Побожьева — проведение исследования, анализ данных, написание текста статьи; И. С. Копецкий — редактирование статьи; А. И. Копецкая — анализ данных, написание текста статьи.

Соблюдение этических стандартов: работа одобрена этическим комитетом Российского национального исследовательского медицинского университета имени Н. И. Пирогова (протокол № 238 от 19 марта 2024 г). Все участники дали добровольное информированное согласие на участие в исследовании.

✉ **Для корреспонденции:** Людмила Владимировна Побожьева
ул. Островитянова, д. 1, стр. 7, г. Москва, 117997; ludmila-stomatolog@mail.ru

Статья получена: 23.04.2025 **Статья принята к печати:** 23.05.2025 **Опубликована онлайн:** 06.06.2025

DOI: 10.24075/vrgmu.2025.030

Microbial plaque forms biofilms on the tooth surface, which represents a major etiological factor of dental caries and inflammatory periodontal diseases [1–3].

A number of studies have proven that it is possible to use the quantitative light-induced fluorescence (QLF) technique as a new method to detect biofilms in the oral cavity [4, 5].

Biofilm removal from the tooth surface is an effective method to prevent the main dental diseases. It seems extremely important to teach patients methods of individual oral hygiene and encourage them to perform oral hygiene regularly on a daily basis. Dentists use visual demonstration of dental plaque localization in clinical practice to teach patients how to take care about the oral cavity [6, 7].

Hygienic indices are widely used to quantify microbial plaque on the tooth surface. To detect microbial plaque, the dental deposits are stained with dyes and assessed through visual control, which does not preclude incorrect interpretation and takes time for accurate calculation and measurement [8, 9].

The advanced noninvasive quantitative light-induced fluorescence (QLF) technique involving the use of the oral camera equipped with software allows one not only to quantify dental plaque, but also measure the area of the microbial plaque buildup and calculate the Simple Hygiene Score (SHS). It should also be noted that software can analyze such parameters, as the lesion area/white spot area (area % px 2), fluorescence loss/average enamel mineral loss (ΔF, %), lesion depth (ΔFmax, %), lesion volume/maximum mineral loss (ΔQ, % px), area showing bacterial activity/extent of bacterial activity in the lesions (ΔR, %), maximum bacterial activity (ΔRmax, %), area of bacterial activity (ΔR Area, %) [10, 11].

Even minimal microbial plaque buildup shows up as red fluorescence [11]. The microbial biofilm produces porphyrin, which is manifested by the color change in vivo [12]. The QLF-D method can be used as an alternative to the existing clinical index methods, regardless of the assessed tooth regions [13, 14]. Microbial plaque detection is accomplished without using dyes [15]. The QLF-D method can be used to teach patients individual oral hygiene [16].

Thus, the use of QLF is of great clinical interest in terms of assessing the oral hygiene status.

The study aimed to assess the oral hygiene status using the quantitative light-induced fluorescence technique.

METHODS

The study involved 204 individuals (132 females and 72 males). Inclusion criteria: females and males seeking care or routine examination; age 18–44 years; no dental arch defects in the frontal section (in individuals with physiological or abnormal bite). Exclusion criteria: patients undergoing orthodontics treatment; prosthetic constructions in the frontal section; age below 18 and over 44 year; acute oral inflammatory disease; decompensated somatic disorder; refusal to participate in the study.

The clinical phase consisted of collecting complaints and history taking, oral cavity examination. Disorders of dental hard tissues and periodontal tissues were diagnosed based on ICD-10.

The DMF index (decayed, missing, and filled index) was determined in all subjects in order to assess the intensity of caries lesions. According to the WHO assessment criteria, five caries intensity levels are distinguished in the age group 33–44 years: very low (0.2–1.5), low (1.6–6.2), medium (6.3–12.7), high (12.8–16.2), very high (16.3 and above).

Oral hygiene status was assessed by the quantitative light-induced fluorescence method. The Q-ray dental software, Qraycam Pro camera (AIOBIO, Republic of Korea), and Inspektor Research Systems detector (Netherlands) were used for QLF. The following indicators were determined to detect microbial plaque buildup and oral hygiene status assessment: Simple Hygiene Score with the range of 0–5; area of bacterial activity (ΔR Area, %).

Clinically, oral hygiene status was determined based on the Green-Vermillion (OHI-S) index. Oral hygiene was assessed as good (values within the range of 0–0.6), satisfactory (0.7–1.6), unsatisfactory (1.7–2.5), or poor (over 2.6). Buccal surface of the teeth 16 and 26, labial surface of the teeth 11 and 31, and lingual surface of the teeth 36 and 46 were examined to determine OHI-S.

Furthermore, the Quigley Hein dental plaque index was determined on the vestibular surface of 12 frontal maxillary and mandibular teeth using the dental plaque indicator (Plaque Test, PRESIDENT). Six index values are distinguished: no plaque, isolated flecks of plaque, band of plaque at the gingival margin, up to 1/3 of the tooth surface covered with plaque, plaque from 1/3 to 2/3 of the surface, plaque on more than 2/3 of the surface.

Statistical processing of the study results was performed using Microsoft Office Excel 2017 (Microsoft Corporation) and the Statistica 12.0 (StatSoft) software package. Relative values were calculated; descriptive statistical methods were applied involving calculation of the mean, average error, and standard deviation.

RESULTS

The gender and age distribution of surveyed individuals is provided in Table 1. The average age of surveyed females was 27.73 (± 1.9) years, and that of surveyed males was 31.54 (± 2.3) years.

Based on the study results, very low caries intensity was revealed in 5.9% of surveyed individuals with the DMF value of 1.5 ± 0.34. Low caries intensity was determined in 13.7% of surveyed individuals with the DMF value of 5.6 ± 0.43. Medium caries intensity was revealed in 35.3% of cases with the average DMF value of 11.3 ± 1.2, high intensity — in 37.3% of cases with the DMF value of 14.6 ± 1.3, very high intensity — in 7.8% of cases with the DMF value of 17.2 ± 0.8 (Fig. 1).

The analysis of the Green-Vermillion index values has shown that the patients' oral hygiene corresponds to good, when the caries intensity is very low or low, to satisfactory, when the caries intensity is moderate-to-high, and to unsatisfactory, when the caries intensity is very high.

Oral hygiene indices (Green-Vermillion and Quigley Hein) are provided in Table 2.

Table 1. Gender and age distribution of subjects

Total number of surveyed individuals, *n*	*n* = 204	
Average age of surveyed individuals, years	29.3 (± 2.4) (min 18 ÷ max 44)	
Gender distribution of surveyed individuals, *n*	Males *n* = 72	Females *n* = 132
Average age of surveyed individuals depending on gender, years	31.54 (± 2.3) (min 18 ÷ max 44)	27.73 (± 1.9) (min 18 ÷ max 42)

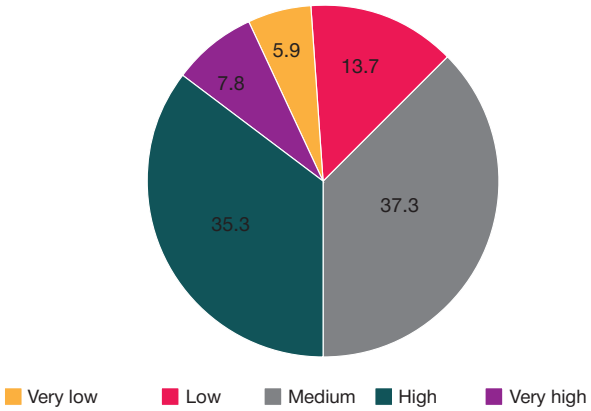

Fig. 1. Distribution of subjects by caries intensity, %

The analysis of the Quigley Hein index values has shown that patients with medium, high, and very high caries intensity need individual oral hygiene improvement (index values above 1) (Fig. 3).

Thus, the results of data interpretation based on the Green-Vermillion and Quigley Hein indices of the surveyed individuals were similar, despite the differences in determination of indices.

Assessment of both indices suggests that oral hygiene of patients with very low or low caries intensity corresponds to good and does not require adjustment, in contrast to the overwhelming majority of individuals with the medium, high, and very high DMF values.

In our study, microbial plaque buildup and oral hygiene estimates based on the Simple Hygiene Score were determined in the region of the maxillary and mandibular incisors and canines. The QLF-D diagnosis allows one to detect even slight dental plaque buildup in red fluorescence, as shown as blue pseudo-stain (Fig. 4).

The quantitative light-induced fluorescence (QLF) method enabled the noninvasive, quick, objective determination of the patients' oral hygiene status (Fig. 5).

Quantitative and qualitative assessment of dental plaque in surveyed individuals is provided in points (range 0–5 points) (Table 3).

Based on the Simple Hygiene Score it was determined that the values were 0–2 points, when the caries intensity was very low or low. When the caries intensity was medium, the Simple Hygiene Score varied between 1 and 5 points, when it was high — 2–5 points, when it was very high — between 3 and 5 points (Fig. 6).

DISCUSSION

In the study we determined hygienic indices in patients with different caries intensity using conventional methods and the quantitative light-induced fluorescence technique. According to the data obtained, when the caries intensity was very low, the Simple Hygiene Score corresponded to 0 and 1

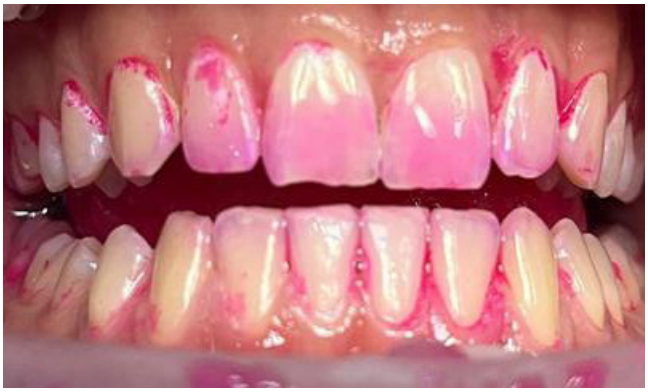

Fig. 2. Patient A., 22 years. Photo protocol of oral hygiene status assessment. DMF — 3, Green-Vermillion index — 0.5, Quigley Hein index — 0.92

(Green-Vermillion — 0.4 ± 0.12, Quigley Hein — 0.2 ± 0.07) ($p < 0.05$). SHS values of 1 and 2 points corresponded to low caries intensity (Green-Vermillion — 0.5 ± 0.23, Quigley Hein — 0.2 ± 0.14) ($p < 0.05$). In these groups, the clinical index values suggest good individual oral hygiene. When the caries intensity is medium, the Simple Hygiene Score varies between 1 and 5 points (Green-Vermillion — 1.2 ± 0.27, Quigley Hein — 1.4 ± 0.32). High caries intensity is characterized by the SHS 2–5 points (Green-Vermillion — 1.5 ± 0.31, Quigley Hein — 1.5 ± 0.28). Very high caries intensity is characterized by the Simple Hygiene Score 3–5 points (Green-Vermillion — 2.3 ± 0.43, Quigley Hein — 2.1 ± 0.35) ($p < 0.05$).

According to the data provided by a number of authors, SHS 0 indicates good oral hygiene status, while SHS 5 indicates poor status [17]. Our study has shown that SHS values of 0, 1, and 2 corresponded to good oral hygiene status. However, the dental plaque distribution and production within the dental arch can vary considerably, as reflected by the Simple Hygiene Score values.

There is a report of the QLF-D limitation when used to assess general oral status. This is due to the fact that QLF reflects well the diagnosis in the region of frontal maxillary and mandibular teeth. Thus, measurement in the region of maxillary molars, as well as on the palatal and lingual tooth surface, it limited due to complexity of taking images of these regions [18]. Our findings have shown that SHS determination in the region of the frontal group of teeth enables quick and reliable detection of microbial plaque buildup. It should be noted that for a number of indices it is necessary to determine dental plaque on the lingual/palatal tooth surface, which is more convenient to do using a probe.

No need to stain dental deposits should be considered an advantage of the method [19].

CONCLUSIONS

It is reasonable to use the QLF method for screening aimed to estimate the patients' individual oral hygiene.

Table 2. Oral hygiene status indices, M ± sd

Caries intensity	Green-Vermillion index	Quigley Hein index
Very low	0.4 ± 0.12	0.2 ± 0.07
Low	0.5 ± 0.23	0.2 ± 0.14
Medium	1.2 ± 0.27	1.4 ± 0.31
High	1.5 ± 0.31	1.5 ± 0.28
Very high	2.3 ± 0.43	2.1 ± 0.35

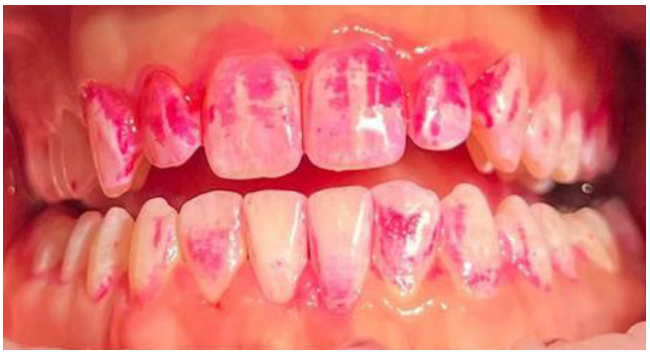

Fig. 3. Patient K., 27 years. Clinical assessment of hygienic indices. DMF — 8, Green-Vermillion index — 1.7, Quigley Hein index — 3.3

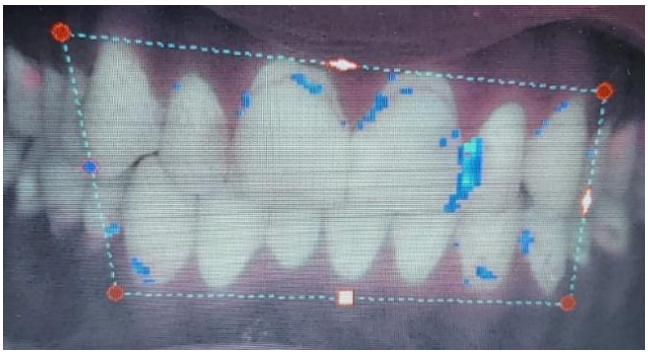

Fig. 5. Patient M., 25 years. The areas covered with dental plaque are analyzed using the software tool. DMF — 13. SHS — 2, area of bacterial activity (Area ΔR) — 30% — 4[%]

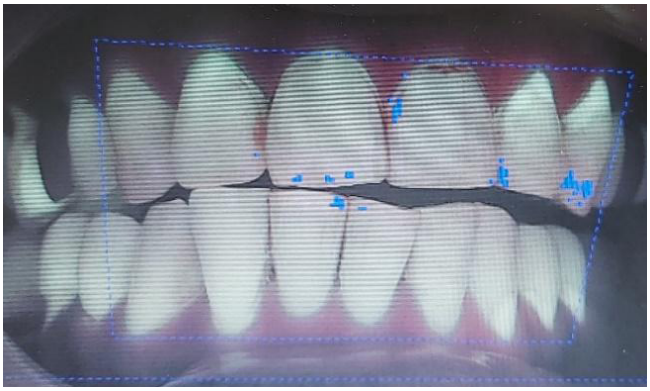

Fig. 4. Patient N., 32 years. Results of the oral hygiene status QLF diagnosis. DMF — 10. SHS — 1, area of bacterial activity (Area ΔR) — 30% — 1[%]

Fig. 6. Patient A., 21 years. Dental plaque assessment involving the use of QLF diagnosis. DMF — 7. SHS — 5, area of bacterial activity (Area ΔR) — 30% — 34[%].

Table 3. Simple Hygiene Score (SHS) in surveyed individuals

Caries intensity	Number of surveyed individuals	Simple Hygiene Score (SHS)
Very low	3	0
	9	1
Low	13	1
	15	2
Medium	2	1
	13	2
	23	3
	22	4
	12	5
High	1	2
	23	3
	25	4
	27	5
Very high	2	3
	5	4
	9	5
Total	204	

The quantitative light-induced fluorescence objectively and transparently reflects the dental plaque buildup and allows one to assess the dynamic changes in SHS. However, the issue of the clinical significance of determining the area of bacterial activity on dental restorations is still poorly understood.

References

1. Valm A.M. The structure of dental plaque microbial communities in the transition from health to dental caries and periodontal disease. J Mol Biol. 2019; 431 (16): 2957–69. DOI: 10.1016/j.jmb.2019.05.016.
2. Mosaddad SA, Tahmasebi E, Yazdanian A, Rezvani MB, Seifalian A, Yazdanian M, et al. Eur. Oral microbial biofilms: an update. J Clin Microbiol Infect Dis. 2019; 38 (11): 2005–19. DOI: 10.1007/s10096-019-03641-9. PMID: 31372904.
3. Velsko IM, Fellows Yates JA, Aron F, Hagan RW, Frantz LAF, Loe L, et al. Microbial differences between dental plaque and historic dental calculus are related to oral biofilm maturation stage. Microbiome. 2019; 7 (1): 102. DOI: 10.1186/s40168-019-0717-3.
4. Hwang H-R, Cho Y-S, Kim B-I. Assessment of clinical applicability of a new plaque scoring system using quantitative light-induced fluorescence-digital. J Dental Hygiene Sci. 2014; 14 (2): 150–7.
5. Klaus K, Glanz T, Glanz AG, Ganss C, Ruf S. Comparison of Quantitative light-induced fluorescence-digital (QLF-D) images and images of disclosed plaque for planimetric quantification of dental plaque in multibracket appliance patients. Sci Rep. 2020; 10 (1): 4478. DOI: 10.1038/s41598-020-61454-9.PMID: 32161288.
6. D'Elia G, Floris W, Marini L, Corridore D, Rojas MA, Ottolenghi L, et al. Methods for evaluating the effectiveness of home oral hygiene measures-a narrative review of dental biofilm indices. Dent J (Basel). 2023; 11 (7): 172. DOI: 10.3390/dj11070172.
7. Soldo M, Matijević J, Malčić Ivanišević A, Čuković-Bagić I, Marks L, Nikolov Borić D, et al. Impact of oral hygiene instructions on plaque index in adolescents. Cent Eur J Public Health. 2020; 28 (2): 103–7. DOI: 10.21101/cejph.a5066.PMID: 32592553.
8. Carvalho AP, Moura MF, Costa FO, Cota LO. Correlations between different plaque indexes and bleeding on probing: A concurrent validity study. J Clin Exp Dent. 2023; 15 (1): e9–e16. DOI: 10.4317/jced.60039.
9. Yoo JMSS, Cho JW, Eom KH, Kim HS, Lee MG, Lee MY. Clinical study on the comparison of various types of the dental plaque indices. Int J Clin Prev Dent. 2007; 3: 111–21.
10. Kim H-E. Quantitative light-induced fluorescence: a potential tool for dental hygiene process. J Dental Hygiene Sci. 2013; 13 (2): 115–24. DOI: 10.1016/j.jds.2012.12.011.
11. Meharry MR, Dawson D, Wefel IS, Harless JD, Kummet CM, Xiao X. The effect of surface defects in early caries assessment using quantitative light-induced fluorescence (QLF) and micro-digital-photography (MDP) J Dent. 2012; 40 (11): 955–61. DOI: 10.1016/j.jdent.2012.08.001. Epub 2012 Aug 11.
12. Oh SH, Choi JY, Lee SR, Kim SH. Evaluation of Periodontal Risk Factors with Quantitative Light-Induced Fluorescence Based Fluorescent Plaque Index, in Comparison to Radiographic and Oral Health Habit Scoring: A Retrospective Case Study. Sensors (Basel). 2021; 21 (17): 5774. DOI: 10.3390/s21175774.
13. Lee J, Lee T, Jung HI, Park W, Song JS. Effectiveness of an Oral Health Education Program Using a Smart Toothbrush with Quantitative Light-Induced Fluorescence Technology in Children. Children (Basel). 2023; 10 (3): 429. DOI: 10.3390/children10030429.
14. H SY. Development of novel dental plaque scoring system using quantitative light induced fluorescence-digital. Dissertation: Yonsei university; 2014.
15. Kim M, Lee S-Y, Cho Y-S. Validity and reliability of the plaque score using Qraycam. J Dental Hygiene Sci. 2015; 15 (3): 377–82. DOI: 10.17135/jdhs.2015.15.3.377.
16. Khudanov B, Jung HI, Kahharova D, Lee J-W, Hamidov I, Lee ES, Kim B-I. Effect of an oral health education program based on the use of quantitative light-induced fluorescence technology in Uzbekistan adolescents. Photodiagn Photodyn Ther. 2018.
17. Akulovich AV, Nikiforova GG, Korostelev AA, Matelo SK. Ispol'zovanie metoda kolichestvennoj svetoinducirovannoj fluorescencii (QLF) dlja diagnostiki sostojanija jemali pri razlichnyh stomatologicheskih vmeshatel'stvah. Parodontologija. 2023; 28 (1): 55–65. Dostupno po ssylke: https://doi.org/10.33925/1683-3759-2023-28-1-55-65. Russian.
18. Hwang H-R, Cho Y-S, Kim B-I. Assessment of clinical applicability of a new plaque scoring system using quantitative light-induced fluorescence-digital. J Dental Hygiene Sci. 2014; 14 (2): 150–7.
19. Jong-Bin Lee, Da-Hye Choi, Yon-Joo Mah, Eun-Kyoung Pang. Validity assessment of quantitative light-induced fluorescence-digital (QLF-D) for the dental plaque scoring system: a cross-sectional study. BMC Oral Health. 2018 20; 18: 187. DOI: 10.1186/s12903-018-0654-8.

Литература

1. Valm A.M. The structure of dental plaque microbial communities in the transition from health to dental caries and periodontal disease. J Mol Biol. 2019; 431 (16): 2957–69. DOI: 10.1016/j.jmb.2019.05.016.
2. Mosaddad SA, Tahmasebi E, Yazdanian A, Rezvani MB, Seifalian A, Yazdanian M, et al. Eur. Oral microbial biofilms: an update. J Clin Microbiol Infect Dis. 2019; 38 (11): 2005–19. DOI: 10.1007/s10096-019-03641-9. PMID: 31372904.
3. Velsko IM, Fellows Yates JA, Aron F, Hagan RW, Frantz LAF, Loe L, et al. Microbial differences between dental plaque and historic dental calculus are related to oral biofilm maturation stage. Microbiome. 2019; 7 (1): 102. DOI: 10.1186/s40168-019-0717-3.
4. Hwang H-R, Cho Y-S, Kim B-I. Assessment of clinical applicability of a new plaque scoring system using quantitative light-induced fluorescence-digital. J Dental Hygiene Sci. 2014; 14 (2): 150–7.
5. Klaus K, Glanz T, Glanz AG, Ganss C, Ruf S. Comparison of Quantitative light-induced fluorescence-digital (QLF-D) images and images of disclosed plaque for planimetric quantification of dental plaque in multibracket appliance patients. Sci Rep. 2020; 10 (1): 4478. DOI: 10.1038/s41598-020-61454-9.PMID: 32161288.
6. D'Elia G, Floris W, Marini L, Corridore D, Rojas MA, Ottolenghi L, et al. Methods for evaluating the effectiveness of home oral hygiene measures-a narrative review of dental biofilm indices. Dent J (Basel). 2023; 11 (7): 172. DOI: 10.3390/dj11070172.
7. Soldo M, Matijević J, Malčić Ivanišević A, Čuković-Bagić I, Marks L, Nikolov Borić D, et al. Impact of oral hygiene instructions on plaque index in adolescents. Cent Eur J Public Health. 2020; 28 (2): 103–7. DOI: 10.21101/cejph.a5066.PMID: 32592553.
8. Carvalho AP, Moura MF, Costa FO, Cota LO. Correlations between different plaque indexes and bleeding on probing: A concurrent validity study. J Clin Exp Dent. 2023; 15 (1): e9–e16. DOI: 10.4317/jced.60039.
9. Yoo JMSS, Cho JW, Eom KH, Kim HS, Lee MG, Lee MY. Clinical study on the comparison of various types of the dental plaque indices. Int J Clin Prev Dent. 2007; 3: 111–21.
10. Kim H-E. Quantitative light-induced fluorescence: a potential tool for dental hygiene process. J Dental Hygiene Sci. 2013; 13 (2): 115–24. DOI: 10.1016/j.jds.2012.12.011.
11. Meharry MR, Dawson D, Wefel IS, Harless JD, Kummet CM, Xiao X. The effect of surface defects in early caries assessment using quantitative light-induced fluorescence (QLF) and micro-digital-photography (MDP) J Dent. 2012; 40 (11): 955–61. DOI: 10.1016/j.jdent.2012.08.001. Epub 2012 Aug 11.
12. Oh SH, Choi JY, Lee SR, Kim SH. Evaluation of Periodontal Risk Factors with Quantitative Light-Induced Fluorescence Based Fluorescent Plaque Index, in Comparison to Radiographic and Oral Health Habit Scoring: A Retrospective Case Study. Sensors (Basel). 2021; 21 (17): 5774. DOI: 10.3390/s21175774.
13. Lee J, Lee T, Jung HI, Park W, Song JS. Effectiveness of an Oral Health Education Program Using a Smart Toothbrush with Quantitative Light-Induced Fluorescence Technology in Children. Children (Basel). 2023; 10 (3): 429. DOI: 10.3390/children10030429.
14. H SY. Development of novel dental plaque scoring system using quantitative light induced fluorescence-digital. Dissertation: Yonsei university; 2014.
15. Kim M, Lee S-Y, Cho Y-S. Validity and reliability of the plaque score using Qraycam. J Dental Hygiene Sci. 2015; 15 (3): 377–82. DOI: 10.17135/jdhs.2015.15.3.377.
16. Khudanov B, Jung HI, Kahharova D, Lee J-W, Hamidov I, Lee ES, Kim B-I. Effect of an oral health education program based on

the use of quantitative light-induced fluorescence technology in Uzbekistan adolescents. Photodiagn Photodyn Ther. 2018.
17. Акулович А. В., Никифорова Г. Г., Коростелев А. А., Мателo С. К. Использование метода количественной светоиндуцированной флуоресценции (QLF) для диагностики состояния эмали при различных стоматологических вмешательствах. Пародонтология. 2023; 28 (1): 55–65. Доступно по ссылке: https://doi.org/10.33925/1683-3759-2023-28-1-55-65.
18. Hwang H-R, Cho Y-S, Kim B-I. Assessment of clinical applicability of a new plaque scoring system using quantitative light-induced fluorescence-digital. J Dental Hygiene Sci. 2014; 14 (2): 150–7.
19. Jong-Bin Lee, Da-Hye Choi, Yon-Joo Mah, Eun-Kyoung Pang. Validity assessment of quantitative light-induced fluorescence-digital (QLF-D) for the dental plaque scoring system: a cross-sectional study. BMC Oral Health. 2018 20; 18: 187. DOI: 10.1186/s12903-018-0654-8.

ANALYSIS OF THE RUSSIANS' AWARENESS OF BONE MARROW DONATION AND THE FEDERAL BONE MARROW DONOR REGISTRY INFRASTRUCTURE

Butunts MA, Dyuzhina KA, Nifatova ES, Muradyan TG ✉

Pirogov Russian National Research Medical University, Moscow, Russia

Bone marrow transplant is the leading method to treat hematologic malignancies, immunodeficiency, and hereditary metabolic disorders. The Federal Bone Marrow Donor Registry effectiveness depends directly on public awareness of bone marrow donation and infrastructure development. A comprehensive approach to public awareness is necessary to increase the system effectiveness. The study aimed to investigate factors that influence joining the Federal Bone Marrow Donor Registry, with a focus on motivation, sources of information, impact of infrastructure, environment, and common myths. The respondents (potential donors registered in the Federal Registry; *n* = 3100) filled an online questionnaire of 24 questions aimed at studying and assessing the socio-demographic characteristics, motivation, sources of information, influence of the environment, awareness of bone marrow donation, and readiness to donate. It was found that young adults aged 18–36 (*n* = 1860) more often join the Federal Registry through informal channels, such as work/school events (*n* = 843; 27.2%), while respondents over the age of 37 (*n* = 1240) prefer healthcare institutions (*n* = 1590; 51.3%). Women make up the majority of potential donors (*n* = 2304; 74.3%), especially in Moscow (*n* = 1650; 74.5%), while higher prevalence of myths is reported for the regions (*n* = 1646; 53.1%). The findings emphasize the need for the differentiated approach to information policy, which will make it possible to increase the donor movement effectiveness nationwide. A key factor in scaling this work is partnership with commercial laboratories, which significantly expands the Federal Registry recruitment network and provides convenient conditions for donors to join.

Keywords: donation, bone marrow, hematopoietic stem cell, transplantation, BMT, HSCT, Federal Bone Marrow Donor Registry

Author contribution: Butunts MA — study planning, literature review, recruiting potential bone marrow donors, cooperation with medical institutions, statistical analysis, manuscript writing; Dyuzhina KA — literature review, data acquisition, analysis, and interpretation, recruiting potential bone marrow donors, cooperation with medical institutions; Nifatova ES — study planning, literature review, recruiting potential bone marrow donors; Muradyan TG — study planning, literature review, data analysis and interpretation, cooperation with medical institutions, statistical analysis, manuscript writing.

Compliance with ethical standards: all the sociological syrvey participants submitted the informed consent to the study; the survey was anonymous, the data were treated confidentially.

✉ **Correspondence should be addressed:** Tigran G. Muradyan
Ostrovityanova, 1/6, ap. 2021, Moscow, 117513, Russia; muradyan@rsmu.ru

Received: 26.05.2025 **Accepted:** 17.06.2025 **Published online:** 26.06.2025

DOI: 10.24075/brsmu.2025.032

АНАЛИЗ ОСВЕДОМЛЕННОСТИ РОССИЯН О ДОНОРСТВЕ КОСТНОГО МОЗГА И ИНФРАСТРУКТУРЫ ФЕДЕРАЛЬНОГО РЕГИСТРА ДОНОРОВ КОСТНОГО МОЗГА

М. А. Бутунц, К. А. Дюжина, Е. С. Нифатова, Т. Г. Мурадян ✉

Российский национальный исследовательский медицинский университет имени Н. И. Пирогова, Москва

Трансплантация костного мозга — ведущий метод лечения злокачественных новообразований крови, иммунодефицитных состояний и наследственных метаболических нарушений. Эффективность Федерального регистра доноров костного мозга напрямую зависит от уровня информированности населения о донорстве костного мозга и развития инфраструктуры. Для повышения эффективности системы необходим комплексный подход к информированию населения. Целью исследования было изучить факторы, влияющие на вступление в Федеральный регистр доноров костного мозга, с акцентом на мотивацию, источники информации, влияние инфраструктуры, окружения и распространенных мифов. Респонденты (потенциальные доноры, состоящие в Федеральном регистре; *n* = 3100) заполняли онлайн-анкету из 24 вопросов, направленных на изучение и оценку социально-демографических характеристик, мотивации, источников информации, влияния окружения, осведомленности о донорстве костного мозга и готовности к донации. Установлено, что молодые люди 18–36 лет (*n* = 1860) чаще вступают в Федеральный регистр через неформальные каналы, такие как акции на работе/учебе (*n* = 843; 27,2%), респонденты старше 37 лет (*n* = 1240) предпочитают медицинские организации (*n* = 1590; 51,3%). Женщины составляют большинство потенциальных доноров (*n* = 2304; 74,3%), особенно в Москве (*n* = 1650; 74,5%), в регионах отмечается более высокая распространенность мифов (*n* = 1646; 53,1%,). Полученные результаты подчеркивают необходимость дифференцированного подхода в информационной политике, что позволит повысить эффективность донорского движения в масштабах страны. Ключевой фактор масштабирования этой работы — партнерство с коммерческими лабораториями, которое значительно расширяет рекрутинговую сеть Федерального регистра и обеспечивает удобные условия для вступления доноров.

Ключевые слова: донорство, костный мозг, гемопоэтические стволовые клетки, трансплантация, ТКМ, ТГСК, Федеральный регистр доноров костного мозга

Вклад авторов: М. А. Бутунц — планирование исследования, анализ литературы, рекрутинг потенциальных доноров костного мозга, взаимодействие с медицинскими организациями, статистический анализ, подготовка рукописи; К. А. Дюжина — анализ литературы, сбор, анализ и интерпретация данных, рекрутинг потенциальных доноров костного мозга, взаимодействие с медицинскими организациями; Е. С. Нифатова — планирование исследования, анализ литературы, рекрутинг потенциальных доноров костного мозга, Т. Г. Мурадян — планирование исследования, анализ литературы, анализ и интерпретация данных, взаимодействие с медицинскими организациями, статистический анализ, подготовка рукописи.

Соблюдение этических стандартов: все участники социологического опроса дали добровольное информированное согласие на проведение исследования; опрос анонимный, данные обрабатываются конфиденциально.

✉ **Для корреспонденции:** Тигран Гагикович Мурадян
ул. Островитянова, д. 1/6, к. 2021, г. Москва, 117513, Россия; muradyan@rsmu.ru

Статья получена: 26.05.2025 **Статья принята к печати:** 17.06.2025 **Опубликована онлайн:** 26.06.2025

DOI: 10.24075/vrgmu.2025.032

Bone marrow and peripheral blood hematopoietic stem cell transplant (BMT/HSCT) represents a high-tech treatment method. It is used for a broad range of disorders, including hematologic malignancies, immunodeficiency, and hereditary metabolic disorders [1]. The method is based on substitution of the recipient's abnormal hematopoiesis through administration of hematopoietic stem cells obtained either from the patient him/herself (autologous HSCT), or from the donor (allogeneic HSCT) [2]. In turn, allogeneic HSCT is classified into procedures involving cells obtained from the HLA-identical related donors, haploidentical related donors, and unrelated bone marrow donors showing acceptable compatibility. Historically, the first successful allogeneic HSCT from the HLA-matched related donor (sister) was performed by R. A. Good in 1968 in the USA in a 5-month-old boy with primary immunodeficiency, while the first successful allogeneic HSCT from the HLA-matched unrelated donor was performed by E. D. Thomas in a 5-year-old child with severe combined immunodeficiency in 1973, also in the USA. In Russia, such intervention was first performed in 1985, and the first pediatric HSCT from the related donor was performed in 1991 by B. V. Afanasyev: a 5-year-old boy with acute lymphoblastic leukemia was the recipient, and his brother was a donor. In recent years, more than 2000 HSCT procedures are annually performed in the country, and the rate of allogeneic procedures is growing steadily (in 2023 it was above 1000 cases) [3].

It should be noted, that the bone marrow donor registry represents a key element of the allogeneic HSCT system. In 2014, a unified Bone Marrow Donor Search (BMDS) database was created in Russia at the Pavlov First Saint Petersburg State Medical University. In 2022, the Federal Registry of the Bone Marrow and Hematopoietic Stem Cell Donors, Donor Bone Marrow and Hematopoietic Stem Cells, Bone Marrow and Hematopoietic Stem Cell Recipients (Federal Registry) was formed, and the Federal Medical Biological Agency was made the Registry operator [4]. Today, it contains about 470,000 records of potential bone marrow donors (potential donors), among them 312,000 are available for search. However, it is necessary to expand the Federal Registry to 1 million people in order to ensure effective selection of potential donors for 80% of patients [5].

It is important to note that the processes ensuring the bone marrow donation are funded from the state budget (HLA typing, medical examination of bone marrow donors, bone marrow donation, transfer of bone marrow donors).

Despite the development of infrastructure, including establishing the recruiting centers (RCs) at blood service facilities and other healthcare institutions, there are still a number of systemic problems. Only 35% of the population are ready to become the bone marrow donors, which is due to low awareness and high rate of myths about the procedure [6]. Thus, 47% of Russians believe that bone marrow donation is a health hazard, and 60% expect painful sensations. Limited access to the recruiting centers represents one more barrier: there are no such centers in nine constituent entities, and in the large constituent entities these are far from sufficient [7]. That produces essential difficulties for potential donors, limiting their access to the RCs and forcing them to travel long distances for biomaterial (venous blood or buccal epithelium) sampling, which can be a barrier to join the Federal Registry. Thus, further development of the Federal Registry requires both proactive media policy and expansion of infrastructure.

The study aimed to identify the key factors that influence the person's readiness for the bone marrow donation and the differences in motivational factors that influence entry into the Federal Bone Marrow Donor Registry depending on the respondent's gender, age, and personal experience, including the impact of the rate of myths, trust in professionals, and the Federal Registry infrastructure.

METHODS

The study was conducted in October–November 2024 using the online questionnaire survey. A total of 6900 potential bone marrow donors registered in the Federal Bone Marrow Donor Registry at the time of the survey recruited by the Pirogov University were invited to take part in the study. An online questionnaire was sent to potential donors via e-mail and messengers using the contact data specified when joining the Federal Registry. Among the potential donors invited to take part in the study, 4664 (67.6%) were females and 2236 (32.4%) were males; the median age was 29.0 years (23–36). A total of 3100 respondents registered in the Federal Bone Marrow Donor Registry, who were recruited by the Pirogov University and filled the questionnaire posted on the Google Forms platform (Google LLC, USA), took part in the survey. The questionnaire comprised 24 mandatory questions aimed at investigating socio-demographic characteristics, motivation, sources of information, influence of the environment, awareness of bone marrow donation, and readiness to donate (Appendix).

The results of the respondent questionnaire survey results were process by conducting statistical analysis using the StatTech 4.8.3 software (StatTech, Russia).

The quantitative indicators were tested for normality using the Kolmogorov–Smirnov test. The non-normally distributed data are presented as the median and quartiles (Me [Q_1–Q_3] — interquartile range (IQR)), categorical variables are presented as absolute and relative rates (*n*, %) with the 95% confidence interval (95% CI), the Clopper–Pearson interval. Comparison of two independent groups based on the quantitative trait (when the distribution was non-normal) was performed using the Mann–Whitney *U* test. Comparison of percentages in four-field tables was performed using the Pearson's chi-squared test (with the expected rates ≥ 10.0), and the odds ratio with the 95% CI was calculated to estimate the effect. The analysis of multi-field tables was conducted using the Pearson's chi-squared test. The data were considered significant at $p < 0.05$.

RESULTS

The questionnaire survey conducted showed that there were 2304 (74.3%) females and 796 (25.7%) males among 3100 (100%) respondents, who completed the survey. The respodents' median age was 31.0 years (24–37). The respondents' median age of joining the Federal Bone Marrow Donor Registry was 30.0 years (23–36). The largest number of respondents joined the Federal Registry in Moscow — 2215 (71.5%), Moscow Region — 284 (9.2%), Omsk Region — 113 (3.6%), and Saint Petersburg — 83 (2.7%) respondents, respectively. As for other constituent entities of the Russian Federation (61 constituent entities), the number of the respondents, who joined the Federal Registry, was 0.1–0.8%.

Among surveyed individuals, 2558 (82.5%) people had heard about bone marrow donation before joining the Federal Registry, while 542 (17.5%) people were not aware of that previously.

Social media (information publics and channel, blogs), information campaigns at work/school, stories told by colleagues/friends/relatives were the main sources of information about bone marrow donation for the respondents. When estimating

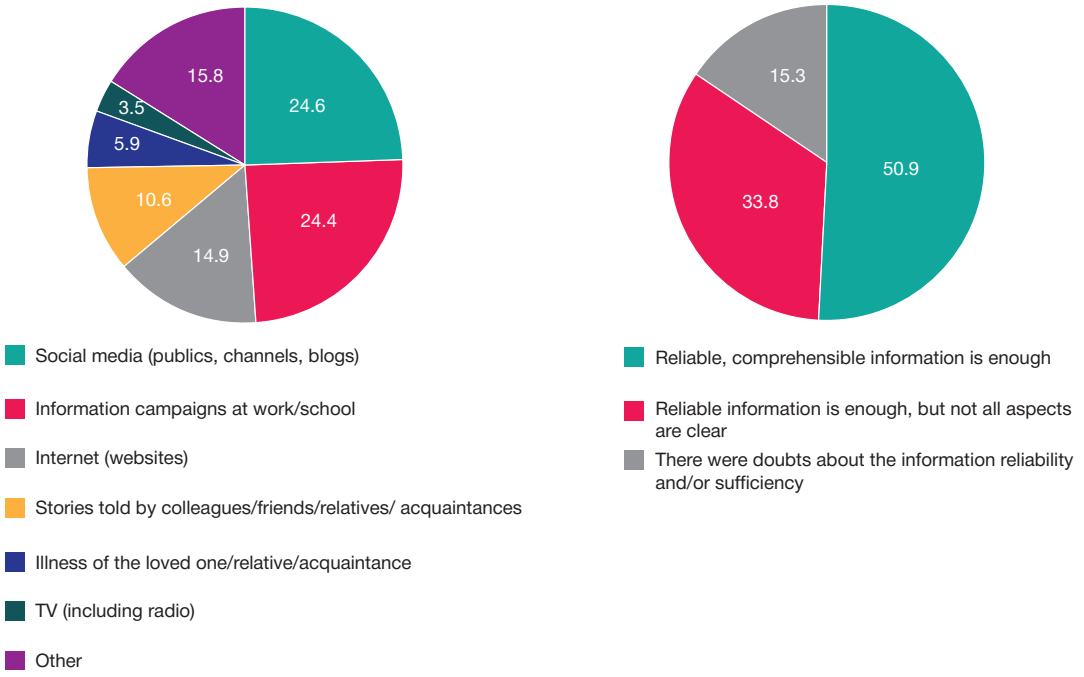

Fig. 1. Channels of information about the Federal Registry: 1 — primary source of information, 2 — completeness and reliability of information, clarity of presentation

reliability of open-source information, 1523 (49.1%) people believed that the information obtained was sufficient and reliable, while 434 (14.0%) expressed doubts about reliability of the information provided (Fig. 1).

Less that a half of the respondents, 1258 (40.6%), knew about the myths related to bone marrow donation, while 1122 (36.2 %) encountered such myths personally. The most common myths were as follows: "The procedure is a health hazard", "The bone marrow is collected from the spine or spinal cord", and "The procedure is very painful" (Fig. 2).

The vast majority of the respondents, 2551 (82.3%), got all the questions about bone marrow donation answered when consulting the Federal Registry expert. In 740 (23.9%) respondents, it was the specialist's advice that helped make the decision to join the Federal Registry (Fig. 3).

The main reasons for joining the Federal Registry were as follows: willingness to health the patients in need of HSCT (2332 people; 75.2%); aspiration to be involved in socially significant activities (666 people; 21.5%). A total of 2273 respondents (73.3%) expressed their willingness to donate bone marrow immediately. Another 623 (20.1%) would like to discuss the issue with their loved ones, but would make the decision independently (Fig. 4).

According to the survey results, only 1175 people (37.9%) received support from their families. Relatives of the majority of the respondents are not registered in the Federal Registry (Fig. 5).

Awareness of the disorders, for which bone marrow transplant is used, is as follows: 2420 people (78.1%) know about these disorders; 2701 respondents (87.1%) have knowledge about the HSCT procedure itself.

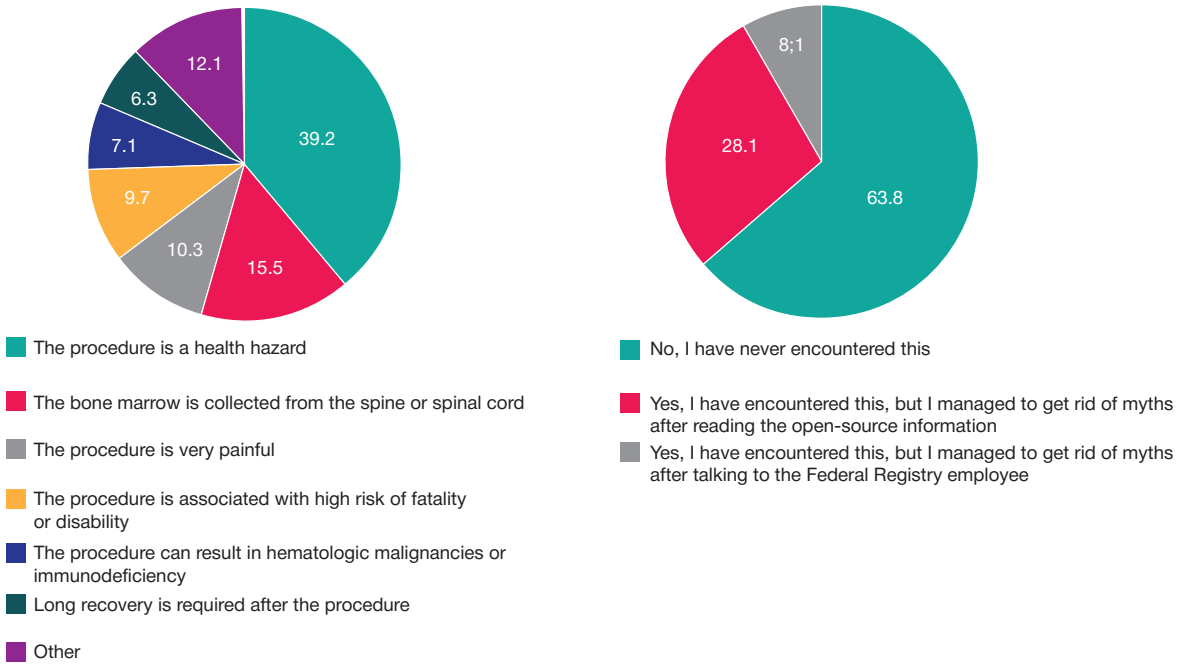

Fig. 2. Myths about bone marrow donation: 1 — the most common myths about bone marrow donation, 2 — experiences in addressing bone marrow donation myths and counterstrategies

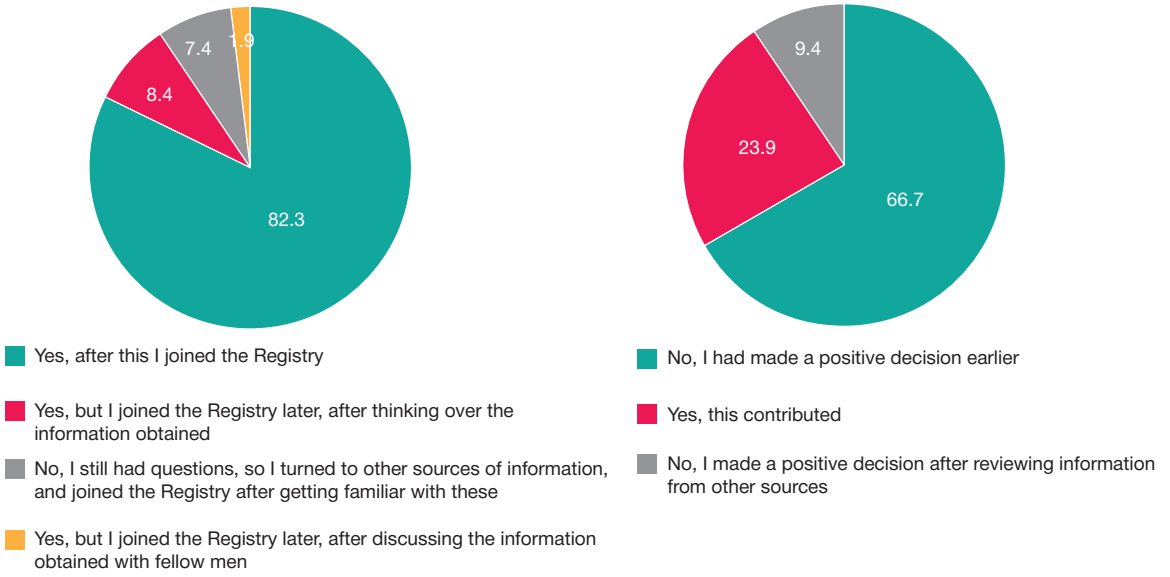

Fig. 3. Consulting the Federal Registry specialist: 1 — potential donors' satisfaction with counseling, 2 — influence on making the decision to join the Federal Registry

As for the sites for joining the Federal Registry, 2638 people (85.1%) did it in their settlements. In 1445 (46.6%) people, the most popular places were commercial partner laboratories of the Pirogov University (Citylab, Russia; KDL Domodedovo-Test, Russia). When assessing convenience of the facilities, where the respondents successfully joined the Federal Registry, 2515 people (81.1%) reported that they were satisfied with the facility location and working hours (Fig. 6).

The feedback on the biological sample receipt in the laboratory and on entering the HLA typing results in the Federal Registry is important for 3025 (97.6%) respondents.

DISCUSSION

The analysis conducted revealed some patterns and trends. Thus, we managed to find out that the respondents under the age of 37 years 27.2% more often joined the Federal Bone Marrow Donor Registry during the donor events at work or in educational institutions. The study participants aged 37–50 years preferred (in 51.3% of cases) joining the Federal Registry at medical laboratories and blood service institutions ($p < 0.001$).

Analysis of the sources of information showed the strongly marked age-related specifics ($p = 0.048$): the youth gets information primarily from the social media (974 people; 31.4%), friends' stories (428 people; 13,8%) and websites (564 people; 18.2%), while people over the age of 37 years trust TV (257 people; 8.3%), official information campaigns (887 people; 28.6%), and medical sources (282 people; 9.1%) more. We revealed weak support of making the decision to join the Federal Registry from loved ones and relatives (1230 people; 39.7%), as well as their low involvement in bone marrow donation: in 2769 (89.3%), their loved ones and relatives are not registered in the Federal Registry.

The structure of motivation also has some age-related features ($p = 0.013$): the youth is characterized by the desire to help (2117 people; 68.3%) and social activity (787 people; 25.4%), while the older generation is guided by personal experience (270 people; 8.7%) and a conscious choice (1897 people; 61.2%). The gender-based analysis revealed greater willingness to donate in males (607 people out of 796; 76.3%) compared to females (1588 people out of 2304; 68.9%). Moreover, young people often agree immediately (1365 people out of 1860; 73.1%), while people over the

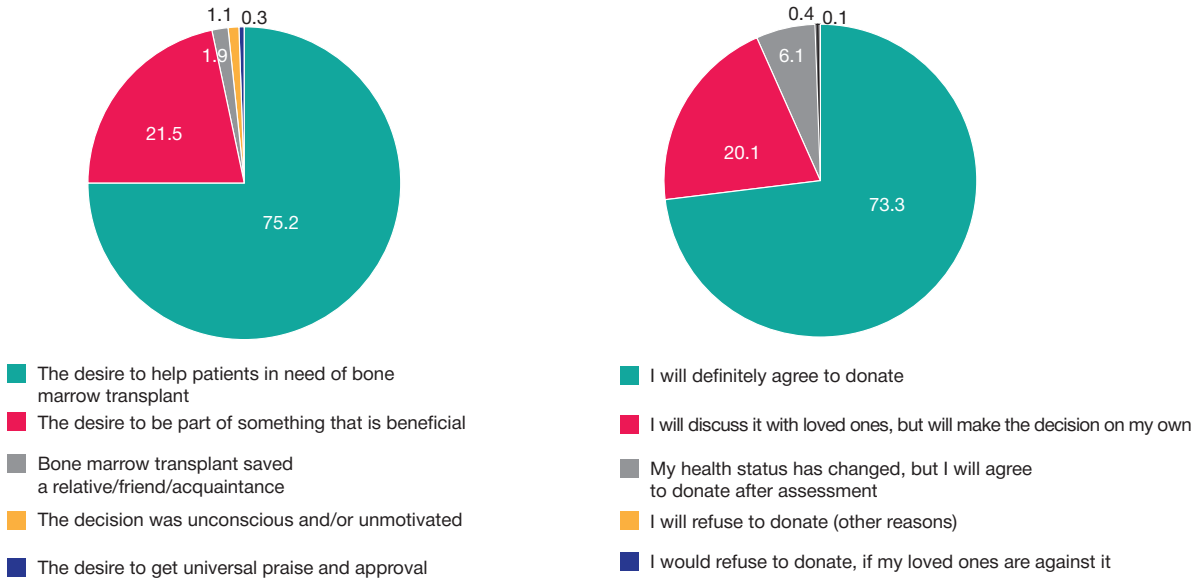

Fig. 4. Motivation to donate bone marrow: 1 — primary motivation to join the Federal Registry, 2 — readiness to donate bone marrow immediately

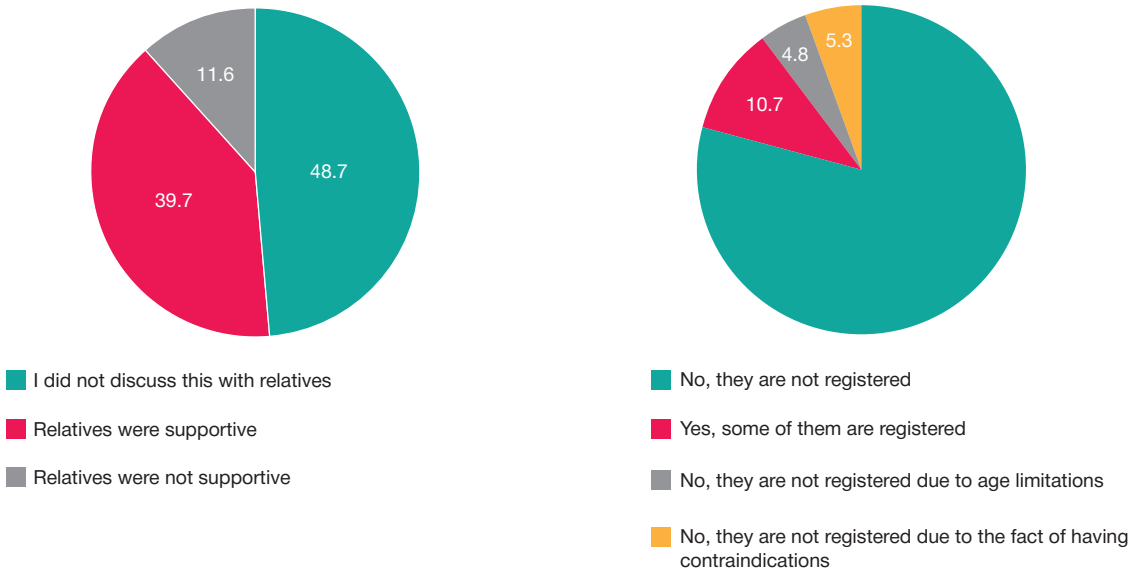

Fig. 5. Support of relatives and their involvement in bone marrow donation: 1 — discussing the plan to join the Federal Registry, 2 — relatives' status in the Federal Registry

age of 37 years need further discussion (786 people out of 1240; 63.4%).

The study has cofirmed a significant influence of myths on decision making (p = 0.047): among 1205 respondents, who had faced those, a total of 172 probable refusals of donation in the future (14.3%) were reported, while only 59 probable refusals (3.1%) were reported among 1895 respondents, who encountered no myths. The youth faces myths more often (792 people out of 1860; 42.6%), than the older generation (369 people out of 1240; 29.8%), and the highest rate of myths is reported for the regions (1646 cases out of 3100; 53.1%) vs. 1004 cases (32.4%) in large cities.

The region and gender-based analysis revealed predominance of females among potential donors in all the regions (2201–2449 people; 71.0–79.0%), with maximum rate in Moscow (1650 females among 2215 donors; 74.5%) and minimum rate in the regions (158–180 females per region, 51.0–58.0%). These data emphasize the need to develop differentiated approaches to information work and donor movement arrangement considering the identified age, gender, and regional features.

CONCLUSIONS

The findings conclusively demonstrate the need for a comprehensive differentiated approach to the development of the Federal Bone Marrow Donor Registry. The data analysis has shown considerable variability of motivation, information channels, and the factors affecting making the decision to join the Federal Registry across varios socio-demographic groups. According to the data, 46.6% of potential donors joined the Federal Registry via commercial partner laboratories of the Pirogov University, while only 11.1% did it in blood service facilities, which confirms the important role of the commercial partner laboratory participation in the Federal Registry development. Such situation results from significant representation of the networks of medical offices of commercial laboratories in both central large cities, where there are blood service institutions, and in the towns with no donor infrastructure, as well as from convenient working hours (most often from 8:00 to 20:00, including weekends). This is especially important for the core audience — young adults (students, employees), whose

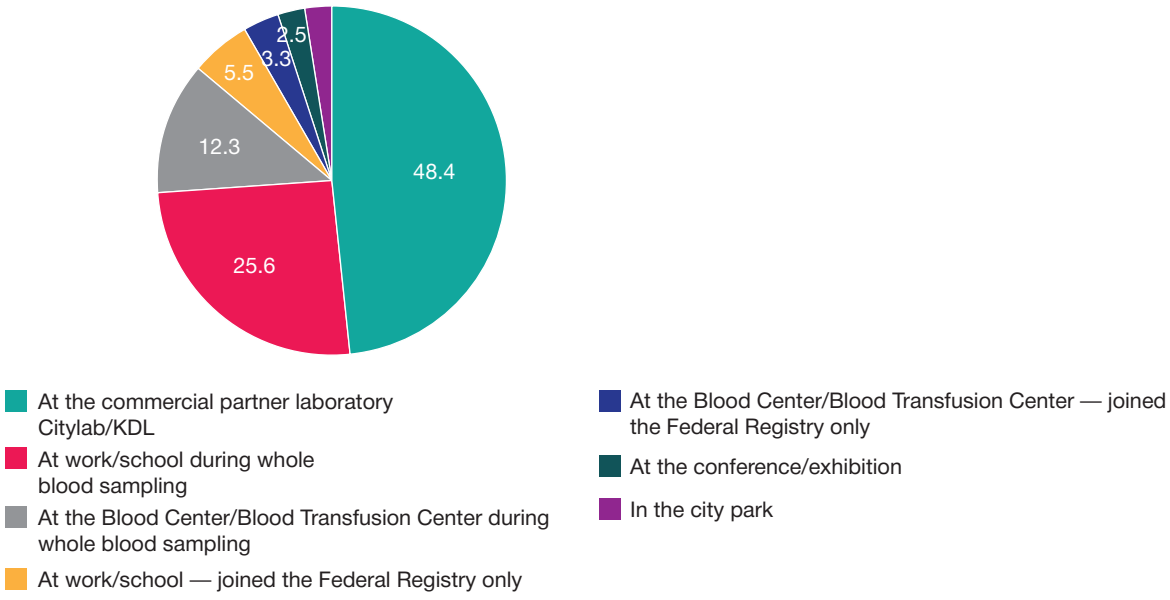

Fig. 6. Sites most convenient for joining the Federal Registry

training or work schedule coincides with the schedule of blood service facilities. Thus, commercial partner laboratories significantly improve accessibility of joining the Federal Registry due to offered convenient terms: schedule and geographical proximity. The study confirms critical importance of the information campaign personalization considering age-and-gender features and regional specifics. Taking into account the influence of relatives on making the decision to join the Federal Registry, special attention should be paid to information work with the older audience, i.e. the young adults' parents, on whom the existing myths and misconceptions of bone marrow donation resulting in the refusal to join the Federal Registry or donate bone marrow to recipients upon receiving the request from the transplant center, are projected. Optimization of the information system and arrangement of bone marrow donation popularization require the development of the multidimensional communication system combining digital technology with conventional formats, as well as strengthening the role of professional medical community in educational work. The feedback from the Federal Registry represents an important aspect of information policy. Implementation of such approach will make it possible to improve the effectiveness of attracting deliberate potential donors to the Federal Bone Marrow Donor Registry and the quality of their support at all stages of cooperation, as well as to achieve the main goal, i.e. the donors' consent to donate bone marrow upon receiving appropriate requests of the transplant centers. Furthermore, reduction of the share of refusals of bone marrow donation will result in more effective spending budget funds through eliminating the costs of expensive laboratory tests: primary and/or follow-up HLA typing of donor blood samples and medical assessment of the bone marrow donors joining the Federal Registry without realizing.

References

1. Afanasiev BV, Zubarovskaya LS, Moiseev IS. Allogennaya transplantatsiya gemopoeticheskikh stvolovykh kletok u detey: nastoyashchee, problemy, perspektivy. Rossiyskiy zhurnal detskoy gematologii i onkologii (RZhDGiO). 2015; 2 (2): 28–42. Available from: https://doi.org/10.17650/2311-1267-2015-2-2-28-42. Russian.
2. Gratwohl A, Pasquini MC, Aljurf M, Atsuta Y, et al. Worldwide Network for Blood and Marrow Transplantation (WBMT). One million haemopoietic stem-cell transplants: a retrospective observational study. Lancet Haematol. 2015; 2 (3): e91–100. Available from: https://doi.org/10.1016/S2352-3026(15)00028-9.
3. Melkova KN. Allogeneic Bone Marrow Transplantation. Klinicheskaya onkogematologiya. 2012; 5 (1): 1–12. Russian.
4. Alyanskiy AL, Makarenko OA, Ivanova NE, Golovacheva AA, Kuzmich EV, Kucher MA, et al. Development of donor bone marrow registry in Russian Federation: experience of Raisa Gorbacheva Memorial Research Institute of Children Oncology, Hematology and Transplantation. Russian Journal of Pediatric Hematology and Oncology. 2016; 3 (2): 68–74. Available from: https://doi.org/10.17650/2311-1267-2016-3-2-68-74. Russian.
5. Gaponova TV. Strategiya formirovaniya registra donorov kostnogo mozga s ispol'zovaniem infrastruktury sluzhby krovi (dissertaciya). 2022. Russian.
6. Akcionernoe obshestvo "Vserossijskij centr izutchenia obshestvennogo mneniya" (VCIOM). Available from: https://wciom.ru/analytical-reviews/analiticheskii-obzor/donorstvo-kostnogo-mozga-neznanie-rozhdaet-stereotipy. Russian.
7. Federalnaja gosudarstvennaja informacionnaia sistema "Ediniy portal gosudarstvennih i municipalnih uslug (funkciy)". Available from: https://www.gosuslugi.ru/help/faq/bone_marrow_registry/102326. Russian.

Литература

1. Афанасьев Б. В., Зубаровская Л. С., Моисеев И. С. Аллогенная трансплантация гемопоэтических стволовых клеток у детей: настоящее, проблемы, перспективы. Российский журнал детской гематологии и онкологии (РЖДГиО). 2015; 2 (2): 28–42. Доступно по ссылке: https://doi.org/10.17650/2311-1267-2015-2-2-28-42.
2. Gratwohl A, Pasquini MC, Aljurf M, Atsuta Y, et al. Worldwide Network for Blood and Marrow Transplantation (WBMT). One million haemopoietic stem-cell transplants: a retrospective observational study. Lancet Haematol. 2015; 2 (3): e91–100. Available from: https://doi.org/10.1016/S2352-3026(15)00028-9.
3. Мелкова К. Н. Аллогенная трансплантация костного мозга. Клиническая онкогематология. 2012; 5 (1): 1–12.
4. Alyanskiy AL, Makarenko OA, Ivanova NE, Golovacheva AA, Kuzmich EV, Kucher MA, et al. Development of donor bone marrow registry in Russian Federation: experience of Raisa Gorbacheva Memorial Research Institute of Children Oncology, Hematology and Transplantation. Russian Journal of Pediatric Hematology and Oncology. 2016; 3 (2): 68–74. Available from: https://doi.org/10.17650/2311-1267-2016-3-2-68-74. Russian.
5. Гапонова Т. В. Стратегия формирования регистра доноров костного мозга с использованием инфраструктуры службы крови (диссертация). 2022.
6. Акционерное общество «Всероссийский центр изучения общественного мнения» (ВЦИОМ). Доступно по ссылке: https://wciom.ru/analytical-reviews/analiticheskii-obzor/donorstvo-kostnogo-mozga-neznanie-rozhdaet-stereotipy.
7. Федеральная государственная информационная система «Единый портал государственных и муниципальных услуг (функций)». Доступно по ссылке: https://www.gosuslugi.ru/help/faq/bone_marrow_registry/102326.

INTRANASAL LIPOPOLYSACCHARIDE ADMINISTRATION TO SPRAGUE-DAWLEY RATS AS A BIOMODEL OF ACUTE RESPIRATORY DISTRESS SYNDROME

Kiseleva VV[1]✉, Vishnyakova PA[2], Kosyreva AM[3], Kananykhina EYu[3], Emelianov II[1], Elchaninov AV[3], Fatkhudinov TH[3]

[1] Patrice Lumumba Peoples' Friendship University of Russia, Moscow, Russia
[2] Kulakov National Medical Research Center for Obstetrics, Gynecology and Perinatology, Moscow, Russia
[3] Petrovsky National Research Centre of Surgery, Moscow, Russia

High fatality rate and the lack of pathophysiological therapy are typical for acute respiratory distress syndrome (ARDS). Intratracheal lipopolysaccharide (LPS) administration is used to model ARDS in animals. The method has the limitation of requiring the use of equipment to perform intubation and control the animal's state. The study aimed to assess the possibility of using intranasal LPS administration instead of intratracheal and determine the LPS optimal dose. A total of 150 mL of the *E. coli* O111:B4 LPS (7.5 mg/kg or 15 mg/kg) or 0.9% NaCl was administered to 21 Sprague-Dawley rats. After 48 h blood was collected from the tail vein to determine the white blood cell count and TNFa concentration. The lungs were retrieved to assess dry weight (wet/dry ratio) and to determine the expression of the genes encoding pro- and anti-inflammatory cytokines using real-time PCR. The relative counts of CD68-, CD86-, and MHC II-positive cells in the lung tissue were also evaluated using flow cytometry. The w/d ratio was higher when the dose of 15 mg/kg of body weight was used (p = 0.0228, ordinary one-way Anova). Blood lymphocyte counts were decreased (p = 0.0019, ordinary one-way Anova), and neutrophil counts were increased (p = 0.0021, ordinary one-way Anova) upon administration of both doses. The counts of CD86- (p = 0.0014, ordinary one-way Anova) and MHC II-positive cells (p = 0.0050, ordinary one-way Anova) increased after LPS administration. The *IL10* gene expression was significantly increased upon administration of the dose of 15 mg/kg (p = 0.0024, ordinary one-way Anova), while the *IL4* expression (p = 0.0194, ordinary one-way Anova) was decreased upon administration of the dose of 7.5 mg/kg. Thus, intranasal LPS administration can be used to model ARDS in the Sprague-Dawley rats. Administration of the high dose leads to the rapid development of inflammation in the lung.

Keywords: lipopolysaccharide, LPS, Sprague-Dawley rats, cytokine, animal model, ARDS, expression level

Funding: the study was supported by the Russian Science Foundation (grant No. 24-25-00203).

Acknowledgements: the authors would like to thank D.A. Areshidze, C. Sci. Biol., Head of the Cellular Pathology Laboratory of the Avtsyn Institute of Human Morphology for performing the complete blood count test in animals.

Author contribution: Kiseleva VV — experimental design and procedure, analysis of the results, manuscript writing; Vishnyakova PA — advice on the experimental procedure, material resources, editing; Kosyreva AM — advice on the experimental procedure, editing; Kananykhina EYu, Emelianov II — animal handling; Elchaninov AV — advice on the experimental procedure, material resources, editing; Fatkhudinov TH — material resources for the study.

Compliance with ethical standards: the study was approved by the Ethics Committee of the Avtsyn Institute of Human Morphology (protocol No. 21 dated 29 March 2019). Animals were handled in accordance to the ARRIVE guidelines and the Directive EC 2010/63/EU on the protection of animals used for scientific purposes.

✉ **Correspondence should be addressed:** Victoria V. Kiseleva
Oparina, 4, Moscow, 117997, Russia; victoria.kurnosova.1991@gmail.com

Received: 21.04.2025 **Accepted:** 06.05.2025 **Published online:** 20.05.2025

DOI: 10.24075/brsmu.2025.027

ИНТРАНАЗАЛЬНОЕ ВВЕДЕНИЕ ЛИПОПОЛИСАХАРИДА КРЫСАМ SPRAGUE-DAWLEY КАК БИОМОДЕЛЬ ОСТРОГО РЕСПИРАТОРНОГО ДИСТРЕСС-СИНДРОМА

В. В. Киселева[1]✉, П. А. Вишнякова[2], А. М. Косырева[3], Е. Ю. Кананыхина[3], И. И. Емельянов[1], А. В. Ельчанинов[3], Т. Х. Фатхудинов[3]

[1] Российский университет дружбы народов имени Патриса Лумумбы, Москва, Россия
[2] Национальный медицинский исследовательский центр акушерства, гинекологии и перинатологии имени В. И. Кулакова, Москва, Россия
[3] Российский научный центр хирургии имени Б. В. Петровского, Москва, Россия

Для острого респираторного дистресс-синдрома (ОРДС) характерны высокая частота летальных исходов и отсутствие патофизиологической терапии. Для воспроизведения у животных ОРДС используют интратрахеальное введение липополисахарида (ЛПС). Ограничением метода является необходимость использования оборудования для выполнения интубации и контроля за состоянием животного. Целью исследования было оценить возможность использования интраназального введения ЛПС вместо интратрахеального и определить его оптимальную дозу. ЛПС *E. coli* O111:B4 7,5 мг/кг или 15 мг/кг или NaCl 0,9% в объеме 150 мкл вводили 21 крысе Sprague-Dawley. Через 48 ч кровь из хвостовой вены отбирали для определения лейкоцитарной формулы и концентрации TNFa. Легкие извлекали для оценки сухого остатка (Wet/dry ratio), определения уровней экспрессии генов про- и противовоспалительных цитокинов методом ПЦР-РВ, определения относительного количества CD68, CD86 и MHC II положительных клеток в ткани легкого методом проточной цитометрии. W/d ratio было выше при дозе 15 мг/кг массы тела (p = 0,0228, Ordinary one-way Anova). В крови содержание лимфоцитов было снижено (p = 0,0019, Ordinary one-way Anova), а нейтрофилов повышено (p = 0,0021, Ordinary one-way Anova) при обеих дозах введения. Количество CD86 (p = 0,0014, Ordinary one-way Anova) и MHC II положительных клеток (p = 0,0050, Ordinary one — way Anova) повышалось после введения ЛПС. Уровень экспрессии гена IL10 был значимо повышен при дозе 15 мг/кг (p = 0,0024, Ordinary one-way Anova), а IL4 (p = 0,0194, Ordinary one-way Anova) снижен при дозе 7,5 мг/кг. Таким образом, интраназальное введение ЛПС может быть использовано для воспроизведения ОРДС у крыс Sprague-Dawley. Высокая доза введения приводит к быстрому развитию воспалительных процессов в легких.

Ключевые слова: липополисахарид, ЛПС, крысы Sprague-Dawley, цитокин, модель на животных, ОРДС, уровень экспрессии

Финансирование: работа поддержана Российским научным фондом (номер гранта 24-25-00203).

Благодарности: авторы благодарят руководителя лаборатории патологии клетки НИИ морфологии человека имени А. П. Авцына к. б. н. Д. А. Арешидзе за измерение показателей общей формулы крови животных.

Вклад авторов: В. В. Киселева — дизайн и проведение эксперимента, анализ полученных результатов, написание статьи; П. А. Вишнякова — консультирование по вопросам проведения эксперимента, материальная база, редактирование; А. М. Косырева — консультирование по вопросам проведения эксперимента, редактирование; Е. Ю. Кананыхина, И. И. Емельянов — работа с животными; А. В. Ельчанинов — консультирование по вопросам проведения эксперимента, материальная база, редактирование; Т. Х. Фатхудинов — материальная база исследования.

Соблюдение этических стандартов: исследование одобрено этическим комитетом НИИ морфологии человека имени А. П. Авцына (протокол № 21 от 29 марта 2019 г.). Все манипуляции с животными проводили в соответствии с рекомендациями ARRIVE и Директивой ЕС 2010/63/EU о защите животных, используемых в научных целях.

✉ **Для корреспонденции:** Виктория Викторовна Киселева
ул. Опарина, д. 4, г. Москва, 117997, Россия; victoria.kurnosova.1991@gmail.com

Статья получена: 21.04.2025 **Статья принята к печати:** 06.05.2025 **Опубликована онлайн:** 20.05.2025

DOI: 10.24075/vrgmu.2025.027

Acute lung injury and acute respiratory distress syndrome (ARDS), representing its most severe form, are complex, multifactorial disorders. Today, there is no pathophysiological therapy for ARDS, and treatment remains exclusively symptomatic, which makes studies of this disorder relevant [1]. The use of animal models is essential for both assessment of pathophysiological processes associated with the disease development and estimation of potential drug efficacy.

The effectiveness of human ARDS reproduction in an animal model is assessed based on the presence of major morphological alterations that are typical for the disorder: presence of intra-alveolar edema; elevated neutrophil counts in the interalveolar septa; hyaline membrane formation leading to the interalveolar septa thickening; formation of microthrombi [2]. The extent of these alterations is usually assessed within 24 h; longer times after the LPS administration remain understudied.

Various animal species, from rodents to anthropoid apes, are used to model ARDS [3]. ARDS is most often simulated in mice and rats due to maximum affordability and ease of handling. Several approaches to ARDS modeling are distinguished: direct and indirect lung injury (intranasal/intratracheal or intravenous administration of the bacterial wall lipopolysaccharide (LPS) of Gram-negative bacteria), as well as combined models.

LPS consists of three parts determining its immunogenicity. The A lipid “anchors” the LPS molecule in the cell wall of Gram-negative bacteria and binds the O-chain on the bacterial surface via the core polysaccharide. The O-chain is unique for each bacterium; it provides the basis for serotyping historically used for identification of Gram-negative bacteria. It is believed that bacteria that form smooth colonies have a less pyrogenic O-chain consisting of the repeating disaccharides, and LPS from the bacterium having no O-chain is the most immunogenic.

The benefit of using LPS to model ARDS is represented by its relative affordability and the possibility of standardizing the experiments. However, it is worth remembering that LPS formulations often contain contaminants, such as bacterial lipoproteins, which can affect the LPS biological effects.

After entering the body LPS is recognized by the Toll-like receptor 4 (TLR4) on the surface of monocytes, macrophages, and dendritic cells. The lipopolysaccharide-binding protein (LBP) and CD14, playing the role of co-receptors in this interaction, contribute to activation of the MyD88 and TRIF-dependent signaling pathways [4]. These cascade reactions lead to activation of the transcription factors NF-κB/MAPK (mitogen-activated protein kinases) and IRF3, respectively. As a result, production of pro-inflammatory cytokines TNFα, IL6, IL1β and type I interferons is stimulated, which mediates the development of inflammation [4].

ARDS modeling involving the use of intratracheal LPS administration is currently used more often than intranasal administration, which results from the more targeted effect on the lower respiratory tract. However, such an approach requires the use of specific equipment for LPS delivery in the lower respiratory tract through the nose or through drug administration via the tracheal incision, which increases the animal's recovery time and bears the risk of the surgical wound infection. This may increase both the research time frame and the financial resources required to implement the research. Furthermore, there are data suggesting comparable effects of both administration methods. Comparison of intranasal and intratracheal administration of the O55:B5 Escherichia coli LPS was performed in 12 female C57Bl/6 J mice by the researchers from Canada guided by Fatemeh Khadangi. One LPS dose and withdrawal of animals from the experiment after 24 h were used. The authors showed that the administration route did not affect the inflammation severity; however, lower variability of the studied parameters (cell counts and total protein levels in bronchoalveolar lavage, dry lung weight, inflammation severity based on the lung histological slides, and mechanical ventilation indicators) within the group when using intranasal administration [5].

Other authors have shown that intratracheal administration of the *E. coli* O111:B4 LPS results in bronchopneumonia, increased counts of bone marrow-derived macrophages and macrophages with inflammatory phenotype in bronchoalveolar lavage. The development of local inflammation in the lung was reflected in high expression of pro-inflammatory cytokines and low expression of anti-inflammatory cytokines. High serum C-reactive protein levels were reported at the systemic level [6].

The study aimed to assess the possibility of using intranasal LPS administration to Sprague-Dawley (SD) rats for ARDS simulation and compare alterations in the rat lung after a single administration of LPS in a dose of 7.5 mg/kg or 15 mg/kg.

METHODS

Intranasal LPS administration

Male Sprague-Dawley rats weighting 250–280 g were obtained from the Stolbovaya breeding nursery (Moscow Region, Russia). The animals were kept with natural light, at a temperature of 20–22 °C and relative air humidity of 60–70%. The animals had ad libitum access to the drinking water and pelleted feed (Laboratorsnab LLC, Russia).

The study involved 21 animals. A total of 150 µL of the *E. coli* O111:B4 LPS (Sigma, USA), 7.5 mg/kg or 15 mg/kg, was administered intranasally to experimental animals under heavy injection anesthesia (Zoletil, Virbac, France). The control rats were administered 150 µL of saline (NaCl 0.9%).

Lungs of 10 rats were retrieved 48 h after administration of the 0.9% NaCl (three animals), LPS in a dose of 7.5 mg/kg of body weight (four animals), and LPS in a dose of 15 mg/kg of body weight (three animals) to determine dry weight.

In nine rats (the same groups, three animals per group), the right lung was retrieved 48 h after administration of LPS or 0.9% NaCl. A small part of those was placed in the RNA fixative (Evrogen, Russia) for further RNA extraction, performing RT and PCR aimed at estimating the local inflammation severity. The remaining lung was homogenized, fixed and stained in order to determine the CD68, CD86, and MHC II macrophage markers by flow cytometry. A total of 2–3 mL of blood was collected from the tail vein of the same animals for serum extraction and enzyme-linked immunoassay aimed at assessing the TNFa concentration (Cloude-Clone, #SEA133Ra) and complete blood counts.

Finally, lungs of another three intact animals were used to determine macrophage markers by flow cytometry.

Wet/dry ratio estimation

To assess the edema severity, lungs of 10 animals were retrieved and weighted 48 h after administration of LPS or saline. Re-weighting was performed after 7 days of drying lungs at a temperature of 60 °C. The wet/dry ratio was calculated by dividing the lung weight 48 hours after LPS injection by the weight after drying [8].

RNA extraction, reverse transcription, and PCR

Total RNA was extracted from the samples of the right lung placed in the IntactRNA (Evrogen, Russia) using the Magzol

reagent (Magen, China) in accordance with the manufacturer's instructions in order to determine the expression of the genes encoding pro- (TNFα, IL18, IL13, IL1β) and anti-inflammatory (IL10, IL4) cytokines, genes of the enzymes involved in arginine metabolism (NOS2 and Arg1), and the gene of the NF-kb transcription factor. The first cDNA chain for determination of gene expression was obtained from 1 μg of total RNA using the MMLV RT kit (Evrogen, Russia) in accordance with the manufacturer's instructions.

Real-time PCR was conducted in the volume of 25 μL containing 400 ng of the first cDNA chain using 400 nM of forward and reverse primers (sequences are provided in Table 1) and 5x qPCRmixHS SYBR (Evrogen, Russia). All the reactions were carried out in triplicate in the DTprime DT96 cycler (DNA-Technology, Russia) under the following conditions: initial denaturation — 95 °C 5 min; 40 amplification cycles including denaturation — 95 °C 15 s, annealing — 60 °C 12 s, and elongation — 72 °C 15 s.

Table 1. Key reagents and materials used in the study

Reagents, instruments, and resources	Manufacturer	Catalogue number
Chemical substances, peptides, and recombinant proteins		
E.coli O111:B4 LPS	Sigma-Aldrich, USA	#LPS25
Key commercially available kits		
IntactRNA	Evrogen, Russia	#BC031
ELISA Kit for Tumor Necrosis Factor Alpha (TNFa)	Cloude-Clone, China	#SEA133Ra
MMLV RT kit	Evrogen, Russia	# SK021
Magzol	Magen, China	#R480101
5x qPCRmixHS SYBR	Evrogen, Russia	#PK147L
Instruments		
DTprime DT96	DNA-Technology, Russia	NA
Multiskan FC Microplate Photometer	Thermo Scientific	NA
BD FASC Calibur flow cytometer	Becton, Dickinson and Company, USA	
Animals		
Male Sprague-Dawley rats	Stolbovaya breeding nursery, Russia	NA
Primers 3'-5'		
IL4 For - ATGTAACGACAGCCCTCTGA Rev - AGCACGGAGGTACATCACG	Evrogen, Russia	NA
TNFα For - CCACCACGCTCTTCTGTCTA Rev - GCTACGGGCTTGTCACTCG	Evrogen, Russia	NA
IL1β For - CTGTCTGACCCATGTGAGCT Rev - ACTCCACTTTGGTCTTGACTT	Evrogen, Russia	NA
IL10 For - GCCCAGAAATCAAGGAGCAT Rev - TGAGTGTCACGTAGGCTTCTA	Evrogen, Russia	NA
Arg-1 For - GGATGAGCATGAGCTCCAAG Rev - GCCAGCTGTTCATTGGCTT	Evrogen, Russia	NA
IL18 For - GACAAAAGAAACCCGCCTG Rev - ACATCCTTCCATCCTTCACAG	Evrogen, Russia	NA
IL13 For - CCAGAAGACTTCCCTGTGCA Rev - CCCTCAGTGGCCATAGCG	Evrogen, Russia	NA
NOS2 For - CGCTGGTTTGAAACTTCTCAG Rev - GGCAAGCCATGTCTGTGAC	Evrogen, Russia	NA
NF-kb For - AGAGCAACCGAAACAGAGAGG Rev - TTTGCAGGCCCCACATAGTT	Evrogen, Russia	NA
b2m For - CTCGCTCGGTGACCGTGAT Rev - GGACAGATCTGACATCTCGA	Evrogen, Russia	NA
Other		
Zoletil	VIRBAC, France	NA
Pelleted feed	Laboratorsnab LLC, conformity certificate No. ROSSRU.nO81. B00113, GOST P50258-92, Russia	#ПК-120-1
Floriadae [https://floreada.io/]	Online tool for cytometry data calculation [7]	NA

Specificity of the product yielded was tested by the PCR product melting curve analysis using the Real Time PCR software tool (DNA-Technology, Russia). Threshold cycles (Ct) for all the studied genes were determined based on the fluorescent signal accumulation curve. Relative gene expression was calculated by the 2^(-ΔΔCt) method. The housekeeping beta-2 microglobulin gene was used to normalize the expression of each gene.

Flow cytometry

Levels of the pan-macrophagal marker CD68, CD86 typical for pro-inflammatory macrophages, and MHC II typical for anti-inflammatory macrophages were assessed by flow cytometry. For that lungs of 12 animals (intact animals, animals post administration of the 0.9% NaCl and LPS in a dose of 7.5 mg/kg or 15 mg/kg; three animals per group) were mechanically homogenized, then passed through a cell strainer with the pore diameter of 100 μm to eliminate the remaining large fragments and fixed with the 2% paraformaldehyde. A total of 106 cells were used for permeabilization with the Inside Perm reagent (#130-090-477, Miltenyi, Germany). CD68 was stained with FITC (#130-133-301, Miltenyi, Germany) or CD68 PE-Vio 770 (#130-134-152 Miltenyi, Germany), CD86 with Vio Bright FITC (#130-109-180 Miltenyi, Germany), and MHC II with PE (#205308, Biolegent). At least 50,000 events were acquired using a BD FACS Calibur flow cytometer (USA). The relative number of CD68, CD86 *и* MHC II-positive cells was assessed using the Floriadae online tool [7].

Enzyme-linked immunoasay

To determine serum TNFα concentration, 2 mL of blood were collected from the tail vein of the SD rat under heavy anesthesia into test tubes with clotting activator. Centrifugation was performed at 3200 rpm for 20 min. Then serum was collected in the new tubes and stored at –20 °C. Assay was performed using the ELISA Kit for Tumor Necrosis Factor Alpha (TNFa) (Cloude-Clone, China, #SEA133Ra) in accordance with the manufacturer's instructions. Optical density was determined at the wavelength of 450 nm using the Multiskan FC Microplate Photometer (Thermo Scientific, USA).

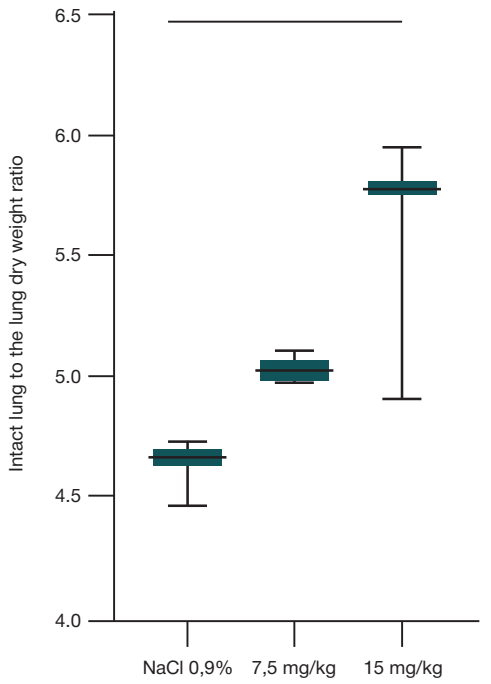

Fig. 1. Results of the lung dry weight determination performed 48 h after the intranasal *E. coli* O111:B4 LPS administration. Significantly high W/D relative to the control group was determined upon administration of the dose of 15 mg/kg of body weight ($p = 0.0228$, ordinary one-way Anova)

Statistical analysis

Statistical analysis was performed using the Prism 8.0 software. The Mann–Whitney U test was used when comparing two groups; ordinary one-way ANOVA was used when comparing a larger number of groups. The differences were considered significant at $p < 0.05$. Box plots including the median and the upper/lower extremes were used for graphic representation of the data.

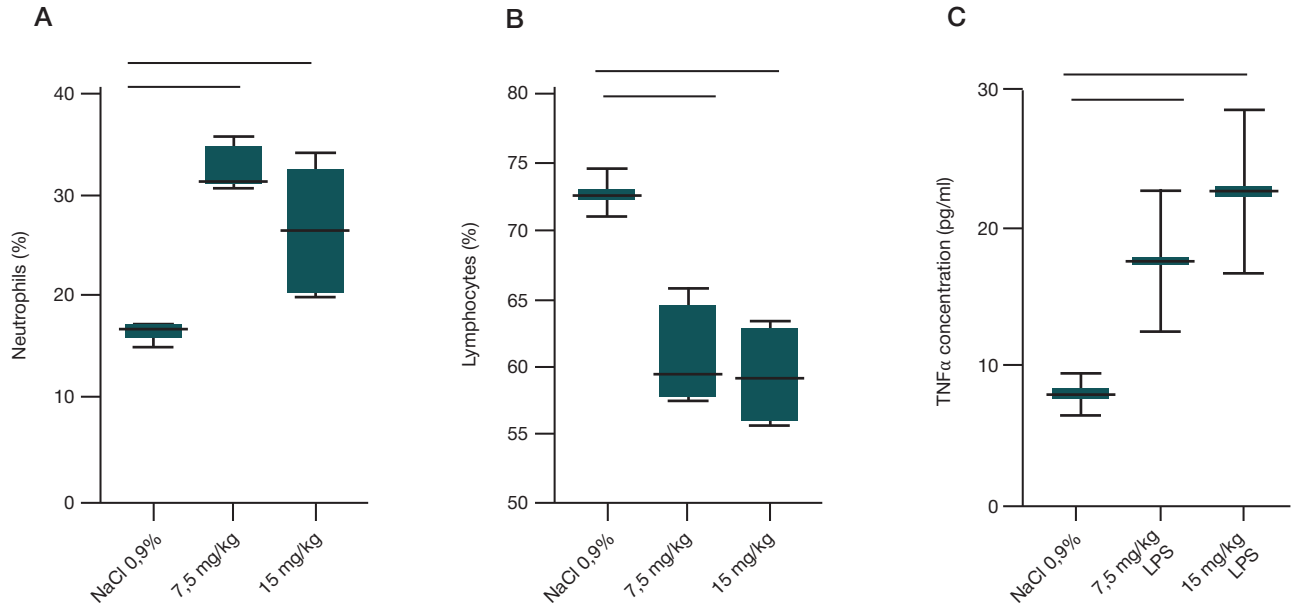

Fig. 2. Complete blood count alterations 48 h after the intranasal LPS administration (A) and serum TNFα concentrations (B). **A**. Relative lymphocyte counts are decreased compared to the control group ($p = 0.0019$, ordinary one-way Anova), while neutropil counts are elevated upon administration of both doses ($p = 0.0021$, ordinary one-way Anova). **B**. A more than 4-fold increase in serum concentration of the TNFα pro-inflammatory cytokine relative to the control group was observed after the LPS administration, but the differences were non-significant

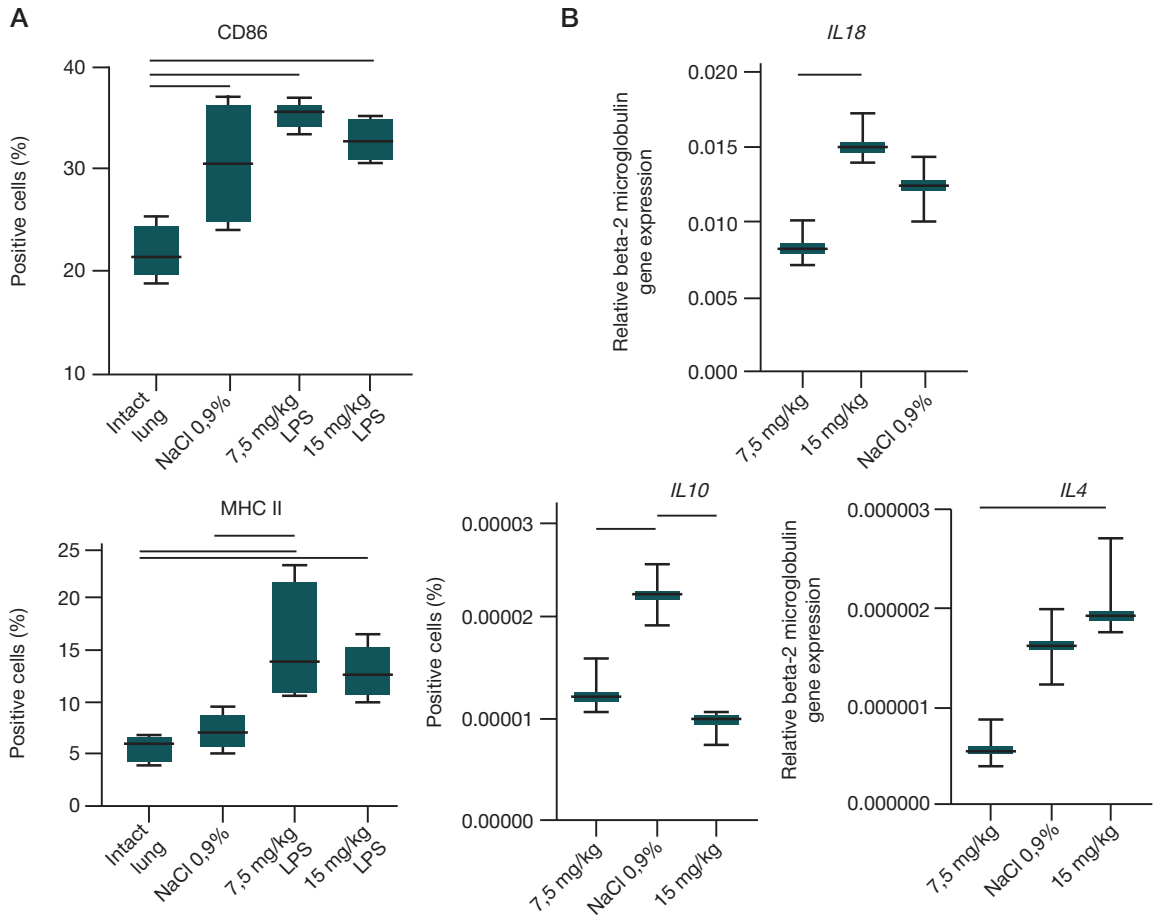

Fig. 3. Lung tissue alterations 48 h after the intranasal LPS administration. **A**. The counts of cells carrying the marker that is typical for CD86 pro-inflammatory macrophages are elevated relative to the intact lung in all groups (p = 0.0014, ordinary one-way Anova). The counts of cells carrying the marker that is typical for MHC II anti-inflammatory macrophages (p = 0.0050, ordinary one-way Anova) are significantly increased relative to the intact lung after intranasal administration of both LPS doses. The counts of MHC II-positive cells are elevated relative to the group administered saline after LPS administration in a dose of 7.5 mg/kg of body weight. **B**. When the LPS dose of 15 mg/kg of body weight was administered, there was a significant increase in the *IL10* gene expression (ordinary one-way Anova, p = 0.0024) relative to the group administered saline (0.9% NaCl group). *IL4* expression decreased (ordinary one-way Anova, p = 0.0194) upon administration of the dose of 7.5 mg/kg of body weight. As for genes *IL18* and *IL10*, the significantly high expression was reported after administration of the LPS dose of 15 mg/kg of body weight (ordinary one-way Anova, p (IL18) = 0.009, p (IL10) = 0.0024)

RESULTS

The development of acute lung injury was assessed primarily based on the wet-to-dry ratio (W/D), which is an objective indicator of lung tissue water content and reflects the development of the exudative phase of acute respiratory distress syndrome (ARDS). The entire lung was used to determine the W/D ratio. A significantly high W/D relative to the control group was determined after administration of the dose of 15 mg/kg of body weight (p = 0.0228, ordinary one-way Anova) (Fig. 1).

At the systemic level intranasal administration of both LPS doses resulted in the significantly low relative lymphocyte counts (p = 0.0019, ordinary one-way Anova) and significantly high neutrophil counts (p = 0.0021, ordinary one-way Anova).

After LPS administration the experimental rats showed a more than 4-fold increase in serum concentrations of the TNFα pro-inflammatory cytokine compared to the control group, however, the differences were non-significant (Fig. 2).

It is well known that macrophages determine the ARDS outcome. That is why the relative counts of cells carrying the CD68 pan-macrophagal marker and the markers reported for both pro-inflammatory and anti-inflammatory macrophages (CD86 and MHC II, respectively) were assessed in the rat lung homogenates during the next stage [9–11]. Experimental animals showed significantly high levels of CD86-positive cells in the lung relative to intact animals after administration of both LPS doses (p = 0.0014, ordinary one-way Anova); when the LPS dose of 7.5 mg/kg of body weight was used, the significantly high levels of MHC II-positive cells were also observed (p = 0.0050, ordinary one-way Anova) (Fig. 3).

The development of local inflammation was assessed through determining the expression of genes of the TNFα, IL1β, IL13, and IL18 pro-inflammatory cytokines, gene of the NF-kb transcription factor, genes of IL10 and IL4 anti-inflammatory cytokines, as well as genes of the enzymes involved in arginine metabolism, NOS2 and Arg1 (Fig. 3).

Expression of the IL10 gene was significantly increased in the experimental animals administered LPS in a dose of 15 mg/kg of body weight (ordinary one-way Anova, p = 0.0024), while the IL4 expression was decreased in those administered the dose of 7.5 mg/kg of body weight (ordinary one-way Anova, p = 0.0194) compared to the animals administered saline. As for genes IL18 and IL10, there were significant differences between the animals administered different LPS doses (ordinary one-way Anova, p = 0.009 and 0.0024, respectively).

Comparison of the extent of the expression change (2^(-ΔΔCt)) after administration of two LPS doses relative to the group administered saline using the Mann–Whitney U test showed a significant increase in expression of the IL18 pro-inflammatory cytokine and IL10 anti-inflammatory cytokine genes after administration of the dose of 15 mg/kg of body weight (Table 2).

Table 2. Changes in expression of the studied genes in the rat lung after administration of two LPS doses relative to the control group

2^(-ΔΔCt) relative to the 0.9% NaCl group, administration of the dose of 7.5 mg/kg	2^(-ΔΔCt) relative to the 0.9% NaCl group, administration of the dose of 15 mg/kg	*P* value, Mann–Whitney U test (comparison of two doses)
Genes of pro-inflammatory cytokines and transcription factor		
TNFα		
0.58 (± 0.66)	0.77 (± 0.14)	0.7
IL18		
0.69 (± 0.12)	1.25 (± 0.13)	0.05
IL13		
1.11 (± 0.1)	1.09 (± 0.62)	0.35
IL1β		
0.34 (± 0.32)	0.79 (± 0.21)	0.1
NF-kb		
0.73 (± 0.14)	1.11 (± 0.26)	0.1
Genes of anti-inflammatory cytokines		
IL10		
1.41 (± 0.31)	2.44 (± 0.34)	0.05
IL4		
0.9 (± 0.11)	0.51 (± 0.47)	0.35
Genes of the enzymes involved in arginine metabolism		
NOS2		
2.19 (± 1.00)	1.19 (± 0.26)	0.1
Arg1		
0.64 (± 0.44)	1.05 (± 0.3)	0.2

DISCUSSION

Modeling ARDS to study its pathogenesis and search for potential therapy is a non-trivial task, which is largely due to the pathogenetic features' complex nature.

It is common to distinguish three disease phases, regardless of the cause: exudative, proliferative, and fibrotic. The ARDS exudative phase lasts 1–7 days. During this period the damaging factors lead to disruption of the blood-air barrier and the development of intra-alveolar edema [1]. In the majority of papers, neutrophil infiltration of the inter-alveolar septa and the development of intra-alveolar edema are assessed in the lung within 24 h. ARDS model validation within 48 h is a feature of this study. The significantly high ratio of the lung weight after retrieval of the lung from the animal's body to its dry weight, when administered the *E. coli* O111:B4 LPS dose of 15 mg/kg of body weight, suggests high liquid content in the lung tissue, which indicates the exudative phase of the disease.

At the systemic level the signs of inflammatory response development were reported, which was indicated by the significantly low relative lymphocyte counts and significantly high neutrophil counts. Lymphocytes are cells of the adaptive immune system that help the body to withstand invasion of pathogenic microorganisms, including via attraction of neutrophils to the foci of infection during acute inflammation. The cascade of reactions resulting in bone marrow stimulation and the release of a large number of neutrophils into the circulatory system is triggered under the LPS exposure [12]. Low lymphocyte counts can result from redistribution of cells to the inflammatory focus [13]. Similar alterations were revealed when sequencing mononuclear blood cells in individuals suffering from ARDS relative to healthy donors. Low counts of the major lymphocyte representatives, B cells and CD4 T cells, were reported [14].

The phenomenon referred to as "cytokine storm" that is characterized by high blood levels of pro-inflammatory cytokines (TNFα, IFNγ, IL6, IL1β) is a typical feature of ARDS. It has been shown that TNFα is involved in the development of fever, systemic inflammation enhancement, antimicrobial response activation, and increase in secretion of other pro-inflammatory cytokines (such as IL6). TNFα activates the NF-kB transcription factor that stimulates numerous genes involved in inflammatory response [15].

The lung is a barrier organ with the enormously developed system of protection against microorganisms. Macrophages are the first cells responding to foreign invasion. Two types of macrophages are distinguished in the lung: alveolar macrophages inhabiting the alveoli and interstitial macrophages found in the interstitial space [16]. Phenotype of the first is described as pro-inflammatory with high expression of IL10 and TGFβ [17]. Interstitial macrophages currently represent an extensively studied cell population [16]. Macrophages recruited from blood monocytes have a phenotype that is close to pro-inflammatory. These express large amounts of the co-stimulatory CD86 molecules essential for adequate antigenic signal transduction in complexes with the type 1 major histocompatibility complex (MHC I) molecules [9]. The disease outcome depends on the balance between two states of alveolar macrophages. Furthermore, it has been shown that the MHC IIhi memory cell population is formed of those in case of viral disease [18, 19]. Pro-inflammatory macrophages predominate over anti-inflammatory cells in the exudative phase. Activation of the macrophage pattern recognition receptors leads to generation of the inflammasome, in which caspase-1 contributes to the IL1 and IL18 maturation. The disease progression can be severe, if the inflammasome maturation process is disturbed. In the ARDS proliferative phase, pro-inflammatory macrophages are replaced by the anti-inflammatory macrophages that

remove cellular debris and release anti-inflammatory cytokines. It has been shown that abnormal efferocytosis can result in the prolonged inflammation observed in ARDS; moreover, at this stage excessive participation of anti-inflammatory macrophages in matrix reorganization processes can lead to chronic fibrosis and occlusion of blood vessels [20]. Thus, the increased counts of the CD86 and MHC II-positive cells we have revealed suggest that the lung macrophages are in the transitional state 48 h after the intranasal LPS administration: between pro-inflammatory and anti-inflammatory [18].

At the gene level it has been reported that intranasal administration of the LPS in a dose of 15 mg/kg of body weight results in alteration of expression of the genes encoding both pro- and anti-inflammatory cytokines (IL18 and IL10, respectively). Furthermore, the use of the higher dose significantly activated the anti-inflammatory immune response, which was indicated by high *IL10* gene expression [21]. IL10 plays an ambiguous role in the ADRS pathogenesis: it can both contribute to the disease resolution through inhibition of pro-inflammatory cytokine (such as TNFα, IL1β, IL6, and IFNγ) secretion and complicate the disease due to the decreased stem cell differentiation into type II pneumocytes, thereby preventing lung recovery [22]. High *IL10* expression can potentially be an indicator of macrophage polarization into the anti-inflammatory phenotype, which is consistent with high levels of MHC II-positive cells based on the flow cytometry results [17].

The IL18 pro-inflammatory cytokine that was first described as a factor inducing interferon IFNγ through effects of both innate and adaptive immune response is involved in protection against infectious agents and anti-tumor immunity. Activation of the innate immunity pattern recognition receptors (PRR) in the lung leads to activation of the NF-kb transcription factor in the epithelial and endothelial cells, as well as in the resident immune cells. NF-kb, in turn, contributes to the increase of pro-IL1β, pro-IL18, and pro-caspase-1, the mature forms of which that trigger the vicious circle of inflammation are formed in inflammasomes. IL18 is a potent chemoattractant for neutrophils, the increased counts of which in the lung represent the most important sign of the ARDS acute phase; this is consistent with our data on high IL18 gene expression after administration of the LPS dose of 15 mg/kg of body weight, as well as on high neutrophil counts in blood.

CONCLUSIONS

Intranasal administration of the LPS of the external wall of Gram-negative bacteria to Sprague-Dawley rats within 48 h leads to the development of processes typical for the ARDS exudative and proliferative phases: pulmonary edema, decreased lymphocyte counts and increased neutrophil counts in blood, increased serum levels of TNFα. LPS administration in a dose of 15 mg/kg leads to the rapid development of inflammation in the lung, and after 48 h, a significant activation of anti-inflammatory responses can be observed. Thus, the use of the O111:B4 LPS intranasal administration in a dose of 15 mg/kg of body weight to Sprague-Dawley rats can be used to model ARDS in order to assess the efficacy of drug therapy, including cell-based therapy, based on such indicators, as dry weight of the lung, counts of the CD86 and MHC II-positive cells in the lung homogenates, and *IL10* and *IL18* gene expression.

References

1. Bos LDJ, Ware LB. Acute respiratory distress syndrome: causes, pathophysiology, and phenotypes. The Lancet. 2022; 400: 1145–56.
2. Aeffner F, Bolon B, Davis IC. Mouse Models of Acute Respiratory Distress Syndrome. Toxicol Pathol. 2015; 43: 1074–92.
3. Matute-Bello G, Frevert CW, Martin TR. Animal models of acute lung injury. American Journal of Physiology-Lung Cellular and Molecular Physiology. 2008; 295: L379–99.
4. Soloveva T, Davydova V, Krasikova I, Yermak I. Marine Compounds with Therapeutic Potential in Gram-Negative Sepsis. Mar Drugs. 2013; 11: 2216–29.
5. Khadangi F, Forgues A-S, Tremblay-Pitre S, Dufour-Mailhot A, Henry C, Boucher M, et al. Intranasal versus intratracheal exposure to lipopolysaccharides in a murine model of acute respiratory distress syndrome. Sci Rep. 2021; 11: 7777.
6. Kosyreva AM, Miroshnichenko EA, Tsvetkov IS, Lokhonina AV, Sentyabreva AV, Dzhalilova DSh, et al. Morphofunctional Characteristics of Lung Macrophages in Rats with Acute Respiratory Distress Syndrome. Bull Exp Biol Med. 2023; 175: 822–7.
7. Available from: https://floreada.io/.
8. Parker JC, Townsley MI. Evaluation of lung injury in rats and mice. American Journal of Physiology-Lung Cellular and Molecular Physiology. 2004; 286: L231–46.
9. Vishnyakova P, Poltavets A, Karpulevich E, Maznina A, Vtorushina V, Mikhaleva L, et al. The response of two polar monocyte subsets to inflammation. Biomedicine & Pharmacotherapy. 2021; 139: 111614.
10. Chistiakov DA, Killingsworth MC, Myasoedova VA, Orekhov AN, Bobryshev YV. CD68/macrosialin: not just a histochemical marker. Laboratory Investigation. 2017; 97: 4–13.
11. Murray PJ, Allen JE, Biswas SK, Fisher EA, Gilroy DW, Goerdt S, et al. Macrophage Activation and Polarization: Nomenclature and Experimental Guidelines. Immunity. 2014;41:14–20.
12. Qazi MR, Bogdanska J, Butenhoff JL, Nelson BD, DePierre JW, Abedi-Valugerdi M. High-dose, short-term exposure of mice to perfluorooctanesulfonate (PFOS) or perfluorooctanoate (PFOA) affects the number of circulating neutrophils differently, but enhances the inflammatory responses of macrophages to lipopolysaccharide (LPS) in a similar fashion. Toxicology. 2009; 262: 207–14.
13. Chakraborty S, Zawieja SD, Wang W, Lee Y, Wang YJ, von der Weid P-Y, et al. Lipopolysaccharide modulates neutrophil recruitment and macrophage polarization on lymphatic vessels and impairs lymphatic function in rat mesentery. American Journal of Physiology-Heart and Circulatory Physiology. 2015; 309: H2042–57.
14. Torres M, Casado G, Vigón L, Rodríguez-Mora S, Mateos E, Ramos-Martín F, et al. Changes in the immune response against SARS-CoV-2 in individuals with severe COVID-19 treated with high dose of vitamin D. Biomedicine & Pharmacotherapy. 2022; 150: 112965.
15. Riyaz Tramboo S, Elkhalifa AME, Quibtiya S, Ali SI, Nazir Shah N, Taifa S, et al. The critical impacts of cytokine storms in respiratory disorders. Heliyon. 2024; 10: e29769.
16. Hou F, Xiao K, Tang L, Xie L. Diversity of Macrophages in Lung Homeostasis and Diseases. Front Immunol. 2021; 12.
17. Fakoya AO, Naeem A, Louisdon P, Histology. Alveolar Macrophages. Available from: https://www.ncbi.nlm.nih.gov/books/NBK513313/#:~:text=Alveolar%20macrophages%20produce%20anti%2Dinflammatory,processes%20and%20promote%20tissue%20repair.
18. Morrell ED, Bhatraju PK, Mikacenic CR, Radella F, Manicone AM, Stapleton RD, et al. Alveolar Macrophage Transcriptional Programs Are Associated with Outcomes in Acute Respiratory Distress Syndrome. Am J Respir Crit Care Med. 2019; 200: 732–41.
19. Yao Y, Jeyanathan M, Haddadi S, Barra NG, Vaseghi-Shanjani M, Damjanovic D, et al. Induction of Autonomous Memory Alveolar

Macrophages Requires T Cell Help and Is Critical to Trained Immunity. Cell. 2018; 175: 1634–50.e17.
20. Mahida RY, Scott A, Parekh D, Lugg ST, Hardy RS, Lavery GG, et al. Acute respiratory distress syndrome is associated with impaired alveolar macrophage efferocytosis. European Respiratory Journal. 2021; 58: 2100829.
21. Couper KN, Blount DG, Riley EM. IL-10: The Master Regulator of Immunity to Infection. The Journal of Immunology. 2008; 180: 5771–7.
22. Sun Z, Chen A, Fang H, Sun D, Huang M, Cheng E, et al. B cell-derived IL-10 promotes the resolution of lipopolysaccharide-induced acute lung injury. Cell Death Dis. 2023; 14: 418.

Литература

1. Bos LDJ, Ware LB. Acute respiratory distress syndrome: causes, pathophysiology, and phenotypes. The Lancet. 2022; 400: 1145–56.
2. Aeffner F, Bolon B, Davis IC. Mouse Models of Acute Respiratory Distress Syndrome. Toxicol Pathol. 2015; 43: 1074–92.
3. Matute-Bello G, Frevert CW, Martin TR. Animal models of acute lung injury. American Journal of Physiology-Lung Cellular and Molecular Physiology. 2008; 295: L379–99.
4. Soloveva T, Davydova V, Krasikova I, Yermak I. Marine Compounds with Therapeutic Potential in Gram-Negative Sepsis. Mar Drugs. 2013; 11: 2216–29.
5. Khadangi F, Forgues A-S, Tremblay-Pitre S, Dufour-Mailhot A, Henry C, Boucher M, et al. Intranasal versus intratracheal exposure to lipopolysaccharides in a murine model of acute respiratory distress syndrome. Sci Rep. 2021; 11: 7777.
6. Kosyreva AM, Miroshnichenko EA, Tsvetkov IS, Lokhonina AV, Sentyabreva AV, Dzhalilova DSh, et al. Morphofunctional Characteristics of Lung Macrophages in Rats with Acute Respiratory Distress Syndrome. Bull Exp Biol Med. 2023; 175: 822–7.
7. Онлайн-программа для обсчета цитометрических данных. Доступно по ссылке: https://floreada.io/.
8. Parker JC, Townsley MI. Evaluation of lung injury in rats and mice. American Journal of Physiology-Lung Cellular and Molecular Physiology. 2004; 286: L231–46.
9. Vishnyakova P, Poltavets A, Karpulevich E, Maznina A, Vtorushina V, Mikhaleva L, et al. The response of two polar monocyte subsets to inflammation. Biomedicine & Pharmacotherapy. 2021; 139: 111614.
10. Chistiakov DA, Killingsworth MC, Myasoedova VA, Orekhov AN, Bobryshev YV. CD68/macrosialin: not just a histochemical marker. Laboratory Investigation. 2017; 97: 4–13.
11. Murray PJ, Allen JE, Biswas SK, Fisher EA, Gilroy DW, Goerdt S, et al. Macrophage Activation and Polarization: Nomenclature and Experimental Guidelines. Immunity. 2014;41:14–20.
12. Qazi MR, Bogdanska J, Butenhoff JL, Nelson BD, DePierre JW, Abedi-Valugerdi M. High-dose, short-term exposure of mice to perfluorooctanesulfonate (PFOS) or perfluorooctanoate (PFOA) affects the number of circulating neutrophils differently, but enhances the inflammatory responses of macrophages to lipopolysaccharide (LPS) in a similar fashion. Toxicology. 2009; 262: 207–14.
13. Chakraborty S, Zawieja SD, Wang W, Lee Y, Wang YJ, von der Weid P-Y, et al. Lipopolysaccharide modulates neutrophil recruitment and macrophage polarization on lymphatic vessels and impairs lymphatic function in rat mesentery. American Journal of Physiology-Heart and Circulatory Physiology. 2015; 309: H2042–57.
14. Torres M, Casado G, Vigón L, Rodríguez-Mora S, Mateos E, Ramos-Martín F, et al. Changes in the immune response against SARS-CoV-2 in individuals with severe COVID-19 treated with high dose of vitamin D. Biomedicine & Pharmacotherapy. 2022; 150: 112965.
15. Riyaz Tramboo S, Elkhalifa AME, Quibtiya S, Ali SI, Nazir Shah N, Taifa S, et al. The critical impacts of cytokine storms in respiratory disorders. Heliyon. 2024; 10: e29769.
16. Hou F, Xiao K, Tang L, Xie L. Diversity of Macrophages in Lung Homeostasis and Diseases. Front Immunol. 2021; 12.
17. Fakoya AO, Naeem A, Louisdon P. Histology. Alveolar Macrophages. Available from: https://www.ncbi.nlm.nih.gov/books/NBK513313/#:~:text=Alveolar%20macrophages%20produce%20anti%2Dinflammatory,processes%20and%20promote%20tissue%20repair.
18. Morrell ED, Bhatraju PK, Mikacenic CR, Radella F, Manicone AM, Stapleton RD, et al. Alveolar Macrophage Transcriptional Programs Are Associated with Outcomes in Acute Respiratory Distress Syndrome. Am J Respir Crit Care Med. 2019; 200: 732–41.
19. Yao Y, Jeyanathan M, Haddadi S, Barra NG, Vaseghi-Shanjani M, Damjanovic D, et al. Induction of Autonomous Memory Alveolar Macrophages Requires T Cell Help and Is Critical to Trained Immunity. Cell. 2018; 175: 1634–50.e17.
20. Mahida RY, Scott A, Parekh D, Lugg ST, Hardy RS, Lavery GG, et al. Acute respiratory distress syndrome is associated with impaired alveolar macrophage efferocytosis. European Respiratory Journal. 2021; 58: 2100829.
21. Couper KN, Blount DG, Riley EM. IL-10: The Master Regulator of Immunity to Infection. The Journal of Immunology. 2008; 180: 5771–7.
22. Sun Z, Chen A, Fang H, Sun D, Huang M, Cheng E, et al. B cell-derived IL-10 promotes the resolution of lipopolysaccharide-induced acute lung injury. Cell Death Dis. 2023; 14: 418.

NEWBORN SCREENING IN NORTH OSSETIA IN 2023–2024

Zinchenko RA[1]✉, Tebieva IS[2,3], Zakharova EYu[1], Shchagina OA[1], Lotnik EE[1], Gabisova YuV[3], Khokhova AV[2,3], Bakin NV[1], Marakhonov AV[1]

[1] Research Centre for Medical Genetics, Moscow, Russia
[2] North-Ossetian State Medical Academy, Vladikavkaz, Russia
[3] Republican Children's Clinical Hospital, Vladikavkaz, Russia

Mass screening of newborns for 36 hereditary diseases in the Russian Federation will enable the reduction of childhood disability and mortality from hereditary disorders, as well as the identification of all-Russian and regional population-genetic features of the screened disorders. The study aimed to assess the results of newborn screening (NBS), including expanded newborn screening (ENBS), in the Republic of North Ossetia-Alania obtained between January 1, 2023, and December 31, 2024, as well as to study clinical and population-genetic characteristics of the diseases screened in the region. In phase I of assessment, biochemical testing, tandem mass spectrometry, and DNA diagnostics were performed, and the TREC/KREC levels were determined in 14,994 newborns. In 355 cases (2.36%), positive values were revealed. In phase II, the necessary laboratory and subsequent confirmatory DNA diagnostics were carried out in 324 cases (91.2%): repeated analysis by MS/MS and DNA diagnostics (for hereditary metabolic diseases), immunophenotyping (for primary immunodeficiency states). During the 2-year study, a total of 37 diagnoses were established, which accounted for 0.25% of all children screened in phase I and clearly indicated the program's success and effectiveness. We managed to verify the specific spectrum of mutations characteristic of phenylketonuria (PKU) and medium-chain fatty acid acyl-CoA dehydrogenase deficiency (MCADD). The frequency of the disorder assessed within the framework of newborn screening was determined. The frequency of all PKU forms was 1 : 1153 newborns, and the frequency of MCADD was 1 : 789 newborns surveyed. All children are listed as sick in the medical genetic consultation of the Republic of North Ossetia-Alania; they receive treatment in accordance with the clinical guidelines.

Keywords: newborn screening, expanded newborn screening, hereditary pathology, phenylketonuria, medium-chain fatty acid acyl-CoA dehydrogenase deficiency

Funding: the study was funded by the federal and regional budgets in terms of implementing expanded newborn screening and supported as part of the State Assignment of the Research Centre for Medical Genetics and the Ministry of Health of the Republic of North Ossetia–Alania.

Author contribution: Tebieva IS, Gabisova YuV, Khokhova AV — data acquisition, establishing the diagnosis; Zinchenko RA, Tebieva IS — study planning, manuscript writing; Zakharova EYu, Shchagina OA, Lotnik EE, Bakin NV, Marakhonov AV — molecular genetic testing; Zinchenko RA, Tebieva IS, Zakharova EYu — manuscript editing.

Compliance with ethical standards: the study was approved by the Ethics Committee of the Research Centre for Medical Genetics (protocol No. 7 dated 20 December 2017), it was compliant with the standards of Good Clinical Practice and evidence-based medicine. All patients submitted informed consent to participate in the study.

✉ **Correspondence should be addressed:** Rena A. Zinchenko
Moskvorechie, 1, 115522, Moscow, Russia; renazinchenko@mail.ru

Received: 22.04.2025 **Accepted:** 19.05.2025 **Published online:** 30.05.2025

DOI: 10.24075/brsmu.2025.029

НЕОНАТАЛЬНЫЙ СКРИНИНГ В СЕВЕРНОЙ ОСЕТИИ ЗА 2023–2024 ГГ.

Р. А. Зинченко[1]✉, И. С. Тебиева[2,3], Е. Ю. Захарова[1], О. А. Щагина[1], Е. Е. Лотник[1], Ю. В. Габисова[3], А. В. Хохова[2,3], Н. В. Бакин[1], А. В. Марахонов[1]

[1] Медико-генетический научный центр имени Н. П. Бочкова, Москва, Россия
[2] Северо-Осетинская государственная медицинская академия Министерства здравоохранения России, Владикавказ, Россия
[3] Республиканская детская клиническая больница, Владикавказ, Россия

Массовое обследование новорожденных в Российской Федерации на 36 наследственных заболеваний позволит снизить детскую инвалидность и смертность от наследственной патологии и выявить общероссийские и региональные популяционно-генетические особенности скринируемой патологии. Целью исследования было оценить результаты неонатального скрининга (НС), включая расширенный неонатальный скрининг (РНС) в Республике Северная Осетия-Алания (РСО-Алания) в период с 01.01.2023 по 31.12.2024, и изучить клинические и популяционно-генетические особенности скринируемых заболеваний в регионе. На I этапе обследования у 14 994 новорожденных проведены биохимические исследования, тандемная масс-спектрометрия, ДНК-диагностика и определение уровня TREK/KREK. В 355 случаях (2,36%) выявлены позитивные значения. На II этапе в 324 (91,2%) случаях проведена необходимая лабораторная и последующая подтверждающая ДНК-диагностика: повторный анализ в МС/МС и ДНК-диагностика (для наследственных болезней обмена веществ), иммунофенотипирование (для первичных иммунодефицитных состояний). В ходе двухлетнего исследования поставлено 37 диагнозов, что составляет 0,25% от всех детей, охваченных скринингом на I этапе, и однозначно свидетельствует об успешности и результативности данной программы. Удалось верифицировать специфический спектр мутаций, характерных для фенилкетонурии (ФКУ) и недостаточности ацил-КоА-дегидрогеназы жирных кислот со средней длиной углеродной цепи (MCADD). Определена частота встречаемости патологии, исследуемой в рамках неонатального скрининга. Частота всех форм ФКУ составила 1 : 1153 новорожденных, а частота MCADD — 1 : 789 обследованных новорожденных. Все дети состоят на диспансерном учете в медико-генетической консультации РСО-Алания, получают лечение в соответствии с клиническими рекомендациями.

Ключевые слова: неонатальный скрининг, расширенный неонатальный скрининг, наследственная патология, фенилкетонурия, недостаточность ацил-КоА-дегидрогеназы, жирные кислоты со средней длиной углеродной цепи

Финансирование: исследование выполнено из средств федерального и регионального бюджетов в части реализации расширенного неонатального скрининга, а также при финансовой поддержке Государственного задания ФГБНУ «МГНЦ» Минобрнауки России и Минздрава РСО-Алания.

Вклад авторов: И. С. Тебиева, Ю. В. Габисова, А. В. Хохова — сбор данных, постановка диагноза; Р. А. Зинченко, И.С. Тебиева — планирование исследования, написание текста; Е. Ю. Захарова, О. А. Щагина, Е. Е. Лотник, Н. В. Бакин, А. В. Марахонов — проведение молекулярно-генетических исследований; Р. А. Зинченко, И. С. Тебиева, Е. Ю Захарова — редактирование текста.

Соблюдение этических стандартов: исследование одобрено этическим комитетом ФГБНУ Медико-генетический научный центр имени Н. П. Бочкова (протокол № 7 от 20 декабря 2017 г.), соответствует стандартам добросовестной клинической практики и доказательной медицины. Все пациенты подписали добровольное информированное согласие на участие в его проведении.

✉ **Для корреспонденции:** Рена Абульфазовна Зинченко
ул. Москворечье, д. 1, 115522, г. Москва, Россия; renazinchenko@mail.ru

Статья получена: 22.04.2025 **Статья принята к печати:** 19.05.2025 **Опубликована онлайн:** 30.05.2025

DOI: 10.24075/vrgmu.2025.029

Newborn screening has been demonstrating its effectiveness in detecting congenital and hereditary disorders (CHDs) at the early preclinical stage for decades. Mass screening of newborns was launched on January 1, 2023, in the Russian Federation (RF). Today, it is divided into newborn screening (NBS) and expanded newborn screening (ENBS). In the regions, NBS is conducted in order to detect five CHDs: phenylketonuria, congenital hypothyroidism, cystic fibrosis, galactosemia, and congenital adrenal cortex dysfunction (PKU, CH, CF, GAL, CACD, respectively). ENBS is implemented in 10 interregional 3A-level ENBS centers in order to detect 29 hereditary metabolic diseases (HMDs), spinal muscular atrophy (SMA), and severe T-cell and B-cell primary immunodeficiency (PID) [1].

The Decree of the Government of the Republic of North Ossetia–Alania (RNO-Alania) approved the regional program of NBS and ENBS implementation; regulations governing this trial were developed; officials responsible for the implementation of all screening phases were determined, and routing of patients within the framework of the existing infrastructure was arranged.

The study aimed to assess the results of NBS and ENBS in the RNO-Alania reported between January 1, 2023 and December 31, 2024, as well as to determine clinical and population genetic characteristics of the diseases screened.

METHODS

In phase I of screening, capillary blood sampling from the newborn's heel was performed on day 2 in full-term babies and on day 7 in preterm babies using two assay sheets: one with five blood spots for NBS and another with three blood spots for ENBS. The referral with supporting data is generated using the following module: Obstetrics and Neonatology Vertical Integrated Medical and Information System (VIMIS AKiNEO). The data on the children at risk are conveyed to the officials responsible for ENBS arrangement in the constituent entity within 24 hours. In the following 48 h, biomaterial re-collection from children at risk is arranged, and the biomaterial is transferred to the 3B level reference center, the Research Centre for Medical Genetics, where the exact diagnosis of CHD is established or ruled out, for confirmatory diagnostics [2].

Initial examination of the children born in the RNO-Alania being part of the NBS, is conducted at the Medical Genetic Consultation (MGC) of the Republican Children's Clinical Hospital of the RNO-Alania. The levels of biochemical markers in whole blood samples are determined by the time-resolved immunofluorescence method using the DELFIA Neonatal (Finland) and FAVR (Russia) reagents in the Victor-2 system (Wallak, Finland). The measurement results are entered into the computer program for data processing and acquisition. To establish the diagnosis, the values of biochemical markers should be as follows: phenylalanine (PA) > 2 mg% — for the diagnosis of PKU; thyroid-stimulating hormone (TSH) > 20 μIU/L — for CH, immunoreactive trypsin (IRT) > 70 ng/mL — for CF, 17-hydroxyprogesterone (17-OHP) > 30 nmol/L — for CACD in full-term babies and > 60 mmol/L — for CACD in preterm babies, galactose > 400 nmol/L (7 μmol/L) — for GAL. Initial examination being part of ENBS is conducted at the Research Institute — Regional Clinical Hospital No. 1 named after Professor S. V. Ochapovsky of the Ministry of Health of the Krasnodar Krai: testing for HMDs (including PKU) is performed by tandem mass spectrometry (MS/MS); testing for SMA and PID is accomplished via qualitative identification of the homozygous deletion of exon 7 in the SMN1 gene and quantification of the TREC, KREC DNA involving the use of the Neoscreen SMA/TREC/KREC system (DNA-Technology TS, Russia).

In phase II of the assessment, the following essential biomaterial samples must be made available for the Research Centre for Medical Genetics:

HMDs — dried blood spots on the assay sheet, liquid blood in the test tube with EDTA (non-frozen, at least 2.5 mL) and urine (at least 5 mL);

SMA — dried blood spots on the assay sheet, liquid blood in the test tube with EDTA (non-frozen, at least 2.5 mL);

PID in phase I — dried blood spots on the assay sheet, in phase II — liquid blood in the test tube with EDTA (non-frozen, two test tubes) for immunophenotyping and DNA diagnostics.

Confirmatory diagnostics is accomplished via repeated analysis of amino acids and acylcarnitines by MS/MS, determination of urinary levels of organic acids by gas chromatography–mass spectrometry (GC–MS), and DNA diagnostics. In the second phase of testing for PID, immunophenotyping (IPT) is performed at the Dmitry Rogachev National Medical Research Center of Pediatric Hematology, Oncology and Immunology of the Ministry of Health of the RF.

RESULTS

A total of 15,153 babies were born in the Republic during the studied period. A total of 15,059 (taking into account those who died before sampling) were to be assessed. Parents of 65 newborns submitted the informed refusal of screening, and blood was collected from 14,994 babies. The survey covered 99.56% of newborns.

In all 14,994 cases, tandem mass spectrometry was conducted in phase I, of those, in 355 cases (2.36%), the screening results were positive.

Since the Republic represents the region with high ethno-cultural diversity and close ties with the Caucasian and Transcaucasian territories, a large number of children are traditionally born there, who later move to other regions of the RF (Chechen Republic, Republic of Ingushetia, Stavropol Krai, etc.) and abroad (South Ossetia, Georgia, Armenia, etc.). In this regard, in 31 cases (8.8%), information about the results of assessment performed within the framework of ENBS was shared with the officials responsible for the implementation of screening in adjacent constituent entities of the RF. Considering this fact, 324 newborns out of 355 were assessed in phase II, which accounted for 91.2%.

Testing for aminoacidopathies

Given the fact that testing for PKU was performed by the biochemical method within the framework of NBS and by MS/MS within the framework of ENBS, we had an opportunity to compare the data of the testing conducted and draw a conclusion about the MS/MS higher informativity in terms of PKU detection.

Based on the DNA diagnostics data, alterations of the *PAH* gene nucleotide sequence typical for PKU in the homozygous and compound heterozygous state were found in 13 patients. The PKU frequency determined based on the tandem mass spectrometry results was 1 : 1165 newborns and 1 : 1153 surveyed newborns (95% CI: 1 : 675 – 1 : 2166). All children are on the MGC dietitian's D list. The dynamic changes in PA levels and the treatment tactics are determined in accordance with the Federal Clinical Guidelines. Only two children need foods for special medical purposes (FSMP), while in other patients, PA levels do not exceed 6 mg% (360 μM/L) [3].

Table 1. Biochemical and molecular genetic characteristics of patients with PKU

№	PA level in phase I mg%/μM/L)*	Phe/Tyr**	FSMP	Ethnicity	Allele 1 (RefSeq NM_000277.3)	Allele 2 (RefSeq NM_000277.3)
1	1.77/142	2.35	–	Ossetians	c.529G>A (p.Val177Met)	c.119C>T (p.Ser40Leu)
2	0.28/131	2.1	–	Ossetians	c.842C>T (p.Pro281Leu)	c.529G>A (p.Val177Met)
3	3.74/273	2.48	–	Ossetians	c.631C>A (p.Pro211Thr)	c.631C>A (p.Pro211Thr)
4	1.98/149	1.78	–	Ossetians	c.529G>A (p.Val177Met)	c.842C>T (p.Pro281Leu)
5	6.77/405	9.05	+	Ossetians	c.1222C>T (p.Arg408Trp)	c.1222C>T (p.Arg408Trp)
6	2.3/145	2.31	–	Ossetians	c.529G>A (p.Val177Met)	c.1222C>T (p.Arg408Trp)
7	4.79/321	3.66	–	Ossetians	c.842C>T (p.Pro281Leu)	c.722G>A (p.Arg241His)
8	2.4/140	2.2	–	Armenians	c.1208C>T (p.Ala403Val)	c.506G>A (p.Arg169His)
9	38/550	8.8	+	Ossetians	c.842C>T (p.Pro281Leu)	c.1222C>T (p.Arg408Trp)
10	1.9/143	1.98	–	Ossetians	c.533A>T (p.Glu178Gly)	c.490A>G (p.Ile164Val)
11	2.73/286	4.46	–	Female Georgian/Ossetian	c.842C>T (p.Pro281Leu)	c.631C>A (p.Pro211Thr)
12	***/240	2.9	–	Ossetians	c.898G>T (p.Ala300Ser)	c.631C>A (p.Pro211Thr)
13	***/141	2.15	–	Ossetians	c.842C>T (p.Pro281Leu)	c.529G>A (p.Val177Met)

Note: * — PA reference range — 0–2 mg% for NBS, 0–120 μM/L for ENBS; ** — Phe/Tyr ratio reference range 0.25–6.5; *** — not tested for PKU in the MDC of the Republican Children's Clinical Hospital of RNO-Alania due to the lack of reagents.

Biochemical and molecular genetic characteristics of the patients identified are provided in Table 1.

The most common was the "severe" mutation c.842C>T (p.Pro281Leu), in which the residual activity of the PAH enzyme is 2%, the number of heterozygous alleles is 6, homozygous — 0. Among the general sample, the frequency of occurrence is 23%, among representatives of the Ossetian nationality — 27%.

The second most frequent genetic variant was c.529G>A (p.Val177Met), data on PAH activity are not presented in the literature, the frequency of heterozygous carriage is 5, which amounted to 19% in the general sample and 22% among the titular nation. In third place were two variants: "severe" mutation c.1222C>T, (p.Arg408Trp) (residual PAH activity — 2%) and "mild" c.631C>A (p.Pro211Thr) (residual PAH activity — 72%): 1 homozygous case and 2 heterozygous carriers. They accounted for 15% of the total sample and 18% among Ossetians. The remaining variants are found in single heterozygous variants and demonstrate high residual activity of the PAH protein. Patients do not require diet therapy, and therefore the mutations can be classified as "mild" [4, 5]. Thus, out of 13 patients, only two (15.3%) with genotypes with two severe mutations (R408W/R408W and P281L/R408W) require diet therapy.

Impaired mitochondrial fatty acid β-oxidation

The diagnosis belonging to the group of hereditary mitochondrial fatty acid β-oxidation disorders (FAODs) was established in 19 patients based on the MS/MS data and DNA diagnostics: medium-chain fatty acid acyl-CoA dehydrogenase deficiency (MCADD).

The frequency of this disorder in the RNO-Alania was 1 : 789 (95% CI: 1 : 506 – 1 : 1310). The MS/MS data and molecular genetic characteristics of patients with MCADD are provided in Table 2.

In 20 newborns, acylcarnitine levels significantly exceeding reference values were revealed in phase II of diagnostics. However, in case 18, one heterozygous c.985A>G (p.Lys329Glu) mutation was found. The whole genome sequencing in the "trio" format is scheduled for this family, and the case is not considered in the further discussion.

Among 19 patients with two verified mutations, 16 are Ossetians, who were not born into consanguineous marriages. Patients 15 and 16 were monozygotic twins, their parents were Russians. Patient 12 was born into an interethnic marriage between the Ossetian and the female Tabasaran.

In five cases, the c.388-19T>A variant was in the homozygous state. Furthermore, a total of 11 compound heterozygous carriers were identified, which accounted for 55.26% of the entire sample and about 65.62% of the titular nation representatives.

The c.985A>G (p.Lys329Glu) variant ranking second in frequency was found (in the homozygous state in one patient and in the heterozygous carrier state in four cases), which accounted for 15.78% in the entire sample and 18.75% in Ossetians.

The c.134A>C (p.Gln45Arg) ranking third in frequency was found in the compound heterozygous state in four cases, accounting for 10.52 and 12.5% in the entire and titular groups, respectively.

Other variants are sporadic; these account for 18.44% in the entire sample and 3.13% in Ossetians.

It should be noted that the most pronounced changes in the C6, C8, and C10 levels (between 9 and 22 μmol/L) were observed in those having genotypes containing the c.985A>G (p.Lys329Glu) and c.388-19T>A variants in both homozygous and compound heterozygous state.

All children are in the MGC dietitian's and geneticist's D list. The dynamic changes in acylcarnitine levels are determined by MS/MS in accordance with the generally accepted guidelines. The children's condition was stable, and no metabolic crises, hypoglycemic conditions were observed. The identified patients' parents underwent Sanger sequencing in the "trio" format within the framework of the supplementary agreement between the Republican Children's Clinical Hospital of the RNO-Alania and the Research Centre for Medical Genetics; the parents are healthy carriers of the variants identified. During medical genetic counseling of families, prevention of long periods of fasting was discussed, especially in children having intercurrent infectious diseases, in order to prevent metabolic crises, as well as the need for immediate hospitalization in the Republican Children's Clinical Hospital and glucose infusion in case of metabolic crisis [4, 6].

One more case of detecting a disease from the organic aciduria group is as follows: the diagnosis of 3-methylcrotonyl-CoA carboxylase deficiency in a Kumyk child having the MCCC2

Table 2. MS/MS data and molecular genetic characteristics of patients with MCADD

№	Biochemistry indicators based on MS/MS data*	Ethnicity	Genotype (RefSeq NM_000016.6)
1	C6 — 1,04; C6DC — 0,34; C8 — 3,80; C10 — 0,52; C10:1 — 0,21	Ossetians	c.388-19T>A /c.388-19T>A
2	C6 — 1,74; C6DC — 0,52; C8 — 9,78; C8:1 — 0,17; C10 — 0,95; C10:1 — 0,49; C10:2 — 0,03	Ossetians	c.134A>C (p.Gln45Arg)/c.388-19T>A
3	C6 — 1,11; C8 — 4,98; C10 — 0,65; C10:1 — 0,30 + (Phe — 172)**	Ossetians	c.388-19T>A/ c.388-19T>A
4	C6 — 1,50; C6DC — 0,51; C8 — 6,46; C10 — 0,93; C10:1 — 0,45	Ossetians	c.388-19T>A/c.999_1011dup(p.Gln338Ter)
5	C6 — 3,53; C6DC — 1,02; C8 — 17,10; C8:1 — 0,23; C10 — 1,50; C10:1 — 0,58	Ossetians	c.985A>G (p.Lys329Glu)/c.985A>G(p.Lys329Glu)
6	C6 — 0,56; C8 — 1,57; C10:1 — 0,25	Ossetians	c.388-19T>A/c.999_1011dup(p.Gln338Ter)
7	C6 — 0,92; C6DC — 0,47; C8 — 5,25; C10 — 0,83; C10:1 — 0,26	Ossetians	c.388-19T>A/c.388-19T>A
8	C6 — 2,38; C6DC — 0,88; C8 — 12,95; C10 — 1,2; C10:1 – 0,36	Ossetians	c.985A>G (p.Lys329Glu)/c.388-19T>A
9	C6 — 1,22; C6DC — 0,41; C8 — 6,70; C10 — 0,82; C10:1 — 0,57	Ossetians	c.388-19T>A/c.985A>G (p.Lys329Glu)
10	C6 — 1,52; C6DC — 0,50; C8 — 6,10; C10 — 0,77; C10:1 — 0,38	Ossetians	c.388-19T>A/c.388-19T>A
11	C6 — 2,13; C6DC — 0,53; C8 — 9,11; C10 — 1,20; C10:1 — 0,57	Ossetians	c.388-19T>A/c.388-19T>A
12	C6 — 1,50; C6DC — 0,60; C8 — 9,79; C10 — 1,19; C10:1 — 0,44	Ossetian/female Tabasaran	c.388-19T>A/c.985A>G (p.Lys329Glu)
13	C8 — 0,45; C10 — 0,48	Ossetians	c.1091T>C, p.(Ile364Thr)/ c.388-19T>A
14	C6 — 1,31; C8 — 3,76; C10 — 0,44; C10:1 — 0,31	Ossetians	c.388-19T>A/c.461T>G, p.Leu154Trp
15	C6 — 1,24; C8 — 3,59; C10 — 0,41; C10:1 — 0,39	Ossetians (monozygotic twins)	c.388-19T>A/c.400_401delATinsCA, p.(Ile134His)
16	C6 — 1,38; C8 — 4,13; C10 — 0,49; C10:1 — 0,45		c.388-19T>A/c.400_401delATinsCA, p.(Ile134His)
17	C6 — 2,15; C8 — 10,5; C10 — 1,18; C10:1 — 0,45	Ossetians	c.134A>C (p.Gln45Arg)/c.388-19T>A
18	C6 — 0,38; C8 — 0,59; C10 — 0,73; C10:1 — 0,25	Ossetians	c.985A>G (p.Lys329Glu)/***
19	C6 — 3,57; C8 — 22,4; C10 — 1,97; C10:1 — 0,72	Ossetians	c.134A>C (p.Gln45Arg)/c.985A>G (p.Lys329Glu)
20	C6 — 1,28; C8 — 5,13; C10 — 0,61; C10:1 — 0,316	Ossetians	c.388-19T>A/c.134A>C (p.Gln45Arg)

Note: * — reference values for the studied indicators (μM/L): C8 — 0–0.26; C10 — 0–0.32; C6DC — 0–0.45; C10:1 — 0–0.14; ** — case of detecting MCADD and PKU; *** — mutation not found when performing the ACADM whole gene sequencing, the whole genome sequencing is recommended.

c.1082G>A (p.Arg361Gln) mutation in the homozygous state. The child's condition is stable, and the development is age-appropriate. The child is on the MGC dietitian's D list in the Republican Children's Clinical Hospital.

Testing for spinal muscular atrophy

Five newborns were included in the group at risk in phase I of ENBS during the studied period, among them the diagnosis of SMA was established in three cases. The SMA frequency was 1 : 4998 newborns (95% CI: 1 : 1711 – 1 : 24,235), which was generally consistent with the data provided in the world's and domestic literature. The average global prevalence of SMA is 1 : 6000 – 1 : 10,000 newborns, the prevalence in Saudi Arabia is 1 : 7000, the prevalence in Egypt and Libya is 1 : 12,500, and the prevalence in the RF is 1 : 5184 [7]. The SMA diagnostics is accomplished in accordance with the existing diagnostic algorithms within the framework of the clinical guidelines [8].

Table 3 provides the SMA patient assessment results and the therapy prescribed.

Based on the assessment results, in accordance with the guidelines of the Federal Council of the National Medical Research Center for Children's Health, two patients were administered Onasemnogene abeparvovec at the age of 1.5 months and 1 month; Risdiplam was recommended in one case.

The patients are on the neurologist's and geneticist's list.

Testing for primary immunodeficiency (PID)

In the studied period, the diagnosis of PID was established in none of the children in the region. However, in phase I of ENBS, 30 cases of low TREC/KREC were reported, among those, seven children died before blood re-sampling later (if premature), before reaching the post-conceptual age of 37 weeks. In 23 cases, the further scheduled assessment showed that all indicators were within reference ranges. It is assumed that the prevalence of PID in the region is below 1 : 14 994 newborns (95% CI: 0 – 1 : 4065).

Testing for five CHDs within the framework of newborn screening

Testing was performed in 14,994 cases. We have earlier reported epidemiological and molecular genetic characteristics of the disorders screened in the RNO-Alania [9]. The values provided that have been acquired during conventional biochemical screening confirm the results obtained previously for CH, CF, GAL, and CACD. Table 4 presents the results of the 2-year study conducted within the framework of NBS at the MGC of the Republican Children's Clinical Hospital of the

Table 3. SMA patient assessment results, timing of the beginning therapy and drugs used for treatment

Year	SMN1 gene copy number	SMN2 gene copy number	AAV9 carrier state	Therapy	Beginning of treatment (months)
2023	0	3	neg*	Onasemnogene abeparvovec	1.5
2023	0	4	neg	Risdiplam	1.5
2024	0	2	neg	Onasemnogene abeparvovec	1

Note: neg* — negative.

Table 4. NBS results, 2023–2024

Year	PKU		CH		CF		GAL		CACD	
	n	F (95% CI)	*n*	F (95% CI)	*n*	F (95% CI)	*n*	F (95% CI)	*n*	F (95% CI)
2023	3	1 : 2999 (1 : 1285 – 1 : 9235)	2	1 : 2999 (1 : 1285 – 1 : 9235)	0	0 (0 – 1 : 4065)	0	0 (0 – 1 : 4065)	1*	1 : 7500 (1 : 2076 – 1 : 61,904)

Note: *n* — number of patients, F — frequency, 95% CI — 95% confidence interval; * — CACD caused by 3β hydroxysteroid dehydrogenase deficiency that is rare in other world's populations and the RF, but typical for Ossetians, has been detected.

RNO-Alania, showing a low rate of PKU detection based on NBS compared to ENBS.

Comparison of NBS and ENBS in the diagnosis of PKU shows higher sensitivity of MS/MS contributing to the identification of patients with mild PKU having confirmed genetic variants in the *PAH* gene, who need monitoring and clinical follow-up.

DISCUSSION

Aminoacidopathies

We had an opportunity to assess PA levels (among 28 other indicators) in the MS/MS format within the framework of ENBS. The data obtained have radically changed the existing knowledge about the PKU population genetic features in the region. Thus, in 2012, PKU frequency in the Republic was interpreted as 1 per 23,000 newborns. This suggested a low prevalence of the disorder in the region, since the diagnosis of PKU was considered as a variant of severe hyperphenylalaninemia (HPA) with the PA levels above 10 mg%, in which mandatory nutritional therapy is prescribed [10]. Later, when cooperating with the Research Centre for Medical Genetics, we had an opportunity to perform DNA diagnostics in all the children identified based on the screening results (PA levels above 2 mg%) and included in the list due to the diagnosis of HPA. The testing results have showed that the frequency of all PKU forms turned out to be 1 : 4864 (95% CI), while the frequency of cases with severe variants requiring nutritional therapy was 1 : 22,374 (95% CI), and that of mild forms – 1 : 6216 (95% CI). The range of molecular genetic features of the disorder also turned out to be specific due to common nature of two mutations, c.842C>T (p.Pro281Leu) (PAH residual activity 0–2%) and c.631C>A (p.Pro211Thr) (PAH residual activity 72%), which are not that frequent anywhere in the world. Furthermore, we have earlier reported the p.Pro281Leu and p.Pro211Thr carrier state in the population with the frequency of 1 : 26 (95% CI), which allowed us to assume considerably higher prevalence of this aminoacidopathy in the RNA-Alania [5, 10], as confirmed by the ENBS results.

The 2-year study conducted within the framework of NBS revealed five PKU cases, and that conducted within the framework of ENBS proved the fact of high prevalence of mild PKU in the region — 1 : 1363 newborns (95% CI), high frequency of all PKU forms — 1 : 1153 (95% CI) and 1 : 7497 (95% CI) for severe forms, for which variants of two severe mutations were reported.

Organic acidurias

According to various sources, the prevalence of MCAD deficiency in the countries of Europe and the USA is 1 : 8300 — 1 : 15,000 newborns. Based on the results of our study, the prevalence of the disorder is 1 : 789 surveyed newborns. According to the literature data, the frequency of this HMD in the world is as follows: 1 : 22,000 in the Czech Republic, 1 : 27,139 in Norway, higher frequency of 1 : 4900 — 1 : 8500 is reported for Germany, 1 : 23,000 in Italy, 1 : 10,000 — 1 : 30,000 in the USA, and the highest frequency of 1 : 4000 is reported for Qatar [11–12]. Exact epidemiological data for Russia have not been published, but preliminary calculations have revealed no important specifics [4].

In 90–95% of cases, a point mutation in exon 11, in which adenine is replaced by guanine at position 985 of the gene (c.985A>G), is found. Other genetic variants that are much less common have also been reported [13–16]. High prevalence of the c.985A>G carrier state has been shown (1 : 52 in Switzerland, 1 : 58 in the UK), along with its decrease from north to south, which is likely to result from the "founder effect" in the ancient German population [17].

The clinical picture of the disease is extremely variable: from asymptomatic to the rapidly developing severe disease [6, 18].

According to the data obtained during ENBS implementation, the unique range of the *ACADM* gene variants was revealed in the region. Thus, the c.985A>G (p.Lys329Glu) variant that is most common according to the data of the world's and domestic literature [4, 15, 19, 20], in our study has been reported for only one case in the homozygous state and for four cases in the compound heterozygous state, i.e. it accounts for only 15.78% in the entire sample and 18.75% in Ossetians. While the c.388-19T>A variant turned out to be the most common in the studied population: 55.26% in the entire sample and about 65.62% in the titular nation representatives. This variant is not found in population databases (gnomAD without frequency). ClinVar contains the mutation description and links to two studies out of the large number of reports in the world's literature, where the disorder is mentioned [16, 21].

The c.388-19T>A was first described in 2012 based on the results of the large-scale Danish study focused on MCADD as previously unregistered and identified based on the screening results of two newborns (unrelated) with the c.388-19T>A/c.244_245dup genotype [21]. It has been proven that mutational sequence alterations occur in the *ACADM* gene intron 5. These dramatically decrease the strength of the wild-type acceptor

splice sites, while generating new competing, stronger splice sites, causing serious cleavage disorders, up to mRNA degradation resulting from the nonsense-mediated decay, and directly altering the encoded ACADM protein amino acid structure.

To date, all the patients identified are under the age of three years, but metabolic crises have not been reported in any of them. This can be associated with mild variants of the mutations identified and the efforts of parents in terms of preventing long fasting periods.

The fact should be noted that no MCADD cases were reported in the Republic before the beginning of the screening period, but patients with hypoglycemic conditions, unclear metabolic crises, especially against the background of respiratory or acute intestinal infectious diseases, were, of course, encountered in the practice of pediatric endocrinologists, pediatricians, infectious disease specialists, and resuscitators. However, the causes of these conditions were not verified due to the lack of the possibility of conducting MS/MS in the region and insufficient physicians' awareness about this disorder.

In our opinion, a very interesting case is a rare combination of PKU and MCADD in one patient (No. 6 in Table 1 and No. 3 in Table 2), who does not need nutritional therapy with limited PA intake and who has no metabolic crises due to the presence of "mild" mutations associated with both disease entities.

CONCLUSIONS

In general, NBS and ENBS implemented in the RNO-Alania can be acknowledged as an effective method for preclinical diagnosis of CHDs, which is considered to be effective when detecting 0.1% of abnormality in the entire cohort of surveyed children. In our study, 37 established diagnoses account for 0.25% of all the children screened in phase I, which clearly demonstrates the program's success and effectiveness. We have shown higher MS/MS sensitivity in detection of mild PKU compared to the standard biochemical method used during NBS. On the one hand, diagnostics in the tandem mass spectrometry format has considerably reduced the percentage of false positive results. On the other hand, the detection rate of this disorder has increased, even against the background of PA values that are slightly above the standard values. During the study, we have also managed to verify the range of mutations typical for PKU and MCADD and determine their frequency in the region. The frequency of all PKU forms is 1 : 1153 newborns, and the MCADD frequency is 1 : 789 newborns. The opportunities that are presented to the scientific community and practitioners as the scientific and technical progress evolves, specifically the ENBS introduction, directly affect the evolution of our views regarding mutations associated with CHDs and their population genetic features in various ethnic groups. Comprehensive assessment of patients and their parents conducted within the framework of ENBS not only contributes to preclinical diagnosis and timely start of treatment of rare disorders, which have remained undiagnosed until now, but also makes it possible to inform the sick child's parents about further family planning and prevention of the CHD spread across the population when providing medical genetic counseling.

References

1. Voronin SV, Kucev SI. Neonatal'nyj skrining na nasledstvennye zabolevanija v Rossii: vchera, segodnja, zavtra. Neonatologija: novosti, mnenija, obuchenie. 2022; 10 (4): 34–39. DOI: https://doi.org/10.33029/2308-2402-2022-10-4-34-39. Russian.
2. Voronin SV, Zaharova EYu, Bajdakova GV, Marahonov AV, Shhagina OP, Ryzhkova NV, i dr. Rasshirennyj neonatal'nyj skrining na nasledstvennye zabolevanija v Rossii: pervye itogi i perspektivy. Pediatrija im. G. N. Speranskogo. 2024; 103 (1): 16–29. DOI: 10.24110/0031-403X-2024-103-1-16-29. Russian.
3. Associacija medicinskih genetikov. Sojuz pediatrov Rossii. Associacija zdorov'ja detej. Klinicheskie rekomendacii. Klassicheskaja fenilketonurija i drugie vidy giperfenilalaninemii. 2025, 112 c. Russian.
4. Kucev SI, redaktor. Nacional'noe rukovodstvo. M.: GOJeTAR-Medicina, 2023; 360 s. DOI:10.33029/9704-7737-3-NEO-2023-1-360. Russian.
5. Tebieva IS, Mishakova PV, Gabisova YV, Khokhova AV, Kaloeva TG, Marakhonov AV, et al. Genetic Landscape and Clinical Features of Hyperphenylalaninemia in North Ossetia-Alania: high frequency of P281L and P211T genetic variants in the PAH gene. International Journal of Molecular Sciences. 2024; 25 (4): 4598. Available from: https://doi.org/10.3390/ijms25094598.
6. Mihajlova SV, Zaharova EJu, Petruhin AS. Nejrometabolicheskie zabolevanija u detej i podrostkov: diagnostika i podhody k lecheniju. M.: Litterra, 2024; 400 s. ISBN 978-5-4235-0417-5, DOI: 10.33029/4235-0417-5-NEI-2024-1-400. Russian.
7. Megarbane A, Bizzari S, Deepthi A, Sabbagh S, Mansour H, Chouery E, et al. A 20-year Clinical and Genetic Neuromuscular Cohort Analysis in Lebanon: An International Effort. J Neuromuscul Dis. 2022; 9 (1): 193–210. DOI: 10.3233/JND-210652.
8. Associacija medicinskih genetikov. Rossijskaja associacija pediatricheskih centrov. Vserossijskoe obshhestvo nevrologov. Associacija professional'nyh uchastnikov hospisnoj pomoshhi. Federal'nye klinicheskie rekomendacii. Proksimal'naja spinal'naja myshechnaja atrofija 5q. 2023. Russian.
9. Tebieva IS. Jeffektivnost' neonatal'nogo skrininga v vyjavlenii kliniko-genealogicheskih osobennostej nasledstvennyh boleznej i optimizacija sistemy ih diagnostiki i lechenija (dissertacija). Moskva, 2012. Russian.
10. Tebieva IS, Gabisova YuV, Zinchenko RA. Rezul'taty 15-letnego neonatal'nogo skrininga v Respublike Severnaja Osetija-Alanija. Medicinskaja genetika. 2023; 22 (2): 40–47. Russian.
11. Yuan Tian, Xinyun Zhu, Shubo Lv, Chenlu Jia, Linlin Zhang, Min Ni, et al. Analysis of gene mutations of medium-chain acyl-coenzyme a dehydrogenase deficiency (MCADD) by next-generation sequencing in Henan, China. Clinica Chimica Acta. 2022; 536: 155–61. Available from: https://doi.org/10.1016/j.cca.2022.09.008.
12. Pourfarzam M, Zadhoush F. Newborn Screening for inherited metabolic disorders; news and views. J Res Med Sci. 2013; 18 (9): 801–8;
13. Nikolaeva EA, Mamedov IS. Diagnostika i lechenie nasledstvennyh defektov obmena zhirnyh kislot u detej. Rossijskij vestnir perinatologii i pediatrii. 2009; 2: 51–65. Russian.
14. Surkov AN, Gundobina OS, Poljakova SI, Zhurkova NV, Zaharova EYu, i dr. Sluchaj nedostatochnosti acil-KoA-degidrogenazy zhirnyh kislot so srednej dlinoj cepi u rebenka dvuh let. Pediatrija. 2011; 5 (64): 14–18. Russian.
15. Wilcken B, Haas M, Joy P, Wiley V, Chaplin M, Black C, et al. Outcome of neonatal screening for medium-chain acyl-CoA dehydrogenase deficiency in Australia: a cohort study. Lancet. 2007; 369 (9555): 37-42. DOI: 10.1016/S0140-6736(07)60029-4. PMID: 17208640.
16. Li YY, Xu J, Sun XC, Li HY, Mu K. Newborn screening and genetic variation of medium chain acyl-CoA dehydrogenase deficiency in the Chinese population. J Pediatr Endocrinol Metab. 2022; 35 (10): 1264–71. DOI: 10.1515/jpem-2022-0394. PMID: 36068006.
17. Smith EH, Thomas C, McHugh D, Gavrilov D, Raymond K, Rinaldo P, et al. Allelic diversity in MCAD deficiency: the biochemical classification of 54 variants identified during 5 years of ACADM sequencing. Mol Genet Metab. 2010; 100 (3): 241–50. DOI:

10.1016/j.ymgme.2010.04.001. Epub 2010 Apr 8. PMID: 20434380.
18. Waisbren SE. Newborn screening for metabolic disorders. JAMA. 2006; 296 (8): 993–5. DOI: 10.1001/jama.296.8.993. PMID: 16926360.
19. Nikolaeva EA, Semjachkina AN. Sovremennye vozmozhnosti lechenija nasledstvennyh zabolevanij u detej. Roscijskij vestnik perinatologii i pediatrii 2018; 63 (4): 6–14. DOI: 10.21508/1027-4065-2018-63-4-6-14ju. Russian.
20. Andresen BS, Dobrowolski SF, O'Reilly L, Muenzer J, McCandless SE, Frazier DM, et ak. Medium-chain acyl-CoA dehydrogenase (MCAD) mutations identified by MS/MS-based prospective screening of newborns differ from those observed in patients with clinical symptoms: identification and characterization of a new, prevalent mutation that results in mild MCAD deficiency. Am J Hum Genet. 2001; 68 (6): 1408-18. DOI: 10.1086/320602. Epub 2001 May 8. PMID: 11349232; PMCID: PMC1226127.
21. Andresen BS, Lund AM, Hougaard DM, Christensen E, Gahrn B, et al. MCAD deficiency in Denmark. Molecular Genetics and Metabolism. 2012; 106 (2): 175–88. Available from: https://doi.org/10.1016/j.ymgme.2012.03.018.

Литература

1. Воронин С. В., Куцев С. И. Неонатальный скрининг на наследственные заболевания в России: вчера, сегодня, завтра. Неонатология: новости, мнения, обучение. 2022; 10 (4): 34–39. DOI: https://doi.org/10.33029/2308-2402-2022-10-4-34-39.
2. Воронин С. В., Захарова Е. Ю., Байдакова Г. В., Марахонов А. В., Щагина О. П., Рыжкова Н. В. и др. Расширенный неонатальный скрининг на наследственные заболевания в России: первые итоги и перспективы. Педиатрия им. Г. Н. Сперанского. 2024; 103 (1): 16–29. DOI: 10.24110/0031-403X-2024-103-1-16-29.
3. Ассоциация медицинских генетиков. Союз педиатров России. Ассоциация здоровья детей. Клинические рекомендации. Классическая фенилкетонурия и другие виды гиперфенилаланинемии. 2025, 112 с.
4. Куцев С. И., редактор. Национальное руководство. М.: ГОЭТАР-Медицина, 2023; 360 с. DOI:10.33029/9704-7737-3-NEO-2023-1-360.
5. Tebieva IS, Mishakova PV, Gabisova YV, Khokhova AV, Kaloeva TG, Marakhonov AV, et al. Genetic Landscape and Clinical Features of Hyperphenylalaninemia in North Ossetia-Alania: high frequency of P281L and P211T genetic variants in the PAH gene. International Journal of Molecular Sciences. 2024; 25 (4): 4598. Available from: https://doi.org/10.3390/ijms25094598.
6. Михайлова С. В., Захарова Е. Ю., Петрухин А. С. Нейрометаболические заболевания у детей и подростков: диагностика и подходы к лечению. М.: Литтерра, 2024; 400 с. ISBN 978-5-4235-0417-5, DOI: 10.33029/4235-0417-5-NEI-2024-1-400.
7. Megarbane A, Bizzari S, Deepthi A, Sabbagh S, Mansour H, Chouery E, et al. A 20-year Clinical and Genetic Neuromuscular Cohort Analysis in Lebanon: An International Effort. J Neuromuscul Dis. 2022; 9 (1): 193–210. DOI: 10.3233/JND-210652.
8. Ассоциация медицинских генетиков. Российская ассоциация педиатрических центров. Всероссийское общество неврологов. Ассоциация профессиональных участников хосписной помощи. Федеральные клинические рекомендации. Проксимальная спинальная мышечная атрофия 5q. 2023.
9. Тебиева И. С. Эффективность неонатального скрининга в выявлении клинико-генеалогических особенностей наследственных болезней и оптимизация системы их диагностики и лечения (диссертация). Москва, 2012.
10. Тебиева И. С., Габисова Ю. В., Зинченко Р. А. Результаты 15-летнего неонатального скрининга в Республике Северная Осетия-Алания. Медицинская генетика. 2023; 22 (2): 40–47.
11. Yuan Tian, Xinyun Zhu, Shubo Lv, Chenlu Jia, Linlin Zhang, Min Ni, et al. Analysis of gene mutations of medium-chain acyl-coenzyme a dehydrogenase deficiency (MCADD) by next-generation sequencing in Henan, China. Clinica Chimica Acta. 2022; 536: 155–61. Available from: https://doi.org/10.1016/j.cca.2022.09.008.
12. Pourfarzam M, Zadhoush F. Newborn Screening for inherited metabolic disorders; news and views. J Res Med Sci. 2013; 18 (9): 801–8;
13. Николаева Е. А., Мамедов И. С. Диагностика и лечение наследственных дефектов обмена жирных кислот у детей. Российский вестниг перинатологии и педиатрии. 2009; 2: 51–65.
14. Сурков А. Н., Гундобина О. С., Полякова С. И., Журкова Н. В., Захарова Е. Ю. и др. Случай недостаточности ацил-КоА-дегидрогеназы жирных кислот со средней длиной цепи у ребенка двух лет. Педиатрия. 2011; 5 (64): 14–18.
15. Wilcken B, Haas M, Joy P, Wiley V, Chaplin M, Black C, et al. Outcome of neonatal screening for medium-chain acyl-CoA dehydrogenase deficiency in Australia: a cohort study. Lancet. 2007; 369 (9555): 37-42. DOI: 10.1016/S0140-6736(07)60029-4. PMID: 17208640.
16. Li YY, Xu J, Sun XC, Li HY, Mu K. Newborn screening and genetic variation of medium chain acyl-CoA dehydrogenase deficiency in the Chinese population. J Pediatr Endocrinol Metab. 2022; 35 (10): 1264–71. DOI: 10.1515/jpem-2022-0394. PMID: 36068006.
17. Smith EH, Thomas C, McHugh D, Gavrilov D, Raymond K, Rinaldo P, et al. Allelic diversity in MCAD deficiency: the biochemical classification of 54 variants identified during 5 years of ACADM sequencing. Mol Genet Metab. 2010; 100 (3): 241–50. DOI: 10.1016/j.ymgme.2010.04.001. Epub 2010 Apr 8. PMID: 20434380.
18. Waisbren SE. Newborn screening for metabolic disorders. JAMA. 2006; 296 (8): 993–5. DOI: 10.1001/jama.296.8.993. PMID: 16926360.
19. Николаева Е. А., Семячкина А. Н. Современные возможности лечения наследственных заболеваний у детей. Российский вестник перинатологии и педиатрии 2018; 63 (4): 6–14. DOI: 10.21508/1027-4065-2018-63-4-6-14ю.
20. Andresen BS, Dobrowolski SF, O'Reilly L, Muenzer J, McCandless SE, Frazier DM, et ak. Medium-chain acyl-CoA dehydrogenase (MCAD) mutations identified by MS/MS-based prospective screening of newborns differ from those observed in patients with clinical symptoms: identification and characterization of a new, prevalent mutation that results in mild MCAD deficiency. Am J Hum Genet. 2001; 68 (6): 1408-18. DOI: 10.1086/320602. Epub 2001 May 8. PMID: 11349232; PMCID: PMC1226127.
21. Andresen BS, Lund AM, Hougaard DM, Christensen E, Gahrn B, et al. MCAD deficiency in Denmark. Molecular Genetics and Metabolism. 2012; 106 (2): 175–88. Available from: https://doi.org/10.1016/j.ymgme.2012.03.018.

INDIVIDUAL FEATURES OF THE MASTICATORY MUSCLE BIOELECTRICAL ACTIVITY IN ORGANIZATION OF CHEWING FUNCTION

Shishelova AYu[1,2], Guseva OYu[1] ✉, Kopetskiy IS[1], Ansari V[1]

[1] Pirogov Russian National Research Medical University (Pirogov University), Moscow, Russia

[2] Institute of Higher Nervous Activity and Neurophysiology of the Russian Academy of Sciences, Moscow, Russia

The chewing experience acquired during ontogeny may lead to developing functional asymmetry of the masticatory apparatus, adversely affecting the maxillofacial region functions. The study aimed to assess asymmetry of the masticatory muscle activity in healthy individuals showing no dentofacial system dysfunction. In 17 volunteers (6 males, 11 females aged 18–23 years), motor functional asymmetry of the brain was assessed using standard motor tests, and surface electromyogram (EMG) of the masseter (MM) and temporalis muscle (TMs) was recorded on the right and left sides: in the resting state, with the maximum voluntary bite force, during deliberate unilateral mastication (alternately on the left and right sides), and bilateral voluntary chewing. Three groups with various asymmetry manifestations were distinguished and characterized based on the asymmetry indices of standard EMG parameters (integrated EMG (Alint), average amplitude (Alav), and chewing bursts duration (Ald)) of the right and left muscles: 1) showing stable unilateral asymmetry of the MM and TM activity; 2) showing the "dynamic asymmetry" that was different for the MMs and TMs; 3) showing the "adaptive control", when the muscle activity asymmetry was manifested adequately to the chewing test, and Alint of the MMs and TMs reached 40 ± 18% and 97 ± 20% during chewing on the left side, 242 ± 39% and 127 ± 32% during chewing on the right side, 115 ± 12% and 115 ± 24% during bilateral chewing. The major significant between-group differences in Alint, Alav, and Ald were reported for the MMs (the impact of the "group" factor on these indices was as follows: $F = 11.0$, $p < 0.01$; $F = 5.72$ and $F = 3.73$, $p < 0.05$; repeated measures ANOVA). Thus, in young adulthood, some people develop functional asymmetry of the masticatory muscles in the form of excessive predominance of electrical activity on one side of the face with changes in both amplitude and duration of the "chewing" EMG bursts.

Keywords: chewing, electromyography, functional chewing asymmetry, masticatory muscles, neutral bite

Acknowledgements: we would like to thank Professor I.V. Pogabalo for advice on the methods to record and analyze electromyography data.

Author contribution: Shishelova AYu — study idea, concept and design, data acquisition and processing, statistical data processing, manuscript writing and editing; Guseva OYu — study concept and design, data acquisition and processing, literature review, manuscript writing and editing; Kopetskiy IS — manuscript editing and approval before publishing; Ansari V — data acquisition, literature review.

Compliance with ethical standards: the study was approved by the Ethics Committee of the Pirogov Russian National Research Medical University (protocol No. 250 dated 21 April 2025).

✉ **Correspondence should be addressed:** Olga Yu. Guseva
Ostrovityanova, 1, 117513, Moscow, Russia; o-guseva@bk.ru

Received: 19.05.2025 **Accepted:** 09.06.2025 **Published online:** 19.06.2025

DOI: 10.24075/brsmu.2025.031

ИНДИВИДУАЛЬНЫЕ ОСОБЕННОСТИ АСИММЕТРИИ БИОЭЛЕКТРИЧЕСКОЙ АКТИВНОСТИ ЖЕВАТЕЛЬНЫХ МЫШЦ В ОРГАНИЗАЦИИ ЖЕВАТЕЛЬНОЙ ФУНКЦИИ

А. Ю. Шишелова[1,2], О. Ю. Гусева[1] ✉, И. С. Копецкий[1], В. Ансари[1]

[1] Российский национальный исследовательский медицинский университет имени Н. И. Пирогова (Пироговский Университет), Москва, Россия

[2] Институт высшей нервной деятельности и нейрофизиологии Российской академии наук, Москва, Россия

Приобретаемый в онтогенезе опыт жевания может приводить к формированию функциональной асимметрии аппарата жевания с неблагоприятным влиянием на функции челюстно-лицевой области. Целью работы было оценить асимметрию активности жевательных мышц у здоровых людей без дисфункций зубочелюстной системы. У 17 добровольцев (6 мужчин, 11 женщин, 18–23 лет) проводили оценку моторной функциональной асимметрии мозга с помощью стандартных тестов и регистрацию поверхностной электромиограммы (ЭМГ) собственно-жевательных (СЖМ) и височных мышц (ВМ): в покое, при максимальном сжатии челюстей, при жевании — изолированном (поочередно на левой и правой сторонах) и произвольном. На основе индексов асимметрии показателей ЭМГ (общей площади (ИАинт), средней амплитуды (ИАср) и продолжительности жевания (ИАвр)) мышц справа и слева были выделены и описаны три группы с разными проявлениями асимметрии: 1) со стабильной односторонней асимметрией активности СЖМ и ВМ; 2) с «динамичной асимметрией», различной для СЖМ и ВМ; 3) с «адаптивным контролем», когда асимметрия активности мышц была адекватна жевательной пробе. В третьей группе ИАинт для СЖМ и ВМ был равен 40 ± 18% и 97 ± 20% при жевании на левой стороне, 242 ± 39% и 127 ± 32% — на правой, 115 ± 12% и 115 ± 24% при свободном жевании. Основные статистически значимые различия ИАинт, ИАср и ИАвр между группами выявлены для СЖМ (влияние фактора «группа» на данные индексы $F = 11,0$, $p < 0,01$; $F = 5,72$ и $F = 3,73$, $p < 0,05$; ANOVA repeated measures). Таким образом, в молодом возрасте у ряда людей формируется функциональная асимметрия жевательных мышц в виде избыточного преобладания электрической активности на одной стороне лица, с изменением как амплитудного, так и временного компонентов «жевательных» вспышек ЭМГ.

Ключевые слова: жевание, электромиография, функциональная асимметрия жевания, жевательные мышцы, нейтральный прикус

Благодарности: благодарим профессора И. В. Погабало за консультативную помощь по методикам регистрации и анализа электромиограмм.

Вклад авторов: А. Ю. Шишелова — идея, концепция и дизайн исследования, сбор и обработка материала, статистическая обработка данных, написание и редактирование статьи; О. Ю. Гусева — концепция и дизайн исследования, сбор и обработка материала, литературный обзор, написание и редактирование статьи; И. С. Копецкий — редактирование и утверждение статьи для публикации; В. Ансари — сбор материала, литературный обзор.

Соблюдение этических стандартов: исследование одобрено этическим комитетом РНИМУ имени Н. И. Пирогова (протокол № 250 от 21 апреля 2025 г.).

✉ **Для корреспонденции:** Ольга Юрьевна Гусева
ул. Островитянова, д. 1, 117513, г. Москва, Россия; o-guseva@bk.ru

Статья получена: 19.05.2025 **Статья принята к печати:** 09.06.2025 **Опубликована онлайн:** 19.06.2025

DOI: 10.24075/vrgmu.2025.031

Chewing represents a behavioral act culminating in the formation of the food bolus adequate for swallowing [1]. The program of action implemented by the hierarchically organized motor control system of the brain represents one of the key components of the functional system of any behavioral act [2]. The basic rhythmic activity of the masticatory muscles is provided by the brainstem motor program generator coordinating neuronal activity in the trigeminal motor nucleus innervating the masticatory muscles [2]. Excitation of these neurons during chewing is continuously adjusted by sensory signals from the dentofacial system, primarily from the periodontal mechanoreceptors and masticatory muscle proprioceptors [3], as well as from maxillofacial receptors of other types [4], which represents a key link of the innate, and therefore, involuntary mastication component. The cerebral cortex ensures supreme control of the brainstem chewing center via the corticobulbar tract [5–7], thereby also ensuring the conditioned and voluntary chewing component.

Shaping individual characteristics of masticatory activity is determined by the features of the maxillofacial region ontogeny, dentofacial system condition [8], as well as neurophysiology of the brain and chewing experience [9]. Adaptation to the development of the maxillofacial region functions during ontogeny, as well as interhemispheric features of the individual's motor control can result in individual functional asymmetry of chewing. Such asymmetry must manifest itself as predominant activity of the masticatory muscles on one side of the face, regardless of the current dominant side for chewing. Our objective was to assess the possibility of having the masticatory activity functional asymmetry in healthy young adults without any dentofacial system dysfunction. The study aimed to determine the dynamics and asymmetry of the masticatory muscle activity in healthy young volunteers in cases of forced and free chewing side change.

METHODS

Seventeen volunteers (6 males and 11 females, aged 18–23 years) participated in this study. The inclusion criteria: complete, intact dental arches with neutral occlusion (Angle class I on the left and right); no clinical symptoms of the temporomandibular joint (TMJ) abnormality. The exclusion criteria: age under 18 years, pregnancy, almond allergy, patient's refusal to take part in the study. At the beginning of the experiment procedure, motor functional asymmetry of the brain was assessed using standard motor tests (arm crossing test, "applause", leg crossing test) [10]. Then, surface electromyography (EMG) of both left and right masseter muscles (MMs) and temporalis muscles (TMs) was recorded using the 4-channel Synapsis EMG system for dental research (Neurotech, Taganrog, Russia). Pseudo-monopolar EMG electrodes were used. The resting-state EMG was recorded (10 s) with the maximum voluntary bite force (10 s) and during alternate chewing tests, in each of which the subject was chewing one almond nut: 1) deliberate unilateral mastication on the left side; 2) deliberate unilateral mastication on the right side; 3) bilateral voluntary chewing with changing the dominant side in a free manner convenient for the subject. EMG was recorded for 30 s in each chewing test, then the record's fragments from the beginning of mastication to initiation of the swallowing reflex were analyzed. An area

of the integrated EMG (μV*ms), mean voltage (Aav, μV) and duration (s) of the identified bursts were computed for each chewing stroke. The following parameters were measured: total integrated EMG, including the EMG amplitude and temporal characteristics; average amplitude of EMG bursts for the test — indicator showing high correlation with the force of muscle contraction [11]; total duration of the chewing strokes during the chewing test (chewing duration, s). To assess the asymmetry of the paired masticatory muscles' electrical activity, asymmetry indices were calculated for the right and left symmetrical muscles for each test using the formula (X right/X left) — 100%, where X represented an appropriate EMG indicator.

Statistical analysis of the study results was performed using the Statistica 12 software package (StatSoft Inc., USA). To analyze the differences in asymmetry indices based on the set of chewing tests, we used the repeated measures ANOVA (Fisher's *post-hoc* test), while one-way nonparametric Kruskall–Wallis ANOVA was used for the test with maximum bite force. Statistical significance of the differences (p) is shown in the figures.

RESULTS

Primary bilateral asymmetry of muscle's activity was assessed with the integrated EMG asymmetry index (AInt). The dynamic changes in AInt during chewing, test by test, were similar in 88% of subjects (Fig. 1). After switching from unilateral chewing on the left side to unilateral chewing on the right side, AInt rises, what indicates increased muscle activity on the right side compared to the left side. Then, AInt decreased again during bilateral voluntary chewing, remaining higher compared to the first chewing test (in 93% measurements) or similar (and 7%). We divided the subjects into three groups based on the shift of the AInt in accordance with changing the dominant side for chewing. Individuals of group I (with "stable asymmetry", $n = 6$) showed predominance of the MM's and TM's EMG activity on one side of the face in most tests, which was clearly visible in the bilateral chewing test. In two individuals of this group, the muscle's activity was greater on the right side (subgroup Ia; AInt > 100%), while in four individuals it was larger on the left side (subgroup Ib; AInt < 100%) (Fig.1). Individuals of group II (with "dynamic asymmetry", $n = 5$) demonstrated the oppositely directed manifestations of the MM's and TM's activity in some chewing tests. We included the subjects with the lack of the MM and TM adaptation to one or both isolated chewing tests that manifested itself in considerable (> 20%) predominance of appropriate activity on the side opposite to the dominant one in this group of subjects. Furthermore, the AInt reported for one paired muscle group was above 100%, while that for the other group was below 100% (Fig. 1). We assigned individuals, in whom activity of both muscles was larger on the dominant side compared to another side during the unilateral chewing tests, to group III (showing "adaptive control", $n = 6$) (Fig. 1). In three individuals, the dynamic changes in the AInt enabled inclusion in groups II and III. In two of them, TM activity was slightly greater on the right (≤ 20%), when chewing on the left side, in other cases adequate adaptation to chewing on one dominant side was observed. Although the right-sided TM asymmetry persisted in these individuals during bilateral chewing, the differences between the TMs and MMs in the degree of asymmetry decreased. That is why we assigned these subjects to group III. In the third subject, the TM activity was 12% larger on the left side compared to the other, when chewing on the right side, and this feature persisted during bilateral chewing with increasing degree of asymmetry that was oppositely directed in the TMs and MMs. This allowed us to include this subject in group II.

Unilateral masticatory muscle activity predominance revealed in groups Ia and Ib did not match predominance of the

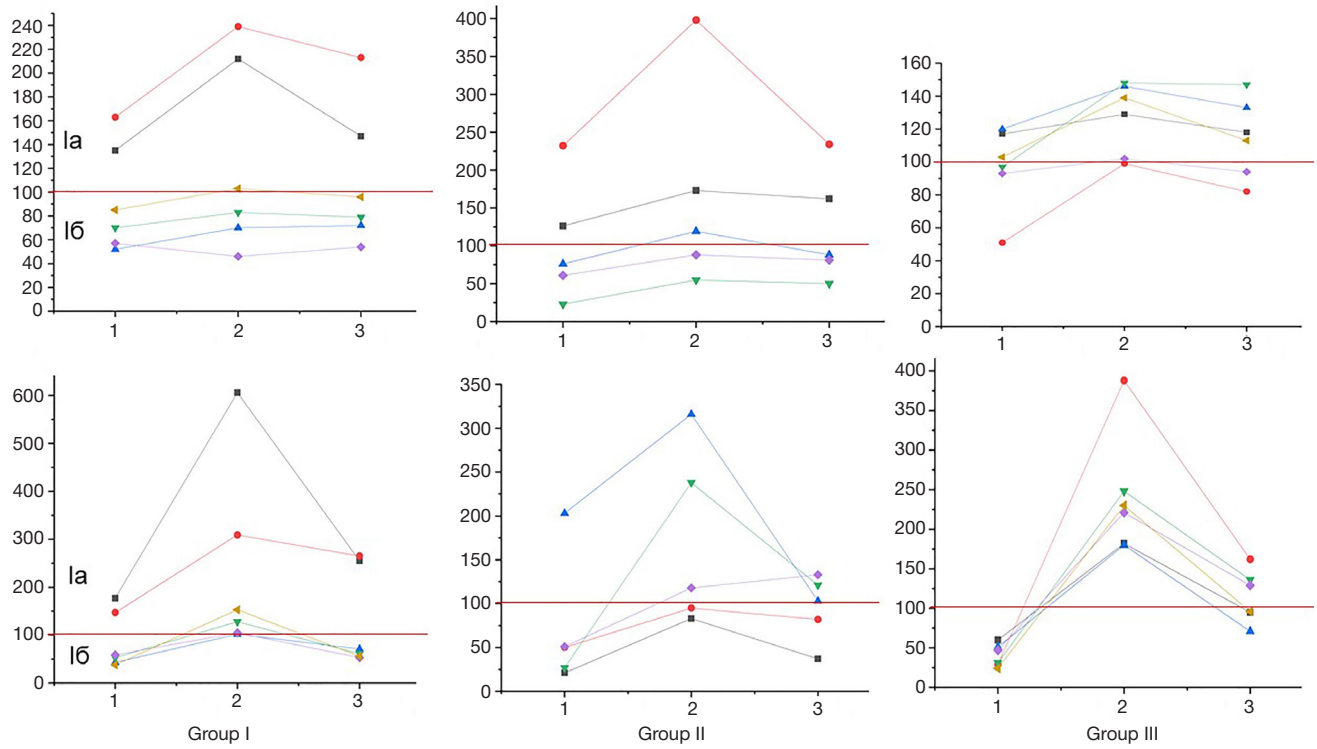

Fig. 1. Individual dynamics of the integrated AMG asymmetry index (Alint) in the identified groups. The x-axis represents the ordinal numbers of the chewing test (see Methods), and the *y*-axis represents Alint values (%). The upper row represents Alint of the temporal muscles, the lower row represents Alint of the masseter muscles. Each line shows individual Alint dynamics in a volunteer

right or left extremity movements during standard motor tests, reflecting the interhemispheric asymmetry in motor control (see Table).

As for the temporalis muscles, the ANOVA analysis revealed a significant impact of the "test" factor on the Alint (F = 19.9; $p < 0.0001$), as well as the trend towards interaction between the "group" and "test" ($p = 0.07$). The significant impact of the "test" (F = 36.6; $p < 0.0001$) and "group" (F = 11.0; $p < 0.01$) on the Alint was reported for the MMs, along with the significant interaction between the "group" and "test" factors (F = 2.76; $p < 0.05$).

In the identified groups, significant differences in the Alint values between the tests were reported for all groups, except for the Ib subgroup (Fig. 2). During unilateral chewing on the right side, the Alint significantly increased relative to the test involving chewing on the left side in subgroup Ia and group II for the TMs, in subgroup Ia, groups II, III for the MMs (post-hoc analysis). Later, during the bilateral chewing test the Alint values decreased in all groups. When comparing Alint during the chewing on the left side and bilateral chewing, the Alint values were significantly lower in the first test compared to bilateral chewing in group II for the TMs and in group III for the MMs.

Significant between-group differences in the Alint values were reported mainly for the MMs (Fig. 2B). The largest number of significant differences was reported for subgroup Ia in comparison with other groups. In the subjects of subgroup Ia, the Alint values were significantly higher compared to other groups in every test (except for the test involving chewing on the left side in the subjects of group II), which indicates marked predominance of the MM activity on the right side. In the subjects of subgroup Ib, the Alint values, in contrast, were significantly lower, than in the subjects of subgroup Ia, in all tests, and lower, than in individuals of group III in the test involving chewing on the right side. We found no significant between-groups differences in the Alint values during chewing tests in the subjects of groups II and III. In the voluntary bilateral chewing test, subjects of group I showed considerable deviation of the Alint values from 100% (> 100% in subgroup Ia and <100% in subgroup Ib), while in other groups the values of this index were close to 100%.

As for the temporalis muscles, significant between-group differences in the Alint values were reported only for the subjects of group I, during chewing on the right side (Fig. 2A). There was lower Alint in the subjects of subgroup Ib compared to the subjects of subgroup Ia and group II.

Then we compared manifestations of the mastication muscle activity asymmetry observed during chewing in the identified groups with the EMG integrated area asymmetry index in the test with maximum bite force (Almbf). In the subjects of subgroup Ia, the TM and MM activity was larger on the right side, while in the majority of subjects of subgroup Ib (75%), it was higher on the left side. In other groups, the majority of subjects showed the TM and MM activity predominance on the right relative to the left side (60 % in group II for both groups of muscles; 83% and 67% in group III for the TMs and MMs, respectively). The Almbf values of the groups are shown in Fig. 3. The differences between groups were non-significant.

Then we analyzed between-group differences in the asymmetry index of the average EMG amplitude (Alav) in the chewing tests. No significant impact of the "group" and "test"

Table. Percentage of subjects (%) with dominant movement of the right limbs in the identified groups

Ia	Iб	II	III
50%	75%	60%	67%

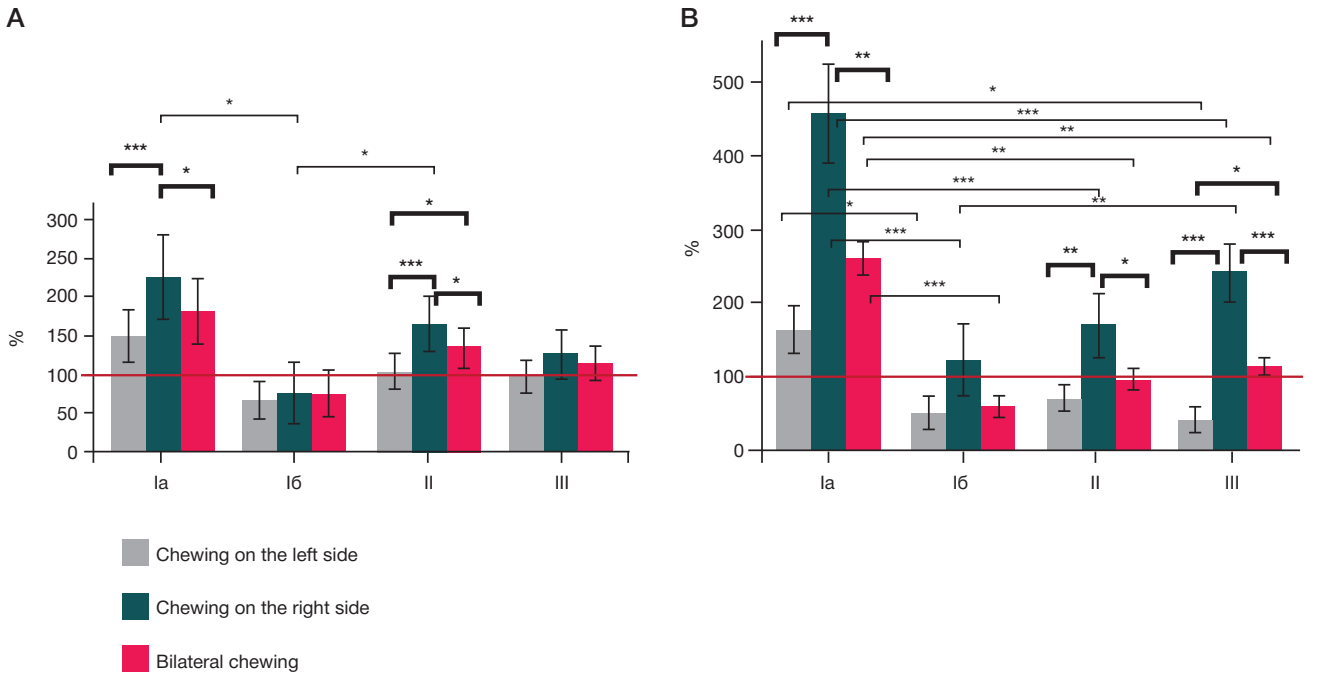

Fig. 2. The integrated EMG asymmetry index (Alint, %) in the chewing tests in the identified groups of volunteers. For each muscle, the bars represent intra-group mean Alint, the whiskers represent the SEM. The *red line* indicates the equal EMG activity of symmetrical muscles (Alint = 100%). **A**. Temporal muscles. **B**. Masseter muscles. Group designations: see text. Significant differences are indicated by *square brackets* above the bars (repeated measures ANOVA, Fisher's *post-hoc* test): within-group differences between the chewing tests are highlighted in *bold*, between-group differences reported during a similar chewing test are highlighted in the *light font* as follows: * — $p < 0.05$; ** — $p < 0.01$; *** — $p < 0.001$

factors on the Alav values was reported for the temporalis muscles. Here, the post-hoc analysis revealed only one between-group difference in Alav during chewing on the left side between subgroup Ib and group II (Fig. 4A).

Significant impact of the "group" ($F = 5.72$; $p = 0.01$) and "test" ($F = 34.17$; $p < 0.0001$) on the Alav values in the chewing tests was reported for the MMs. The dynamics of the Alav shifts test by test in MM was statistically significant in almost all groups. The Alav values increased during chewing on the right side relative to chewing on the left side (post-hoc analysis) in all subjects (Fig. 4B). In the bilateral chewing test, the Alav values significantly decreased in subgroup Ia, groups II, III, and showed a downward trend in subgroup Ib ($p = 0.07$).

The between-group differences in the Alav for the MMs were similar to the differences in the Alint (Fig. 4B). In the subjects of subgroup Ia, the Alav largely exceed 100% in all the tests, which reflected the larger strength of MM contraction on the right side. In the subgroup Ia, the Alav was significantly higher relative to subgroup Ib and group III during chewing on the left side, and higher than all other groups during chewing on the right side. In the bilateral chewing test, the Alav values of the subjects of subgroup Ia were significantly higher compared to the subjects of subgroup Ib, and showed an upward trend relative to the subjects of groups II and III ($p < 0.07$). In the subjects of subgroup Ib, the Alav values were far below 100% in the tests with chewing on the left side and bilateral chewing, which suggests significant predominance of masticatory muscles activity on the left side. The Alav values of the subjects of subgroup Ib were significantly lower compared to the subjects of subgroup Ia in all tests, and the subjects of group III during chewing on the right side. Furthermore, a downward trend of the Alav values relative to group II during chewing on the right side could be noted in the subjects of subgroup Ib ($p < 0.1$). There were no significant differences in the Alav values between group II and other groups. As it was for Alint, the average Alav values during bilateral chewing were much over 100% in the subjects of subgroup Ia, below 100% in subgroup Ib, close to 100% in groups II and III.

Then we assessed the asymmetry index of the total chewing EMG bursts duration ("chewing duration") in the chewing tests (Ald). Significant impact of the "test" factor on the Ald values was reported for the temporalis muscles ($F = 5.09$; $p < 0.05$). No between-group differences in the Ald values were reported for the TMs. The post-hoc analysis revealed significant within-group differences in the Ald values for the TMs between the tests of unilateral chewing on the left and right side in

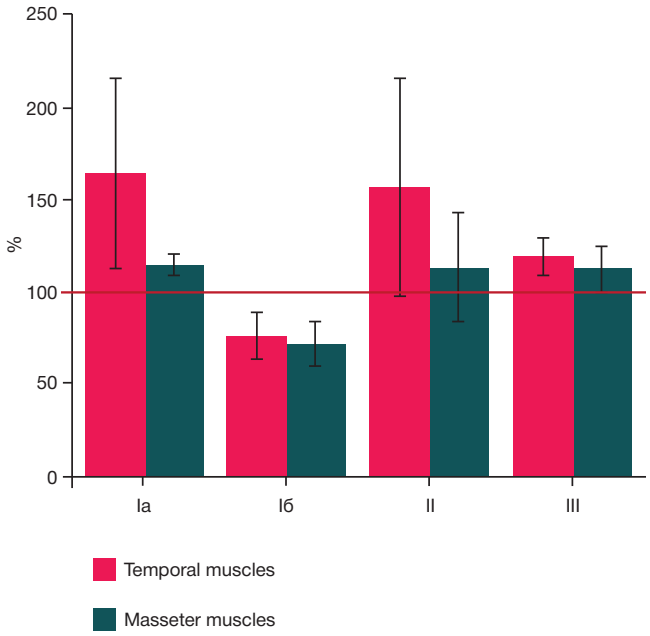

Fig. 3. The integrated EMG asymmetry index in the chewing test with maximum bite force (Almbf, %) in the identified groups of volunteers. For each muscle, the bars represent intra-group mean Almbf, the whiskers represent the SEM. The *red line* indicates the equal EMG activity of symmetrical muscles (Almbf = 100%). Group designations: see text

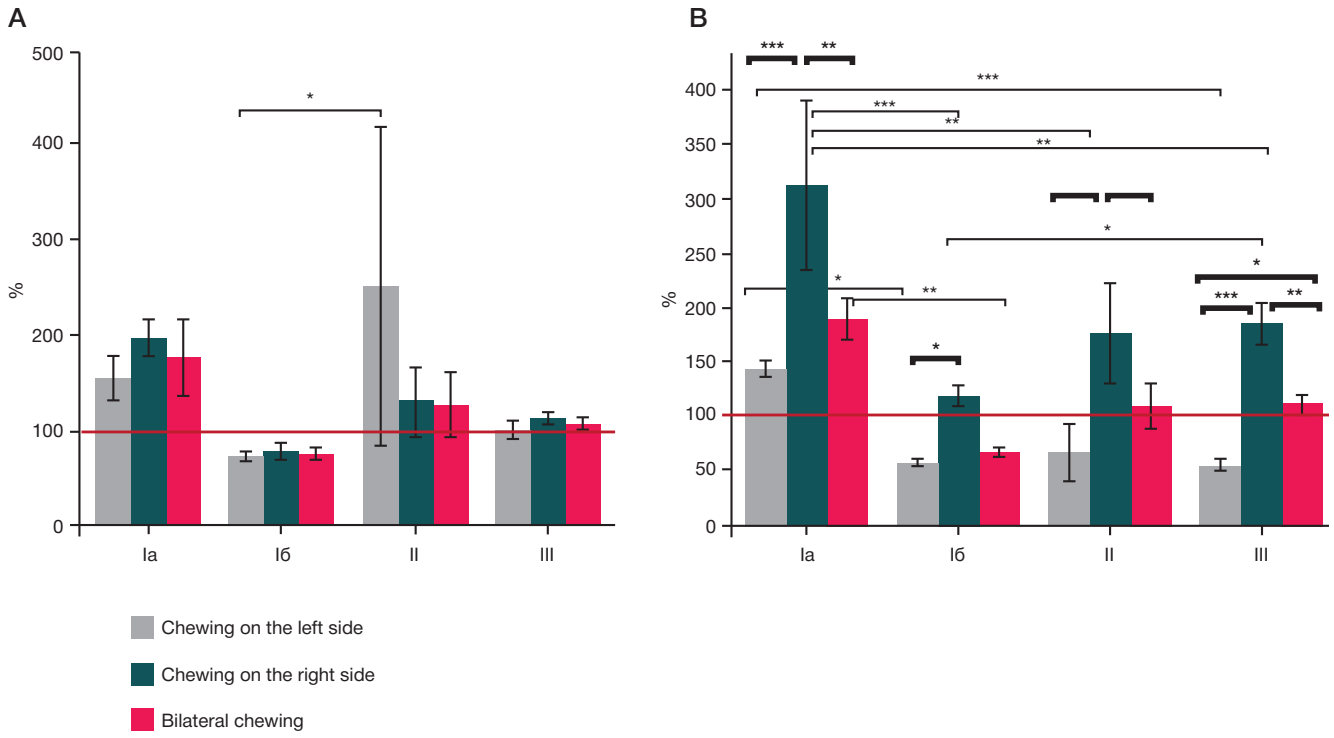

Fig. 4. The asymmetry index of the average EMG amplitude (Alav, %) in the chewing tests in the identified groups of volunteers. For each muscle, the bars represent intra-group mean Alav, the whiskers represent the SEM. The *red line* indicates the equal EMG activity of symmetrical muscles (Alav = 100%). **A**. Temporal muscles. **B**. Masseter muscles. Group designations: see text. Significant differences are indicated by *square brackets* above the bars (repeated measures ANOVA, Fisher's *post-hoc* test): within-group differences between the chewing tests are highlighted in *bold*, between-group differences reported during a similar chewing test are highlighted in the *light font* as follows: * $p < 0.05$; ** $p < 0.01$; *** $p < 0.001$

groups II and III (Fig. 5A). The average AId values of these groups corresponded to the test type: below 100% during chewing on the left side and over 100% during chewing on the right side.

Significant impact of the "group" factor on the AId values was reported for the MMs ($F = 3.73$; $p < 0.05$), along with the interaction between the "group" and "test" factors ($F = 2.97$; $p < 0.05$). Significant within-group differences in the AId

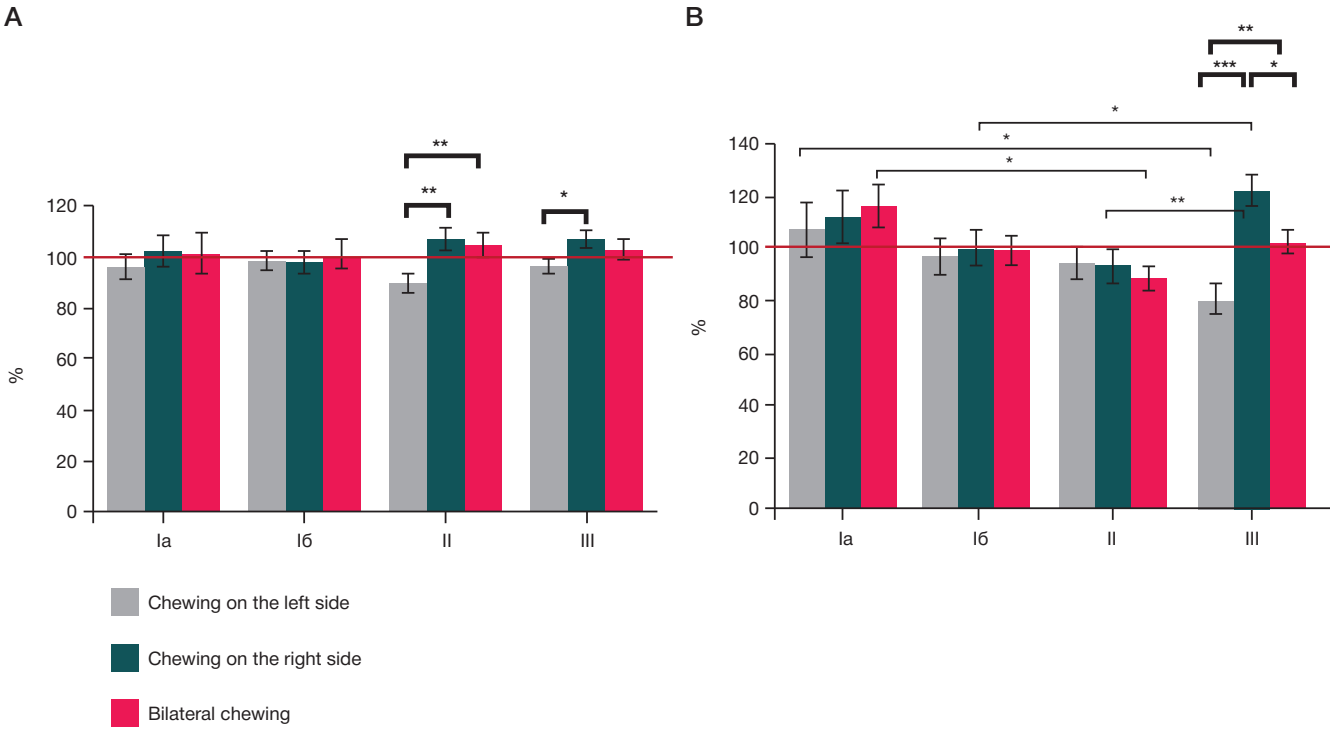

Fig. 5. The asymmetry index of the total chewing bursts duration in EMG (Aid, %) in the chewing tests in the identified groups of volunteers. For each muscle, the bars represent intra-group mean AId, the whiskers represent the SEM. The *red line* indicates the equal EMG activity of symmetrical muscles (AId = 100%). **A**. Temporal muscles. **B**. Masseter muscles. Group designations: see text. Significant differences are indicated by *square brackets* above the bars (repeated measures ANOVA, Fisher's *post-hoc* test): within-group differences between the chewing tests are highlighted in *bold*, between-group differences reported during a similar chewing test are highlighted in the *light font* as follows: * $p < 0.05$; ** $p < 0.01$; *** $p < 0.001$

between the tests were reported only for group III (*post-hoc* analysis; Fig. 5B), where the AId value was lowest during the test with unilateral chewing on the left side (below 100%), which suggests more prolonged MM activity on the left side. In the next test with chewing on the right side, the AId values increased well over 100% in the subjects of group III, which corresponded to more prolonged MM contraction on the right side (Fig. 5B). Then, in the bilateral chewing test, the AId values decreased significantly, getting close to 100%.

The greatest between-group differences in the MM AId values were reported in subgroup Ia, as it was with the other abovementioned asymmetry indices (Fig. 5B). Thus, in the subjects of subgroup Ia, the AId values were significantly higher, than in the subjects of group III in the test with chewing on the left side, compared to the subjects of group II in the bilateral chewing test. In the subjects of subgroup Ib and group II, the AId values were significantly lower, than in the subjects of group III in the test with chewing on the right side.

DISCUSSION

We have distinguished and described several asymmetry types for the activity of paired masticatory muscles based on the EMG data of the masticatory and temporalis muscles of the volunteers having complete intact dental arches with neutral occlusion (Angle I class on the left and on the right), without any clinical symptoms of the TMJ abnormality.

It has been shown that in 35% of subjects asymmetry of the overall electrical activity of paired muscles on the right and left corresponds to the masticatory goal during the chewing. When performing the unilateral chewing tests, activity of muscles of both types in these individuals was significantly larger on the dominant side, while no evident activity asymmetry was observed during bilateral chewing. Thus, the motor control associated with such mastication organization ensures adequate masticatory muscle involvement in the mastication program. That is why these study participants were referred to as the group showing “adaptive control”. The rest of participants showed maladaptive asymmetry of activity of the main masticatory muscles during unilateral and bilateral mastication. Furthermore, 35% of the study participants showed significant predominance of the masticatory muscle bioelectrical activity on one side of the face in all tests. The subjects with such mastication features were referred to as the group with “stable asymmetry”. Other 30% of participants demonstrated the oppositely directed MM and TM activity asymmetry manifestations during chewing, while they showed no predominance of activity on the dominant side for at least one of the studied pairs of muscles during unilateral chewing. This group was referred to as the group with “dynamic asymmetry”. The analysis of the EMG amplitude and temporal components during mastication in the subjects of these groups also revealed significant between-group differences in asymmetry of these indicators. Furthermore, the major differences were reported for the MMs: both between-group and between the tests within each group.

The available literature data on asymmetry of the electrical activity of the leading masticatory muscles in healthy individuals are rather controversial. This is likely to be due to different experimental design. Thus, in a number of studies asymmetry of the masticatory muscle EMG indicators was assessed using the test with maximum bite force only [12, 13]. However, as shown in our study, no full match of the sign of asymmetry of the paired masticatory muscles is observed with maximum bite force and during chewing of the natural substrate. Despite the fact that the trend towards predominance of the MM and TM electrical activity on one side of the face in the test with maximum bite force is preserved in the group with “stable asymmetry”, we have found no significant differences in the integrated EMG asymmetry index values between groups. Since voluntary jaw clenching and chewing food represent behavioral responses of different types aimed at achieving different results, it is reasonable to assume the differences in motor program organization during execution of these tests. In other studies, the masticatory muscle electrical activity was assessed only during unilateral chewing [14, 15], which did not provide a comprehensive view of the mastication motor control organization. Furthermore, the masticatory muscle activity asymmetry is usually assessed without allocating subgroups in accordance with the asymmetry patterns in different tests [13, 15, 16]. This makes comparison of our results with the literature data on assessing the masticatory muscle asymmetry difficult. However, the facts reported in the papers on the topic allow us to suggest what mechanisms underly the identified differences in the masticatory muscle activity asymmetry in the groups we have identified.

The masticatory muscle activity ratio reported during chewing reflects primarily the features of motor control. The lack of TMJ abnormalities, bite abnormalities, and dental lesions in the study participants suggest the key effect of behavioral features on developing the masticatory muscle function asymmetry. The functional interhemispheric asymmetry manifested by dominance of certain arm or leg during movement might be one such factor. The motor tests we have performed [10] have revealed predominance of right-handed individuals in each of the identified groups. This suggests that there is no direct relationship between the presence of interhemispheric asymmetry in organization of motor control of the limbs and masticatory muscles, which seems logical due to various types of behavior involving these groups of muscles.

In our opinion, the lack of the exact match between manifestations of bilateral masticatory muscle activity asymmetry with maximum bite force and during chewing demonstrates different cortical organization of the fast and slow motor unit recruiting in the masticatory muscle contraction during execution of the habitual behavioral action (chewing of food) and in the unfamiliar nonspecific jaw clench test.

It is interesting that the majority of between-group differences in masticatory asymmetry were reported for the MMs. According to the available literature data, the MM and TM control on the right and left side is performed in concert, which, for example, is reflected in the existence of significant correlations between the EMG activity of muscles on the left and right side, as well as between the activity of the right MM and both TMs in the test with maximum bite force [8]. This ensures coordination of muscle contraction during chewing. However, motor control of each muscle is specific, which is, in particular, manifested by low coefficient of the above correlations (not exceeding 0.6), no correlation between the activity of the left MM and both TMs, as well as by different extent of activation of each muscle during execution of various functional tasks (chewing of various substrates, jaw clench, rhythmic jaw movement, etc.) [17]. Thus, individual chewing pattern can be expressed in the varying degree of the MM and TM activity asymmetry.

In a number of studies, it has been found that the contribution of the MMs to the overall electrical activity of these masticatory muscles during chewing of solid food when performing such EMG recording during the chewing tests is larger, than that of the TMs: during both free chewing [16] and

on the dominant side during unilateral chewing [18]. In the latter case, the integrated EMG asymmetry between the dominant and contralateral side is greater for the MMs, than for the TMs [14, 16, 19]. Furthermore, the MM motor control program is more variable, which is indicated, for example, by the increase in the frequency of the MM electrical potential oscillation with the jaws clenched after the short-term normalization of occlusion with a splint in dental patients, along with the lack of significant differences in the frequency of the TM potential oscillation [20]. These facts confirm greater importance of controlling the MM activity compared to the TM activity during organization of chewing, which can result in higher variability of the MM bilateral asymmetry manifestations in individuals having no maxillofacial abnormalities. In this regard, our data reflect mostly manifestations of individual behavioral adaptation of the chewing function. Such behavioral components can affect dental processes. For example, the presence of the TMJ dysfunction can be accompanied by various MM and TM electrical activity shifts and its asymmetry in various studies [21]. The types of the masticatory muscle activity ratio we have reported in healthy individuals will enable more reliable and accurate diagnosis and adjustment of their functional asymmetry.

CONCLUSIONS

Some dentally healthy young adults show unilateral asymmetry of the electrical activity of the temporalis and masseter muscles during chewing that is not correlated to the activity asymmetry with maximum bite force and limb dominance in motor tests. Three groups were distinguished based on the extent of the integrated EMG asymmetry associated with chewing: 1) showing stable predominance of the masticatory muscle activity on one side of the face; 2) showing the oppositely directed asymmetry reported for the temporalis and masseter muscles; 3) showing predominance of muscle activity on the dominant side during unilateral chewing and negligible asymmetry during bilateral chewing. The identified groups also show differences in asymmetry of the EMG indicators characterizing the intensity and duration of masseter muscle excitation during chewing.

References

1. Alyavija O, Nishanova A, Gulyamova S. Funkcional'naja sistema, obespechivajushhaja processy pishhevarenija v rotovoj polosti. Stomatologija. 2018; 1 (70): 54–57. Russian.
2. Gerstner G, Madhavan S and Crane E. Mammalian Oral Rhythms and Motor Control. Biomechanics in Applications. InTech. 2011. Available from: http://dx.doi.org/10.5772/19501.
3. Piancino MG, Isola G, Cannavale R, Cutroneo G, Vermiglio G, Bracco P, Anastasi GP. From periodontal mechanoreceptors to chewing motor control: A systematic review. Arch Oral Biol. 2017; 78: 109–121. DOI: 10.1016/j.archoralbio.2017.02.010.
4. van der Glas HW, van der Bilt A, Abbink JH, Mason AG, Cadden SW. Functional roles of oral reflexes in chewing and biting: Phase-, task- and site-dependent reflex sensitivity. Arch Oral Biol. 2007; 52 (4): 365–369. Available from: https://doi.org/10.1016/j.archoralbio.2006.10.022.
5. Nordstrom MA. Insights into the bilateral cortical control of human masticatory muscles revealed by transcranial magnetic stimulation. Arch Oral Biol. 2007; 52 (4): 338–42. DOI: 10.1016/j.archoralbio.2006.09.013.
6. Onozuka M, Fujita M, Watanabe K, Hirano Y, Niwa M, Nishiyama K, et al. Age-related changes in brain regional activity during chewing: a functional magnetic resonance imaging study. J Dent Res. 2003; 82: 657–660.
7. Quintero A, Ichesco E, Myers C, Schutt R, Gerstner GE. Brain activity and human unilateral chewing: an FMRI study. J Dent Res. 2013; 92: 136–42.
8. Pyo CY, Kim TH, Kim DH. Association between masticatory muscle activity and oral conditions in young female college students. Anat Cell Biol. 2021; 54 (4): 479–88. DOI: 10.5115/acb.21.107.
9. Almotairy N, Kumar A, Trulsson M, Grigoriadis A. Development of the jaw sensorimotor control and chewing — a systematic review. Physiol Behav. 2018; 194: 456–65. DOI: 10.1016/j.physbeh.2018.06.037.
10. Gurizheva MI. Svjazi dvigatel'nyh i vizual'nyh prob, otrazhajushhih funkcional'nuju asimmetriju polusharij golovnogo mozga devushek. Bjulleten' medicinskih internet-konferencij. 2017; 7 (6): 1154–8. Russian.
11. Bogdanov V Type of correlation between bite force and EMG activity of the temporalis and masseter muscles during maximal and submaximal clenching. Folia Medica. 2023; 65 (6): 975–85. Available from: https://doi.org/10.3897/folmed.65.e107180.
12. Ferrario VF, Sforza C, Colombo A, Ciusa V. An electromyographic investigation of masticatory muscles symmetry in normo-occlusion subjects. J Oral Rehabil. 2000; 27 (1): 33–40. DOI: 10.1046/j.1365-2842.2000.00490.x.
13. Hotta GH, Oliveira AIS de, Oliveira AS de, Pedroni CR. Electromyography and asymmetry index of masticatory muscles in undergraduate students with temporomandibular disorders. Brazilian Journal of Oral Sciences. 2015; 14 (2): 176–81. DOI: 10.1590/1677-3225v14n2a15.
14. Kimoto K, Fushima K, Tamaki K, Toyoda M, Sato S, Uchimura N. Asymmetry of masticatory muscle activity during the closing phase of mastication. Cranio. 2000; 18 (4): 257–63. DOI: 10.1080/08869634.2000.11746139.
15. Na SH, Kang DW. Comparative Electromyographic Analysis Of Masticatory Muscles Between Bilateral And Unilateral Masticators. J Korean Acad Prosthodont. 2002; 40 (6): 577–89.
16. Mioche L, Bourdiol P, Martin JF, Noël Y. Variations in human masseter and temporalis muscle activity related to food texture during free and side-imposed mastication. Arch Oral Biol. 1999; 44 (12): 1005–12. DOI: 10.1016/s0003-9969(99)00103-x. PMID: 10669078.
17. Farella M, Palla S, Erni S, Michelotti A, Gallo L. Masticatory muscle activity during deliberately performed oral tasks. Physiol Meas. 2008; 29 (2008): 1397–410. DOI: 10.1088/0967-3334/29/12/004.
18. Fueki K, Yoshida E, Sugiura T, Igarashi Y. Comparison of electromyographic activity of jaw-closing muscles between mixing ability test and masticatory performance test. J Prosthodont Res. 2009; 53 (2): 72–7. DOI: 10.1016/j.jpor.2008.09.003. Epub 2008 Dec 27. PMID: 19318076.
19. Tomonari H, Seong C, Kwon S, Miyawaki S. Electromyographic activity of superficial masseter and anterior temporal muscles during unilateral mastication of artificial test foods with different textures in healthy subjects. Clin Oral Investig. 2019; 23 (9): 3445–55. DOI: 10.1007/s00784-018-2754-x. Epub 2019 Jan 3. PMID: 30607620.
20. Shatrov IM, Zholudev SE. Jelektromiograficheskaja ocenka reakcii zhevatel'nyh i visochnyh myshc na nagruzku kak pokazatel' funkcional'noj adaptacii zubocheljustnoj sistemy. Problemy stomatologii. 2016; 1: 103–9. Russian.
21. Marcelino V, De Rovere S, Paço M, Gonçalves M, Marcelino S, Guimarães AS, et al. Masticatory Function in Individuals with Temporomandibular Disorders: A Systematic Review and Meta-Analysis. Life (Basel). 2023; 13 (2): 472. DOI: 10.3390/life13020472.

Литература

1. Алявия О., Нишанова А., Гулямова С. Функциональная система, обеспечивающая процессы пищеварения в ротовой полости. Стоматология. 2018; 1 (70): 54–57.
2. Gerstner G, Madhavan S and Crane E. Mammalian Oral Rhythms and Motor Control. Biomechanics in Applications. InTech. 2011. Available from: http://dx.doi.org/10.5772/19501.
3. Piancino MG, Isola G, Cannavale R, Cutroneo G, Vermiglio G, Bracco P, Anastasi GP. From periodontal mechanoreceptors to chewing motor control: A systematic review. Arch Oral Biol. 2017; 78: 109–121. DOI: 10.1016/j.archoralbio.2017.02.010.
4. van der Glas HW, van der Bilt A, Abbink JH, Mason AG, Cadden SW. Functional roles of oral reflexes in chewing and biting: Phase-, task- and site-dependent reflex sensitivity. Arch Oral Biol. 2007; 52 (4): 365–369. Available from: https://doi.org/10.1016/j.archoralbio.2006.10.022.
5. Nordstrom MA. Insights into the bilateral cortical control of human masticatory muscles revealed by transcranial magnetic stimulation. Arch Oral Biol. 2007; 52 (4): 338–42. DOI: 10.1016/j.archoralbio.2006.09.013.
6. Onozuka M, Fujita M, Watanabe K, Hirano Y, Niwa M, Nishiyama K, et al. Age-related changes in brain regional activity during chewing: a functional magnetic resonance imaging study. J Dent Res. 2003; 82: 657–660.
7. Quintero A, Ichesco E, Myers C, Schutt R, Gerstner GE. Brain activity and human unilateral chewing: an FMRI study. J Dent Res. 2013; 92: 136–42.
8. Pyo CY, Kim TH, Kim DH. Association between masticatory muscle activity and oral conditions in young female college students. Anat Cell Biol. 2021; 54 (4): 479–88. DOI: 10.5115/acb.21.107.
9. Almotairy N, Kumar A, Trulsson M, Grigoriadis A. Development of the jaw sensorimotor control and chewing — a systematic review. Physiol Behav. 2018; 194: 456–65. DOI: 10.1016/j.physbeh.2018.06.037.
10. Гурижева М. И. Связи двигательных и визуальных проб, отражающих функциональную асимметрию полушарий головного мозга девушек. Бюллетень медицинских интернет-конференций. 2017; 7 (6): 1154–8.
11. Bogdanov V Type of correlation between bite force and EMG activity of the temporalis and masseter muscles during maximal and submaximal clenching. Folia Medica. 2023; 65 (6): 975–85. Available from: https://doi.org/10.3897/folmed.65.e107180.
12. Ferrario VF, Sforza C, Colombo A, Ciusa V. An electromyographic investigation of masticatory muscles symmetry in normo-occlusion subjects. J Oral Rehabil. 2000; 27 (1): 33–40. DOI: 10.1046/j.1365-2842.2000.00490.x.
13. Hotta GH, Oliveira AIS de, Oliveira AS de, Pedroni CR. Electromyography and asymmetry index of masticatory muscles in undergraduate students with temporomandibular disorders. Brazilian Journal of Oral Sciences. 2015; 14 (2): 176–81. DOI: 10.1590/1677-3225v14n2a15.
14. Kimoto K, Fushima K, Tamaki K, Toyoda M, Sato S, Uchimura N. Asymmetry of masticatory muscle activity during the closing phase of mastication. Cranio. 2000; 18 (4): 257–63. DOI: 10.1080/08869634.2000.11746139.
15. Na SH, Kang DW. Comparative Electromyographic Analysis Of Masticatory Muscles Between Bilateral And Unilateral Masticators. J Korean Acad Prosthodont. 2002; 40 (6): 577–89.
16. Mioche L, Bourdiol P, Martin JF, Noël Y. Variations in human masseter and temporalis muscle activity related to food texture during free and side-imposed mastication. Arch Oral Biol. 1999; 44 (12): 1005–12. DOI: 10.1016/s0003-9969(99)00103-x. PMID: 10669078.
17. Farella M, Palla S, Erni S, Michelotti A, Gallo L. Masticatory muscle activity during deliberately performed oral tasks. Physiol Meas. 2008; 29 (2008): 1397–410. DOI: 10.1088/0967-3334/29/12/004.
18. Fueki K, Yoshida E, Sugiura T, Igarashi Y. Comparison of electromyographic activity of jaw-closing muscles between mixing ability test and masticatory performance test. J Prosthodont Res. 2009; 53 (2): 72–7. DOI: 10.1016/j.jpor.2008.09.003. Epub 2008 Dec 27. PMID: 19318076.
19. Tomonari H, Seong C, Kwon S, Miyawaki S. Electromyographic activity of superficial masseter and anterior temporal muscles during unilateral mastication of artificial test foods with different textures in healthy subjects. Clin Oral Investig. 2019; 23 (9): 3445–55. DOI: 10.1007/s00784-018-2754-x. Epub 2019 Jan 3. PMID: 30607620.
20. Шатров И. М., Жолудев С. Е. Электромиографическая оценка реакции жевательных и височных мышц на нагрузку как показатель функциональной адаптации зубочелюстной системы. Проблемы стоматологии. 2016; 1: 103–9.
21. Marcelino V, De Rovere S, Paço M, Gonçalves M, Marcelino S, Guimarães AS, et al. Masticatory Function in Individuals with Temporomandibular Disorders: A Systematic Review and Meta-Analysis. Life (Basel). 2023; 13 (2): 472. DOI: 10.3390/life13020472.

IN VIVO ASSESSMENT OF THE ROLE OF LIVER METABOLISM IN SYDNONE IMINE BIOTRANSFORMATION

Popov NS[1] ✉, Terekhov VM[1], Baranov MS[2], Balabanyan VYu[2], Kaurova DE[2], Myasnyanko IN[2], Terekhova EA[1]

[1] Tver State Medical University, Tver, Russia

[2] Research Institute of Translational Medicine, Pirogov Russian National Research Medical University, Moscow, Russia

Assessment of pharmacologically active molecule biotransformation represents the most important phase of drug development, the results of which make it possible to identify active and toxic metabolites and provide a fundamental basis for the targeted design of new candidate drug molecules. The liver is the main organ involved in biotransformation of drugs. The currently widely used *in vitro* metabolism assessment methods do not allow one to identify products of extrahepatic drug molecule biotransformation. The study aimed to develop an *in vivo* approach to determination of the role of the liver in biotransformation of candidate drug molecules. The approach proposed is based on the vascular liver isolation performed surgically in laboratory rats. The organ involvement in biotransformation of pharmacologically active molecules is exemplified by the leader compound of the sydnone imine group possessing vasodilatory activity. It has been shown that elimination of the liver from systemic blood flow does not result in generation of the test compound metabolites identified by chromatography–mass spectrometry. The findings can provide the basis for prediction of drug pharmacokinetics, efficacy, and safety.

Keywords: biotransformation, pharmacokinetics, sydnone imines, vasodilators, chromatography–mass spectrometry

Funding: the study was carried out under the state assignment for the research project “Development of the Candidate Drug Possessing Mostly Central Vasodilatory Activity for Treatment of Cerebrovascular Disorders”, state registration number 124020900020-4.

Author contribution: Popov NS — search for the BBP2023 compound metabolites, bioanalytical method development, manuscript writing; Terekhov VM — developing the design of vascular liver isolation in rats, surgical procedure; Baranov MS — synthesis of the BBP2023 compound and its metabolites, manuscript writing; Balabanyan VYu — goal setting, developing the study design, manuscript writing, Kaurova DE — literature review, manuscript writing; Myasnyanko IN — synthesis of the BBP2023 compound and its metabolites, manuscript writing; Terekhova EA — developing the design of vascular liver isolation in rats, surgical procedure; all authors contributed to the publication equally, they confirm compliance of authorship with the ICMJE international criteria.

Compliance with ethical standards: the study was approved by the Ethics Committee of the Tver State Medical University (protocol No. 5 dated 19 June 2024). All experiments were conducted in accordance with the principles of Good Laboratory Practice (Order of the Ministry of Health of the Russian Federation No. 708n of 23.08.2010, Directive 2010/63/EU of the European Parliament and of the Council on the protection of animals used for scientific purposes).

✉ **Correspondence should be addressed:** Nikita S. Popov
Sovetskaya, 4, Tver, 170100, Russia; ns.popov@mail.ru

Received: 16.04.2025 **Accepted:** 30.04.2025 **Published online:** 15.05.2025

DOI: 10.24075/brsmu.2025.026

ОЦЕНКА РОЛИ ПЕЧЕНОЧНОГО МЕТАБОЛИЗМА В БИОТРАНСФОРМАЦИИ СИДНОНИМИНОВ *IN VIVO*

Н. С. Попов[1] ✉, В. М. Терехов[1], М. С. Баранов[2], В. Ю. Балабаньян[2], Д. Е. Каурова[2], И. Н. Мяснянко[2], Е. А. Терехова[1]

[1] Тверской государственный медицинский университет, Тверь, Россия

[2] Научно-исследовательский институт трансляционной медицины, Российский национальный исследовательский медицинский университет имени Н. И. Пирогова, Москва, Россия

Исследование биотрансформации фармакологически активных молекул — важнейший этап разработки лекарственных средств, результаты которого позволяют выявить активные и токсичные метаболиты, прогнозировать лекарственные взаимодействия, а также являются фундаментальной основой для целенаправленного конструирования молекул новых лекарственных кандидатов. Основным органом, принимающим участие в биотрансформации лекарств, является печень. Широко используемые в настоящее время методы исследования метаболизма *in vitro* не позволяют выявить продукты внепеченочной биотрансформации лекарственных молекул. Целью исследования было разработать *in vivo* подход к определению роли печени в биотрансформации молекул лекарственных кандидатов. Предложенный подход основан на осуществлении сосудистой изоляции печени у лабораторных крыс, выполненной хирургическим путем. Участие данного органа в биотрансформации фармакологически активных молекул показано на примере соединения-лидера из группы сиднониминов, обладающего сосудорасширяющей активностью. Показано, что исключение печени из системного кровотока не приводит к образованию метаболитов изучаемого соединения, идентифицируемых с помощью хромато-масс-спектрометрии. Полученные результаты могут служить основой для прогнозирования фармакокинетики, эффективности и безопасности лекарственных средств.

Ключевые слова: биотрансформация, фармакокинетика, сиднонимины, вазодилататоры, хромато-масс-спектрометрия

Финансирование: исследование выполнено в рамках государственного задания, тема научно-исследовательской работы: «Разработка лекарственного кандидата, обладающего преимущественно центральным сосудорасширяющим действием для лечения цереброваскулярных патологий», номер госрегистрации — 124020900020-4.

Вклад авторов: Н. С. Попов — поиск метаболитов соединения BBP2023, разработка биоаналитической методики, подготовка рукописи; В. М. Терехов — разработка дизайна сосудистой изоляции печени у крыс, выполнение оперативного вмешательства; М. С. Баранов — синтез соединения BBP2023 и его метаболитов, подготовка рукописи; В. Ю. Балабаньян — постановка цели, разработка дизайна исследования, подготовка рукописи, Д. Е. Каурова — обзор литературы, подготовка рукописи; И. Н. Мяснянко — синтез соединения BBP2023 и его метаболитов, подготовка рукописи; Е. А. Терехова — разработка дизайна сосудистой изоляции печени у крыс, выполнение оперативного вмешательства; все авторы внесли равнозначный вклад в подготовку публикации, подтверждают соответствие своего авторства международным критериям ICMJE.

Соблюдение этических стандартов: исследование одобрено этическим комитетом ФГБОУ ВО Тверской ГМУ Минздрава России (протокол № 5 от 19 июня 2024 г.). Все эксперименты выполнены в соответствии с Правилами лабораторной практики (приказ Минздрава России от 23.08.2010 № 708н, Директива Европейского парламента, Совет Европейского союза 2010/63/ЕС по защите позвоночных животных, используемых для научных целей).

✉ **Для корреспонденции:** Никита Сергеевич Попов
ул. Советская, д. 4, г. Тверь, 170100, Россия; ns.popov@mail.ru

Статья получена: 16.04.2025 **Статья принята к печати:** 30.04.2025 **Опубликована онлайн:** 15.05.2025

DOI: 10.24075/vrgmu.2025.026

Assessment of the candidate molecule biotransformation represents the most important phase of drug development [1]. Generation of toxic drug metabolites is a factor contributing greatly to safety of the ongoing drug therapy and the cause of the pre-clinical and clinical trial failure [2]. In contrast, generation of pharmacologically active metabolites can significantly increase the drug use efficacy [3] and can provide the basis for the design of new drug molecules [4]. The data on drug biotransformation are important at the stage of developing the dosage form composition and production technology [5]; these also allow one to predict many drug interactions [6]. Furthermore, the data on metabolic pathways of the known compounds provide the basis for the targeted design of new candidate drug molecules [7].

The liver is the main organ involved in biotransformation of drugs [8]. The drug candidate metabolism testing in the early development phase is most commonly conducted in vitro via incubation of substances with the liver microsomal fraction containing various enzymes [9–11]. This is a generally accepted, affordable and reproducible approach [12]. Furthermore, this allows one to identify certain cytochromes involved in metabolism of a specific substance [13]. However, such method has a number of fundamental flaws, among which impossibility of identifying products of extrahepatic drug biotransformation can be distinguished [14]. The alternative approach is *in vivo* biotransformation assessment, during which laboratory animals receive the test drug, and after that biomaterial (blood plasma, urine, internal organ fragments) is collected from these animals after a while. Biomaterial is tested in order to detect probable metabolites [15]. The results obtained also cannot give an accurate picture of the liver involvement in drug biotransformation processes.

One of the approaches to determination of the liver involvement in metabolism of pharmacologically active substances represents surgical elimination of the organ from systemic blood flow performed immediately before the test drug administration. Comparison of the results of determining probable metabolites in biomaterial collected from the laboratory animals with vascular liver isolation and without it by chromatography–mass spectrometry makes it possible to draw conclusions about the role of hepatocytes in the test molecule biotransformation.

The study aimed to develop an *in vivo* approach to determination of the role of the liver in biotransformation of candidate drug molecules.

METHODS

All experimental work, including pharmacological and bioanalytical phases, was performed at the research laboratory of the Tver State Medical University.

The BBP2023 leader compound representing a sydnone imine derivative that possessed vasodilator activity was used as an experimental object for assessment of the liver involvement in drug biotransformation (Fig. 1).

In the first phase of the study, the structure of probable BBP2023 compound metabolites, for which accurate monoisotopic mass values were calculated, was predicted based on the knowledge about common xenobiotic biotransformation pathways (Table 1).

In the second phase, a pharmacological experiment was conducted that was aimed at collecting biomaterial (blood plasma) containing probable metabolites. The testing involved male Wistar rats weighing about 250 g (SMK STEZAR LLC breeding nursery, Russia). Cages with animals were kept in a controlled environment (20–26 °C and relative humidity 30–70%). In the rooms, where the animals were kept, a 12 h light/dark cycle was used, along with 8-10 air changes per hour. Rats were fed with the PK-120 complete animal feed (Laboratorkorm LLC, Russia) and were given ad libitum access to filtered tap water. Cleaning of cages, mopping of rooms, and replacement of water bottles with new ones were carried out daily. The animals were deprived of food on the eve of the experiment.

During testing three rats underwent a single intragastric administration of the BBP2023 active pharmaceutical ingredient (API) in the form of the 10% corn oil emulsion in a dose of 1/100 LD_{50}. A total of 0.1 mL of blood was collected from the rat tail vein 3 h after administration of the drug using an insulin syringe containing 2 IU of sodium heparin. The collected blood was

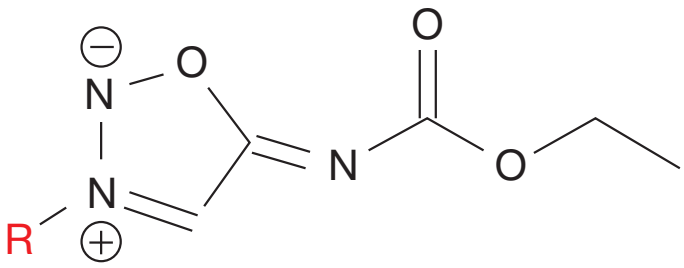

Fig. 1. BBP2023 structural formula, where R is a saturated branched hydrocarbon radical (C_7H_{15})

Table 1. Expected BBP2023 compound biotransformation products and their monoisotopic mass

Probable metabolite	Molecular mass, Da	Probable metabolite	Molecular mass, Da
BBP2023	255.16	R-NH_2	115.13
BBP2023 + OH	271.15	BBP2023 + OH + glucuronic acid	447.19
BBP2023 + 2OH	287.15	BBP2023 - (CO)OC_2H_5 + OH + glucuronic acid	375.16
BBP2023 + 3OH	303.15	R-NH_2 + OH	131.13
BBP2023 - (CO)OC_2H_5	183.14	R-NH_2 + OH + glucuronic acid	307.16
BBP2023 - (CO)OC_2H_5 + OH	199.13	BBP2023 + OH + sulfuric acid	351.11
BBP2023 - (CO)OC_2H_5 + 2OH	215.13	BBP2023 + glutathione	560.23
BBP2023 - (CO)OC_2H_5 - NO	154.15	BBP2023 - (CO)OC_2H_5 - NO+ OH + glucuronic acid	346.17

Note: R — saturated branched hydrocarbon radical (C_7H_{15})

Table 2. Chromatographic parameters for determination of the expected BBP2023 compound biotransformation products

Chromatography system	Agilent Technologies 1260 Infinity II (Agilent Technologies, USA)			
Chromatography column	Agilent InfinityLab Poroshell 120 EC-C18 4.6 × 100 mm, 2.7 µm			
Guard column	Zorbax Eclipse Plus C18 4.6 × 12.5 mm, 5 µm			
Elution solvent A	Deionized water + 0.1% formic acid			
Elution solvent B	Acetonitrile + 0.1% formic acid			
Gradient program	Time, min	Flow rate, mL/min	% A	% B
	0.0 1.0 4.0 8.0 8.01 12.0	0,4	90 90 5 5 90 90	10 10 95 95 10 10
Column thermostat temperature, °C	30			
Sample volume, µL	10			
Total analysis time, min	12			
Injector washing	Via washing port, 3 s, 50% aqueous methanol solution			

immediately transferred to 0.2 mL Eppendorf tubes; plasma was produced using the LMC-4200R laboratory centrifuge (Biosan, Latvia) at room temperature and rotor speed of 3000 rpm for 10 min. A total of 50 µL of plasma collected was combined with 800 µL of methanol supplemented with 0.5% formic acid; samples were vortexed using the Microspin FV-2400 vortex mixer (Biosan, Latvia) for 15 s, kept at a temperature of –40 °C — in the MDF-136 freezer (Sanyo, Japan) for 30 min; after that the supernatant was separated using the D-37520 centrifuge (Sigma, Germany) at 15,000 g and –10 °C — for 20 min. The

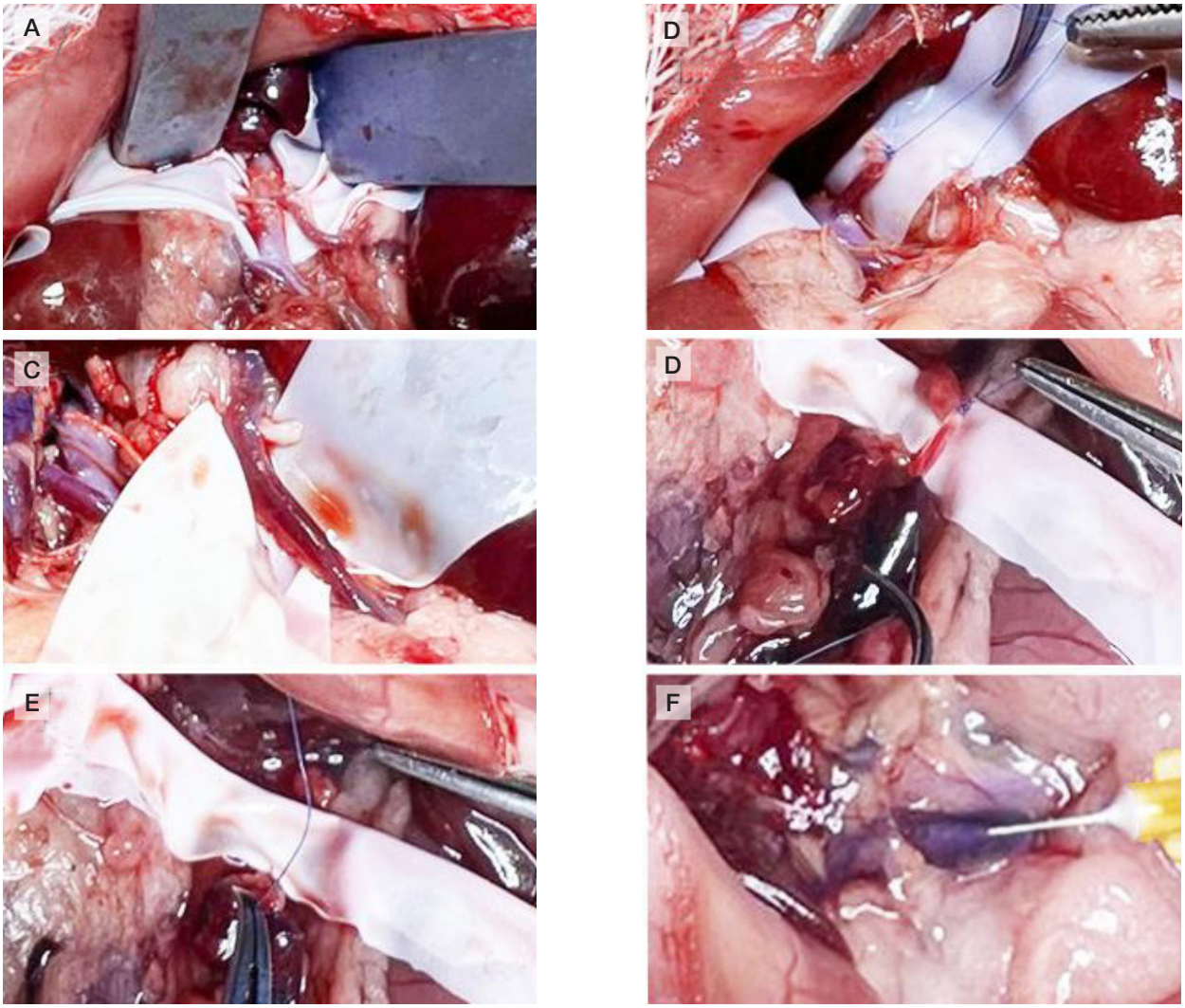

Fig. 2. A. Skeletonization of the abdominal aorta (*aorta abdominalis*) with the celiac trunk (*truncus celiacus*) **B**. Stumps of the celiac trunk with the ligatures placed. **C**. Portal vein (*vena portae*) isolation. **D**. Portal vein with the ligatures placed. **E**. Crossing the portal vein between the ligatures. **F**. Drug injection into the inferior vena cava (*vena cava inferior*). A sterile latex glove was used as a contrast medium during surgery in order to enhance the information content

Tabl3 3. Structural formulae of the identified BBP2023 compound metabolites and MRM transitions used for detection during chromatographic analysis

Structural formula	MRM transition, m/z	Structural formula	MRM transition, m/z
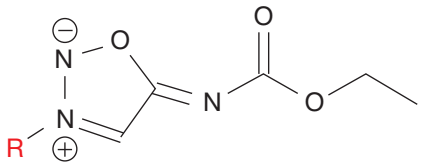	256.2/57.1 256.2/102.1	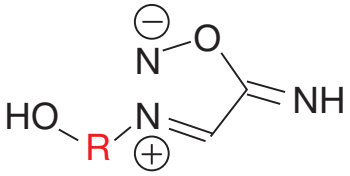	200.1/73.1 200.1/86.1
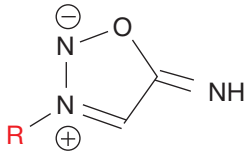	184.1/57.1 184.1/86.1	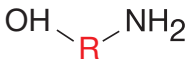	132.1/114.1 132.1/86.1
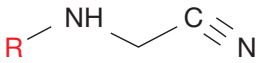	155.2/57.1 155.2/95.0	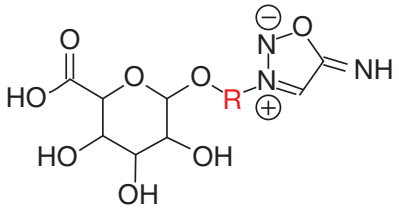	376.2/86.1 376.2/115.1 376.2/183.1
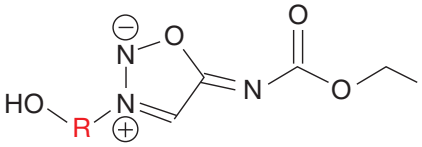	272.2/102.1 272.2/73.1		
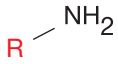	116.1/57.1 116.1/99.1	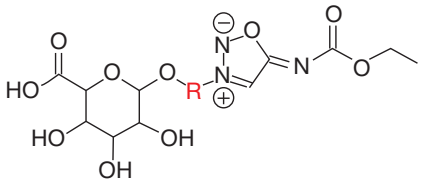	448.2/255.2 448.2/158.1 448.2/102.1
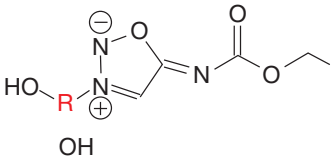	288.2/102.1 288.2/89.1		

Note: R — saturated branched hydrocarbon radical (C_7H_{15}).

supernatant was filtered using the 0.22 μm membrane filter (Laboratoriya Vody, Russia), and injected directly into the electrospray ion source of the AB Sciex 3200 MD Qtrap mass spectrometer (Sciex, Singapore) using the built-in syringe pump at a rate of 10 μL/min. First, mass spectrometry analysis of the BBP2023 compound was conducted in order to identify characteristic product ions (Product Ion mode). Given that fragmentation of potential metabolites can yield product ions overlapping with the BBP2023 compound fragment ions based on the m/z value (mass divided by charge number), the reverse screening of molecular ions was performed for the corresponding product ions (Precursor Ion mode). The signals identified were compared with the theoretically calculated monoisotopic mass values of the expected metabolites. When these values coincided, the BBP2023 compound biotransformation products identified were tested by mass spectrometry in the Product Ion mode in order to indirectly confirm the chemical structure. The mass spectrometry testing results were later used to detect the expected metabolites in the multiple reaction monitoring (MRM) mode when performing chromatography analysis of blood plasma of intact rats and the animals administered the BBP2023 compound. For this purpose, chromatography conditions specified in Table 2 were selected.

To assess the liver involvement in the BBP2023 compound biotransformation, surgery aimed to eliminate this organ from systemic blood flow was performed in three rats in the third phase of the experiment. The animal's fur was completely removed from skin in the surgical site; 0.1% atropine sulfate solution (Dalhimfarm, Russia) in a dose of 0.04 mg/kg was administered subcutaneously for premedication. Rats were in supine position. The upper midline laparotomy was performed under anesthesia achieved via subcutaneous administration of the combination of tiletamine hydrochloride 5 mg, zolazepam 5 mg (Zoletil, Virbac, France), and xylazine 4 mg (Nita-Farm, Russia); intestinal loops were retrieved, pulled to the left, wrapped in napkins soaked in warm sterile saline; the Adson retractor was installed. The portal vein (*vena portae*) and the celiac trunk (truncus celiacus) were isolated, tied up with the USP 3/0 lavsan thread (Medthekhnika, Russia), and crossed between the ligatures (Fig. 2). A key point of the portal vein ligation is that ligature is placed before the branches going to the liver begin to branch out from the vein. After vascular liver isolation, the BBP2023 compound solution (27.5 mg/mL) in a volume of 0.1 mL (1/100 LD_{50}) was injected into the subhepatic segment of the inferior vena cava (*vena cava inferior*) using the insulin syringe with the 30G needle (Inecta, China); a hemostatic sponge (Belcozin Factory, Luga, Russia) was placed onto the

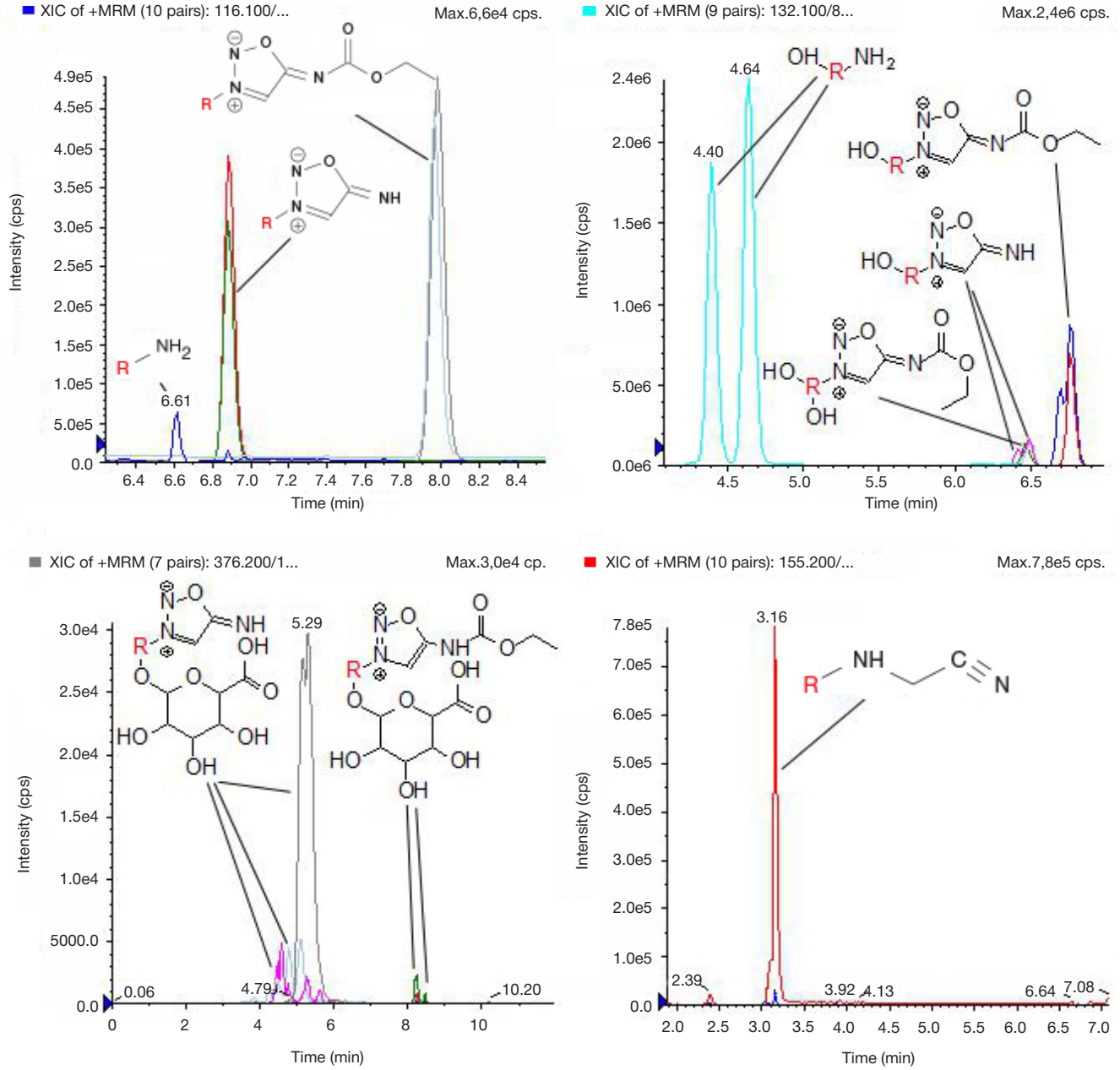

Fig. 3. Fragments of blood plasma chromatograms of the sham-operated animals, which were intravenously administered the BBP2023 compound in a dose of 1/100 LD_{50}. R — saturated branched hydrocarbon radical (C_7H_{15})

puncture site. After achieving hemostasis, the layer by layer closure of the laparotomy wound was performed.

Blood was collected from the rat tail vein 3 h after administration of the drug; plasma collection and sample preparation were performed in accordance with the previously reported method. The samples processed were assessed by chromatography in order to detect the BBP2023 compound metabolites. Furthermore, biomaterial was tested that was collected from intact and sham-operated animals (without liver isolation), which were intravenously administered the drug in the same way. After blood collection the animals were euthanized through carbon dioxide inhalation.

Primary chromatography–mass spectrometry data were processed using the embedded AB Sciex Analyst 1.3.6 software (AB Sciex, USA).

RESULTS

Screening of blood plasma of the rats subjected to intragastric administration of the test drug revealed a metabolite representing the BBP2023 compound devoid of the ethoxycarbonyl group. Furthermore, a product was found formed after the nitrogen monoxide (NO) splitting off the above molecule. This fact may be an indirect evidence of the expected test leader compound pharmacodynamics. Moreover, screening revealed the mono- and dihydroxylated derivatives of the above metabolites and the original compound, as well as the glucuronic acid esters of these compounds (Table 3). Some metabolites identified were synthesized and used as standards when setting the method and performing further chromatographic analysis. The fact that the retention times of these compounds coincide confirms correctness of their identification in the screening phase.

The intact rat plasma testing revealed no chromatographic peaks corresponding to the BBP2023 compound and its metabolites, which confirmed selectivity of the identification method developed. The analysis of plasma samples collected from the sham-operated animals (without liver isolation), which were intravenously administered the test compound in a dose of 1/100 LD_{50} 3 h before blood collection, made it possible

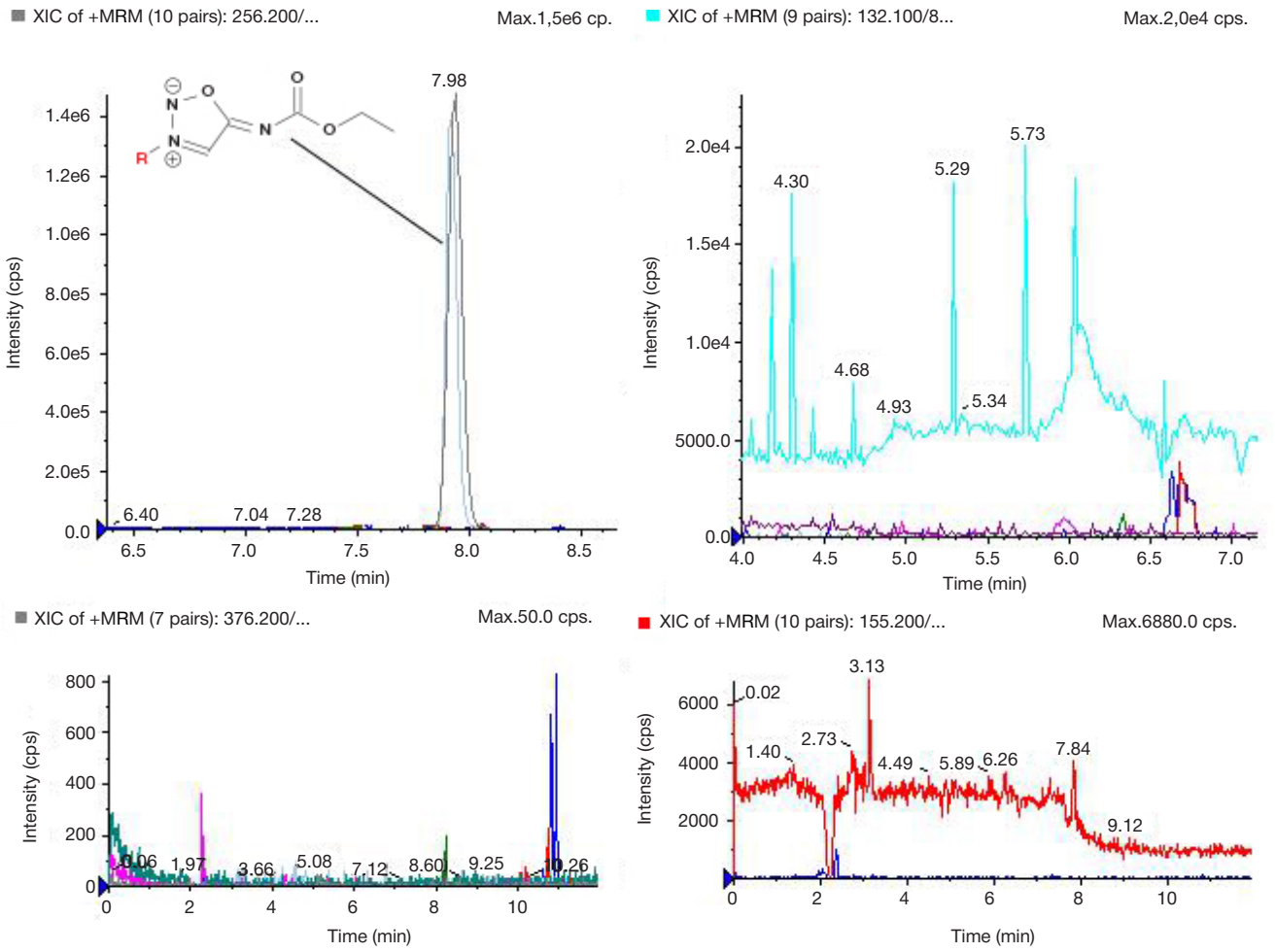

Fig. 4. Fragments of blood plasma chromatograms of the rats with vascular liver isolation, which were intravenously administered the BBP2023 compound in a dose of 1/100 LD_{50}. R — saturated branched hydrocarbon radical (C_7H_{15})

to detect chromatographic signals of all biotransformation products identified in the second phase (Fig. 3).

The results of chromatographic analysis of blood plasma collected from rats, which received the BBP2023 API in the same dose after vascular liver isolation, confirmed the presence of the signal corresponding to the original compound. Furthermore, the chromatographic peak area was on average 2.8 times larger than that obtained when testing biomaterial collected from the sham-operated animals. Furthermore, it was found that there were no peaks corresponding to the earlier detected BBP2023 compound biotransformation products (Fig. 4).

DISCUSSION

The findings allow us to draw a conclusion that the liver is directly involved in production of the identified BBP2023 compound metabolites in rats. The use of perfectly healthy animals was an important factor of the above experiment, since any damage to hepatocytes leading to the emergence of hepatic enzymes in blood can considerably affect reliability of the results obtained. Impossibility of testing the drugs that have exclusively enteral dosage forms represents one of the disadvantages of this approach. In this case, the test substance cannot enter systemic bloodstream due to the ligature placed on the portal vein. Furthermore, one should consider possible interplay between the candidate drug and the components of anesthesia when conducting such an experiment.

One of the options for the implemented approach is the use of temporary restriction of blood flow through the liver by placing surgical clips on the corresponding blood vessels. Blood collection and subsequent blood flow restoration are accomplished after a certain time after drug administration. Blood re-collection after a specified time with subsequent testing of plasma for metabolites will allow one to consider the animal's individual characteristics in terms of certain drug candidate biotransformation. Perhaps, such an approach can be implemented with respect to other organs, such as the kidney.

CONCLUSIONS

The approach to assessment of the role of the liver in biotransformation of candidate molecules at the early stages of drug development proposed in this study is versatile and informative. It can be used as an independent in vivo metabolism assessment method, or to complement the widely used in vitro methods. The results obtained when applying this approach can provide the basis for prediction of drug pharmacokinetics, efficacy, and safety.

References

1. Shanu-Wilson J, Evans L, Wrigley S, Steele J, Atherton J, Boer J. Biotransformation: impact and application of metabolism in drug discovery. ACS Medicinal Chemistry Letter. 2020; 11 (11): 2087–2107. DOI: 10.1021/acsmedchemlett.0c00202.
2. Baillie TA, Rettie AE. Role of biotransformation in drug-induced toxicity: influence of intra-and inter-species differences in drug metabolism. Drug metabolism and pharmacokinetics. 2011; 26 (1): 15–29. DOI: 10.2133/dmpk.DMPK-10-RV-089.
3. Obach RS. Pharmacologically active drug metabolites: impact on drug discovery and pharmacotherapy. Pharmacological reviews. 2013; 65 (2): 578–640. DOI: 10.1124/pr.111.005439.
4. Fura A. Role of pharmacologically active metabolites in drug discovery and development. Drug discovery today. 2006; 11 (3–4): 133–42. DOI: 10.1016/S1359-6446(05)03681-0.
5. Mahanur V, Rajge R, Tawar MA. Review on emerging oral dosage forms which helps to bypass the hepatic first pass metabolism. Asian Journal of Pharmacy and Technology. 2022; 12 (1): 47–52. DOI: 10.52711/2231-5713.2022.00009.
6. Klomp F, Wenzel C, Drozdzik M, Oswald S. Drug–drug interactions involving intestinal and hepatic CYP1A enzymes. Pharmaceutics. 2020; 12 (12): 1201. DOI: 10.3390/pharmaceutics12121201.
7. Cerny MA, Kalgutkar AS, Obach RS, Sharma R, Spracklin DK, Walker GS. Effective application of metabolite profiling in drug design and discovery. Journal of Medicinal Chemistry. 2020; 63 (12): 6387–406. DOI: 10.1021/acs.jmedchem.9b01840.
8. Rai M, Paudel N, Sakhrie M, Gemmati D, Khan IA, Tisato V, Singh AV. Perspective on quantitative structure–toxicity relationship (QSTR) models to predict hepatic biotransformation of xenobiotics. Livers. 2023; 3 (3): 448–62. DOI: 10.3390/livers3030032.
9. Peeters L, Vervliet P, Foubert K, Hermans N, Pieters L, Covaci A. A comparative study on the in vitro biotransformation of medicagenic acid using human liver microsomes and S9 fractions. Chemico-Biological Interactions. 2020; 328: 109192. DOI: 10.1016/j.cbi.2020.109192.
10. Horspool AM, Wang T, Scaringella YS, Taub ME, Chan TS. Human liver microsomes immobilized on magnetizable beads: a novel approach to study in vitro drug metabolism. Drug Metabolism and Disposition. 2020; 48 (8): 645–654. DOI: 10.1124/dmd.120.090696.
11. Ooka M, Lynch C, Xia M. Application of in vitro metabolism activation in high-throughput screening. International journal of molecular sciences. 2020; 21 (21): 8182. DOI: 10.3390/ijms21218182.
12. Knights KM, Stresser DM, Miners JO, Crespi CL. In vitro drug metabolism using liver microsomes. Current protocols in pharmacology. 2016; 74 (1): 7–8. DOI: 10.1002/cpph.9.
13. Venkatakrishnan K, von Moltke LL, Greenblatt DJ. Human drug metabolism and the cytochromes P450: application and relevance of in vitro models. The Journal of Clinical Pharmacology. 2001; 41 (11): 1149–79. DOI: 10.1177/00912700122012724.
14. Pelkonen O, Raunio H. In vitro screening of drug metabolism during drug development: can we trust the predictions? Expert opinion on drug metabolism & toxicology. 2005; 1 (1): 49–59. DOI: 10.1517/17425255.1.1.49.
15. Zhu C, Wan M, Cheng H, Wang H, Zhu M, Wu C. Rapid detection and structural characterization of verapamil metabolites in rats by UPLC–MSE and UNIFI platform. Biomedical Chromatography. 2020; 34 (1): e4702. DOI: 10.1002/bmc.4702.
16. Lee K, Lee JY, Lee K, Jung CR, Kim MJ, Kim JA, Oh SJ. Metabolite profiling and characterization of LW6, a novel HIF-1α inhibitor, as an antitumor drug candidate in mice. Molecules. 2021; 26 (7): 1951. DOI: 10.3390/molecules26071951.

Литература

1. Shanu-Wilson J, Evans L, Wrigley S, Steele J, Atherton J, Boer J. Biotransformation: impact and application of metabolism in drug discovery. ACS Medicinal Chemistry Letter. 2020; 11 (11): 2087–2107. DOI: 10.1021/acsmedchemlett.0c00202.
2. Baillie TA, Rettie AE. Role of biotransformation in drug-induced toxicity: influence of intra-and inter-species differences in drug metabolism. Drug metabolism and pharmacokinetics. 2011; 26 (1): 15–29. DOI: 10.2133/dmpk.DMPK-10-RV-089.
3. Obach RS. Pharmacologically active drug metabolites: impact on drug discovery and pharmacotherapy. Pharmacological reviews. 2013; 65 (2): 578–640. DOI: 10.1124/pr.111.005439.
4. Fura A. Role of pharmacologically active metabolites in drug discovery and development. Drug discovery today. 2006; 11 (3–4): 133–42. DOI: 10.1016/S1359-6446(05)03681-0.
5. Mahanur V, Rajge R, Tawar MA. Review on emerging oral dosage forms which helps to bypass the hepatic first pass metabolism. Asian Journal of Pharmacy and Technology. 2022; 12 (1): 47–52. DOI: 10.52711/2231-5713.2022.00009.
6. Klomp F, Wenzel C, Drozdzik M, Oswald S. Drug–drug interactions involving intestinal and hepatic CYP1A enzymes. Pharmaceutics. 2020; 12 (12): 1201. DOI: 10.3390/pharmaceutics12121201.
7. Cerny MA, Kalgutkar AS, Obach RS, Sharma R, Spracklin DK, Walker GS. Effective application of metabolite profiling in drug design and discovery. Journal of Medicinal Chemistry. 2020; 63 (12): 6387–406. DOI: 10.1021/acs.jmedchem.9b01840.
8. Rai M, Paudel N, Sakhrie M, Gemmati D, Khan IA, Tisato V, Singh AV. Perspective on quantitative structure–toxicity relationship (QSTR) models to predict hepatic biotransformation of xenobiotics. Livers. 2023; 3 (3): 448–62. DOI: 10.3390/livers3030032.
9. Peeters L, Vervliet P, Foubert K, Hermans N, Pieters L, Covaci A. A comparative study on the in vitro biotransformation of medicagenic acid using human liver microsomes and S9 fractions. Chemico-Biological Interactions. 2020; 328: 109192. DOI: 10.1016/j.cbi.2020.109192.
10. Horspool AM, Wang T, Scaringella YS, Taub ME, Chan TS. Human liver microsomes immobilized on magnetizable beads: a novel approach to study in vitro drug metabolism. Drug Metabolism and Disposition. 2020; 48 (8): 645–654. DOI: 10.1124/dmd.120.090696.
11. Ooka M, Lynch C, Xia M. Application of in vitro metabolism activation in high-throughput screening. International journal of molecular sciences. 2020; 21 (21): 8182. DOI: 10.3390/ijms21218182.
12. Knights KM, Stresser DM, Miners JO, Crespi CL. In vitro drug metabolism using liver microsomes. Current protocols in pharmacology. 2016; 74 (1): 7–8. DOI: 10.1002/cpph.9.
13. Venkatakrishnan K, von Moltke LL, Greenblatt DJ. Human drug metabolism and the cytochromes P450: application and relevance of in vitro models. The Journal of Clinical Pharmacology. 2001; 41 (11): 1149–79. DOI: 10.1177/00912700122012724.
14. Pelkonen O, Raunio H. In vitro screening of drug metabolism during drug development: can we trust the predictions? Expert opinion on drug metabolism & toxicology. 2005; 1 (1): 49–59. DOI: 10.1517/17425255.1.1.49.
15. Zhu C, Wan M, Cheng H, Wang H, Zhu M, Wu C. Rapid detection and structural characterization of verapamil metabolites in rats by UPLC–MSE and UNIFI platform. Biomedical Chromatography. 2020; 34 (1): e4702. DOI: 10.1002/bmc.4702.
16. Lee K, Lee JY, Lee K, Jung CR, Kim MJ, Kim JA, Oh SJ. Metabolite profiling and characterization of LW6, a novel HIF-1α inhibitor, as an antitumor drug candidate in mice. Molecules. 2021; 26 (7): 1951. DOI: 10.3390/molecules26071951.

CASE REPORT OF THE PATIENT WITH FOUR MULTIPLE PRIMARY MALIGNANT TUMORS IN THE DUODENUM AND COLON

Popova ES[1] ✉, Agbalyan AN[1], Titov VD[1], Moiseeva VP[1], Mashin SV[2], Anfimiadi VA[1], Zhukov GM[1], Bondarevskaya AO[1], Gavrilyuk LM[1]

[1] Rostov State Medical University, Rostov-on-Don, Russia

[2] Pirogov Russian National Research Medical University, Moscow, Russia

Currently, the occurrence of multiple primary malignant tumors is one of the complex and poorly understood issues of oncology. After the diagnosis of malignant neoplasm is established, the risk of a new primary, non-metastatic tumor increases in a patient. The paper presents a case report of the patient with four multiple primary malignant tumors in the duodenum and colon. Synchronous cancer of the cecum and rectosigmoid junction occurred after 9 months of the duodenal cancer pancreatoduodenal resection, photodynamic therapy, and 12 multiagent chemotherapy courses. The patient received 8 courses of chemotherapy with capecitabine, during which cancer progression was reported, and 16 multiagent chemotherapy courses. Two years later rectal cancer occurred, due to which rectal re-resection was conducted, along with 4 multiagent chemotherapy courses and target therapy. This clinical case emphasizes that it is necessary to perform additional assessment when treating patients with synchronous or metachronous multiple primary tumors to ensure the timely diagnosis and multidisciplinary approach to treatment of cancer patients.

Keywords: duodenal adenocarcinoma, rectal adenocarcinoma, rectosigmoid adenocarcinoma, cecal adenocarcinoma, multiple primary malignant tumors

Author contribution: Popova ES, Titov VD — manuscript writing, editing; Zhukov GM, Agbalyan AN — data analysis, literature review, manuscript writing; Bondarevskaya AO, Gavrilyuk LM — data acquisition, literature review, manuscript writing; Mashin SV, Anfimiadi VA — concept and design, literature review, manuscript writing; Moiseeva VP — literature review, manuscript writing and editing.

Compliance with ethical standards: the patient submitted the informed consent for publication of anonymized personal medical data.

✉ **Correspondence should be addressed:** Ekaterina S. Popova
26 Liniya, 35/2, Rostov-on-Don, 344037, Russia; popovaekse@mail.ru

Received: 07.04.2025 **Accepted:** 19.05.2025 **Published online:** 27.05.2025

DOI: 10.24075/brsmu.2025.028

КЛИНИЧЕСКОЕ НАБЛЮДЕНИЕ ПАЦИЕНТА С ЧЕТЫРЬМЯ ПЕРВИЧНО-МНОЖЕСТВЕННЫМИ ЗЛОКАЧЕСТВЕННЫМИ ОПУХОЛЯМИ ДВЕНАДЦАТИПЕРСТНОЙ И ТОЛСТОЙ КИШКИ

Е. С. Попова[1] ✉, А. Н. Агбалян[1], В. Д. Титов[1], В. П. Моисеева[1], С. В. Машин[2], В. А. Анфимиади[1], Г. М. Жуков[1], А. О. Бондаревская[1], Л. М. Гаврилюк[1]

[1] Ростовский государственный медицинский университет, Ростов-на-Дону, Россия

[2] Российский национальный исследовательский медицинский университет имени Н. И. Пирогова, Москва, Россия

В настоящее время одной из сложных и малоизученных проблем онкологии является возникновение первично-множественных злокачественных опухолей. После установления диагноза злокачественного новообразования у пациентов возрастает риск появления новой первичной неметастатической опухоли. В статье представлено клиническое наблюдение пациента с четырьмя первично-множественными злокачественными опухолями двенадцатиперстной и толстой кишки. Через 9 месяцев после панкреатодуоденальной резекции рака двенадцатиперстной кишки, фотодинамической терапии и 12 курсов ПХТ возник синхронный рак слепой кишки и ректосигмоидного соединения. Проведено 8 курсов химиотерапии капецитобином, на фоне которой отмечено прогрессирование процесса, и 16 курсов ПХТ. Спустя 2 года возник рак прямой кишки, по поводу которого выполнили резекцию прямой кишки, 4 курса ПХТ и таргетную терапию. Данный клинический случай акцентирует внимание на необходимости дополнительных исследований в области терапии пациентов с синхронными или метахронными первичными множественными опухолями, обеспечение своевременной диагностики и мультидисциплинарного подхода к лечению у онкологических пациентов.

Ключевые слова: аденокарцинома двенадцатиперстной кишки, аденокарцинома прямой кишки, аденокарционома ректосигмоидного соединения, аденокарцинома слепой кишки, первично-множественные злокачественные опухоли

Вклад авторов: Е. С. Попова, В. Д. Титов — написание статьи, редактирование; Г. М. Жуков, А. Н. Агбалян — анализ данных, обзор литературы, написание статьи; А. О. Бондаревская, Л. М. Гаврилюк — сбор данных, обзор литературы, написание статьи; С. В. Машин, В. А. Анфимиади — концепция и дизайн, обзор литературы, написание статьи; В. П. Моисеева — обзор литературы, написание и редактирование статьи.

Соблюдение этических стандартов: пациент подписал добровольное информированное согласие на публикацию персональной медицинской информации в обезличенной форме.

✉ **Для корреспонденции:** Екатерина Сергеевна Попова
ул. 26 линия, 35/2, г. Ростов-на-Дону, 344037, Россия; popovaekse@mail.ru

Статья получена: 07.04.2025 **Статья принята к печати:** 19.05.2025 **Опубликована онлайн:** 27.05.2025

DOI: 10.24075/vrgmu.2025.028

After the diagnosis of malignant neoplasm is established, the risk of a new primary, non-metastatic tumor (multiple primary malignant tumor, MPMT) increases in a patient. MPMTs are found in 2–17% of individuals, who have undergone treatment due to the first tumor; their risk of developing MPMT is increased 1.1–1.6-fold relative to the general population [1]. The first mention of MPMT dates back to 1793, when J. Pearson reported the case of metachronous cancer in both breasts and the uterus [2]. In 1947, N.N. Petrov added the description of primary multiplicity criteria in the first Soviet clinical oncology guidelines: "tumors shall not be neither metastatic, brought by the flow of lymph, blood or across the serous cavities, nor imprints developed from contact" [3].

Today, two most common definitions presented in the Surveillance Epidemiology and End Results (SEER) and the International Association of Cancer Registries and International Agency for Research on Cancer (IACR/IARC) are used. According to the guidelines of the SEER database, a 2-month interval should be used for differentiation of synchronous and metachronous MPMTs. At the same time, International Agency for Research on Cancer (IARC) suggests to consider tumors synchronous, when these are diagnosed with an interval less than 6 months (or metachronous, when the interval exceeds 6 months), provided that the tumors are localized in different organs [4].

Small intestine cancer (SIC) is a rare malignant tumor: it is found in about 0.6% of cancer cases and 3–6% of GIT tumor cases; SIC mortality is 0.3% of the total number of fatal outcomes in cancer patients reported all over the world. In 31.6% of cases, early-stage SIC is diagnosed. Overall (5-year) survival rate of patients having localized small intestine cancer reaches 84.8%. According to statistics, the average annual increase in the number of new SIC cases was 2.2% in 2012–2021, while mortality rate increased by an average of 2% annually in 2013–2022 [5, 6]. Primary malignant tumors of the duodenum are rare. These constitute about 61% of all small intestine cancer cases [7]. According to the WHO data, colorectal cancer (CC) ranks second among all causes of cancer mortality all over the world. In 2020, more than 1.9 million new CC cases were reported, and the rate of deaths from this disorder exceeded 930,000 cases [7].

The authors of one retrospective study analyzed 55 CC cases [8] and noted that gastric cancer was the most common malignant neoplasm associated with CC (20% of cases). Next in prevalence were esophageal cancer, uterine cancer and lung cancer; only one patient was diagnosed with duodenal cancer that was found first, while CC was found more than 6 months later [8].

The paper presents a case report of the patient with four multiple primary malignant tumors in the duodenum and colon.

Clinical case description

Female patient L. aged 56 years stays at the cancer hospital in Azov. In 2020, examination conducted due to complaints of weight loss, yellowing of the skin, and itching, revealed a duodenal tumor (based on the EGD data of August 10, 2020): infiltrative and ulcerative c-r in the retrobulbar parts of the duodenum, moderately differentiated adenocarcinoma determined in biopsy specimens, MRI features of tumor lesion of the duodenal wall, head of the pancreas, and parapancreatic tissue. Examination yielded no data confirming other malignant neoplasms; fibrocolonoscopy conducted on August 10, 2020 revealed a polyp 30 cm from the anus. The following diagnosis was established: duodenal cancer cT4N0M0 st. IIb, clinical group 2, obstructive jaundice. Percutaneous transhepatic cholangiostomy was performed on August 13, 2020; the following surgical intervention took place after the bilirubin level were back to normal (total bilirubin 8.8 μmol/L) and preoperative preparation was completed on August 21, 2020: laparotomy, gastro-pancreatoduodenal resection, cholecystectomy with an intraoperative photodynamic therapy session on the bed of the tumor removed. Postoperative period proceeded without complications; the patient received supportive drug therapy that included preventive antibiotics and antithrombotic agents.

The following report was obtained after the surgical material histological examination conducted on August 28, 2020: poorly differentiated adenocarcinoma G3 — high grade with mucosal ulceration, extension into all intestinal wall layers, pancreatic tissue invasion, necrotic foci, lymphoid infiltration along the tumor periphery, perineural invasion, presence of tumor emboli in lymphatic and blood vessels. Sinus histiocytosis, follicular hyperplasia were found in 12 lymph nodes assessed. There was chronic inflammation in the intestinal wall, outside the tumor. There were ectatic acini with the dilated lumen outside the pancreatic tumor. The resection margin showed no signs of tumor growth (Fig. 1).

The following diagnosis was established: duodenal cancer extending into the pancreas pT4bN0M0 st. IIB, clinical group 2.

According to the chemotherapist's advice dated September 15, 2020, the patient was recommended FOLFOX-6 adjuvant multiagent chemotherapy with a satisfactory condition of the patient, complete blood counts and blood biochemistry panel within normal range, after consulting a general practitioner and a cardiologist (if there were no contraindications) throughout 6 months after surgery: 2-h infusion of oxaliplatin (85 mg/m^2) on day 1, intravenous leucovarin 400 (mg/m^2) throughout 2 h with the subsequent bolus of intravenous 5-fluorouracil (400 mg/m^2) and 46-h infusion of 5-fluorouracil (2400 mg/m^2). The interval was 14 days. In October–March 2021, a total of 12 FOLFOX-6 adjuvant multiagent chemotherapy courses were conducted.

The complaints of constipation, tenesmus, mucus discharge from the rectum during bowel movements, fatigue arose almost immediately after the multiple multiagent chemotherapy courses were completed. Two tumors were revealed based on the fibrocolonoscopy data dated April 29, 2021: in the rectosigmoid junction and ascending colon. Report of the histological examination conducted on May 17, 2021: G2 adenocarcinoma (ascending colon), G2 adenocarcinoma (rectosigmoid junction). Abdominal ultrasonography dated April 29, 2021: structural alteration of the left peritoneal lymph

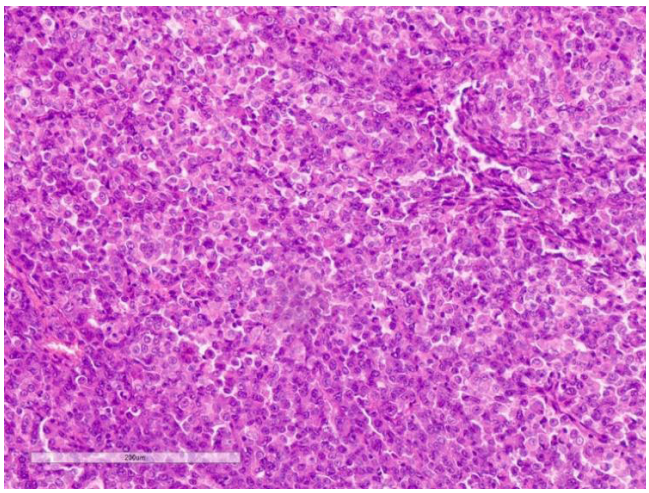

Fig. 1. Surgical material: poorly differentiated duodenal adenocarcinoma, G3

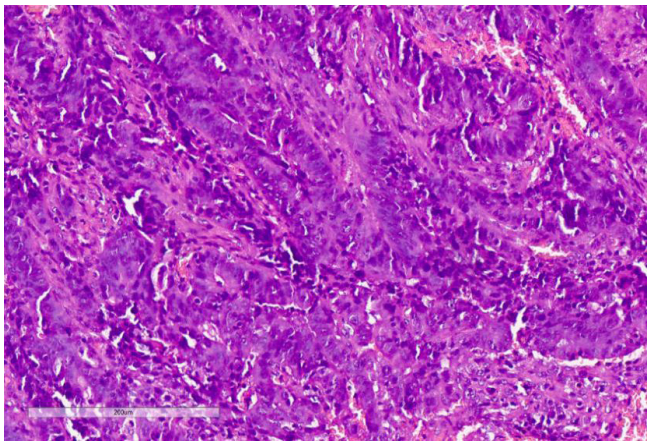

Fig. 2. Surgical material. Moderately differentiated adenocarcinoma, G2

nodes. Spiral computed tomography (CT) of the abdomen dated May 18, 2021: diffuse liver changes, condition after pancreatoduodenal resection.

The following surgical procedure was conducted on May 31, 2021: right hemicolectomy, anterio-superior rectal resection. Postoperative period proceeded without complications. Report obtained after the surgical material histological examination conducted on June 7, 2021: G2 adenocarcinoma invading the subserous layer in the cecum; assessment of the regional lymph nodes revealed metastatic lesions in six of those, G2 adenocarcinoma invading the muscular layer was found in the rectosigmoid junction, no metastasis was found in 8 regional lymph nodes. The resection margins showed no signs of tumor growth. The patient was discharged in fair condition (ECOG-1).

The diagnosis of multiple primary metachronous cancer was established: cecal cancer pT2N1M0 st. III, clinical group 2, rectosigmoid cancer pT2N0M0 st. I, clinical group 2, duodenal cancer extending into the pancreas pT4bN0M0 st. IIB; 12 adjuvant multiagent chemotherapy courses.

According to the chemotherapist's advice dated June 12, 2021, the patient was recommended capecitabine chemotherapy courses. A total of 8 capecitabine chemotherapy courses were conducted between July 2021 and January 2022. At the time of treatment, the patient's condition corresponded to the ECOG score 0–1, the treatment courses were accompanied by the 1st degree gastroenterocolitis. Scheduled clinical supervision was accomplished in accordance with the regulations provided.

In May 2022, a year after surgery due to colorectal malignant neoplasms, the next check-up and spiral CT of the abdomen revealed enlarged paraaortic lymph nodes sized up to 16 mm with unclear margins, "obscure" mesentery, no free fluid in the abdominal cavity, which were considered as metastatic lesion of the retroperitoneal lymph nodes.

The council of physicians decided to conduct FOLFIRI anti-cancer drug therapy. In June–August 2022, a total of five FOLFIRI multiagent chemotherapy courses were conducted: irinotecan 180 mg/m^2 300 mg within a day, calcium folinate 680 mg within a day (400 mg/m^2), 5-fluorouracil 680 mg within a day, infusional 5-fluorouracil 4100 mg through the microinfusion pump within 46 h (2400 mg/m^2).

Spiral CT of the abdomen and pelvis performed on September 20, 2022 revealed metastasis. The patient received 6 FOLFIRI multiagent chemotherapy courses between October 3, 2022 and December 14, 2022.

Based on the results of spiral CT of the chest, abdomen, and pelvis performed on January 23, 2023, a conclusion was drawn about cancer progression due to metastatic lesions in the retroperitoneal and mesenteric lymph nodes.

In February 2023, Aflibercept, the targeted drug (tumor angiogenesis inhibitor) was prescribed; in February–July 2023, a total of 5 r. FOLFIRI multiagent chemotherapy courses + target therapy (infusional Aflibercept 4 mg/kg 260 mg within a day) were conducted.

The patient noted health deterioration (nausea, itching, fatigue) when receiving chemotherapy. In September 2023, routine fibrocolonoscopy revealed a polyp in the transverse colon, which was removed by endoscopy. In February 2024, the patient experienced abdominal pain, as well as blood and mucus discharge during bowel movements again. In April 2024, fibrocolonoscopy performed in the residential clinic revealed the fourth malignant tumor localized in the rectum 8 cm from the anus, proximal to which, 13 cm from the anus, a previously formed intestinal anastomosis showing no signs of tumor infiltration was located. Histological assessment revealed a G2 moderately differentiated adenocarcinoma. Spiral CT of the abdomen conducted on April 24, 2024 revealed wall thickening of the rectosigmoid junction, retroperitoneal lymphadenopathy.

Considering the fact that more than 30 chemotherapy courses had been earlier conducted, it was decided to perform surgery. On May 14, 2024 anterior rectal re-resection was performed. G2 adenocarcinoma in the rectal wall with inflammation, ulceration, and hemorrhage was diagnosed based on the surgical material histological examination conducted on May 28, 2024. The tumor infiltrated into the mucous layer, submucous layer, muscular layer, extended into the pararectal adipose tissue showing perineural invasion, invasion of blood vessels. No signs of lymphatic vessel invasion were found. The resection margins (distal and proximal) showed no signs of tumor growth. No components of the tumor were found in12 lymph nodes isolated from the regional adipose tissue (Fig. 2).

Multiple primary synchronous-metachronous cancer of the middle ampullary rectum pT3N0M0, st. IIa, rectal re-resection, duodenal cancer pT4bN0M0, st. IIb, pancreatoduodenal resection, intraoperative photodynamic therapy in 2020, 12 adjuvant multiagent chemotherapy courses, cecal cancer pT2N1M0 st. III, rectosigmoid cancer pT2N0M0 st. I. In 2021, right hemicolectomy and anterior rectal resection were performed, 8 capecitabine monotherapy courses and 16 multiagent chemotherapy courses were conducted.

According to the chemotherapist's advice dated May 26, 2024, FOLFIRI anti-cancer drug therapy + target therapy with Aflibercept was indicated. The next course started on day 15.

In June–August 2024, a total of 4 FOLFIRI anti-cancer therapy courses + target therapy with Aflibercept were conducted.

During the chemotherapy courses, the patient assessed her condition as satisfactory, she noted increased fatigue and occasional nausea.

Clinical case discussion

Today, the causes of MPMTs are poorly understood. It is assumed that these are affected by several factors, such as advances in early diagnosis and treatment of malignant neoplasms, screening, and scheduled diagnostic tests following identification of the first tumor, due to which the second and subsequent tumors are identified, and the cancer patients' life expectancy increases. It is also important to note the early use of specific anti-tumor treatment, especially the methods having a damaging effect on DNA (radiation therapy and chemotherapy) and used for treatment of the first malignant neoplasm: the immune status deterioration associated with

such treatment can be a ground for the development of subsequent tumors [9]. Furthermore, genetic susceptibility and exposure to environmental factors can play an important role.

A retrospective trial conducted at the Korean cancer center involved analysis of the data of 96,174 adult patients diagnosed with their first cancer in 2003–2022. Among them 87,338 were diagnosed with a single primary malignant neoplasm, while in 8836 patients (9% of the total number) two or more neoplasms were identified. The analysis of median latency period showed that in 44% of patients with multiple primary tumors the second malignant tumor was identified within 1–5 years after the first one. A similar trend was reported for subsequent cancers: 40% of third and 42% of fourth primary tumors were diagnosed within 1–5 years after the previous diagnosis. The decrease in time to the emergence of new tumors: the median interval between the first and second malignant tumors was 4.1 years, between the second and third ones — 2.1 years, between the third and fourth ones — 1.6 years [9].

CONCLUSION

This clinical case emphasizes the importance of prolonged monitoring and regular check-ups for early detection of new malignant tumors after completion of treatment of the first malignant neoplasm. The timely diagnosis and intense surgical treatment can considerably improve the outcome in such patients. In this regard, it is extremely important to ensure the systematic long-term follow-up in order to reveal new malignant neoplasms in such patients. Additional tests are required, especially when treating patients with synchronous or metachronous multiple primary tumors. Furthermore, it is necessary to more thoroughly assess the effects of previous treatment on the outcome, anti-tumor therapy efficacy, and potential toxic effects.

References

1. Vogt A, Schmid S, Heinimann K, et al. Multiple primary tumours: challenges and approaches, a review. ESMO. 2017; 2; 2 (2): e000172. DOI: 10.1136/esmoopen-2017-000172.
2. Owen LJ. Multiple malignant neoplasms. JAMA; 1921; 76: 1329–33.
3. Ganov AM. Jepidemiologija, faktory riska i optimizacija diagnostiki mnozhestvennyh pervichnyh opuholej. M., 1994. Russian.
4. Li, Tao MDa; Wang, et al. Metachronous primary colon and periampullary duodenal cancer: A case report. Medicine. 2021; 100 (3): e24378. DOI: 10.1097/MD.0000000000024378.
5. Li L, Jiang D, Liu H, et al. Comprehensive proteogenomic characterization of early duodenal cancer reveals the carcinogenesis tracks of different subtypes. Nat Commun. 2023; 29; 14 (1): 1751. DOI: 10.1038/s41467-023-37221-5.
6. Reynolds I, Healy P, Mcnamara DA. Malignant tumours of the small intestine. Surgeon. 2014; 12 (5): 263–70. DOI: 10.1016/j.surge.2014.02.003.
7. Li T, Wang X, Chen C, et al. Metachronous primary colon and periampullary duodenal cancer: A case report. Medicine (Baltimore). 2021; 22; 100 (3): e24378. DOI: 10.1097/MD.0000000000024378.
8. Li Q, Zhang B, Niu FN, et al. Clinicopathological characteristics, MSI and K-ras gene mutations of double primary malignancies associated with colorectal cancer. Zhonghua Yi Xue Za Zhi. 2020; 4; 100 (4): 301–6. DOI: 10.3760/cma.j.issn.0376-2491.2020.04.012.
9. Kwon JH, Kim H, Lee JK, et al. Incidence and Characteristics of Multiple Primary Cancers: A 20-Year Retrospective Study of a Single Cancer Center in Korea. Cancers (Basel). 2024. 26; 16 (13): 2346. DOI: 10.3390/cancers16132346.

Литература

1. Vogt A, Schmid S, Heinimann K, et al. Multiple primary tumours: challenges and approaches, a review. ESMO. 2017; 2; 2 (2): e000172. DOI: 10.1136/esmoopen-2017-000172.
2. Owen LJ. Multiple malignant neoplasms. JAMA; 1921; 76: 1329–33.
3. Ганов А. М. Эпидемиология, факторы риска и оптимизация диагностики множественных первичных опухолей. М., 1994.
4. Li, Tao MDa; Wang, et al. Metachronous primary colon and periampullary duodenal cancer: A case report. Medicine. 2021; 100 (3): e24378. DOI: 10.1097/MD.0000000000024378.
5. Li L, Jiang D, Liu H, et al. Comprehensive proteogenomic characterization of early duodenal cancer reveals the carcinogenesis tracks of different subtypes. Nat Commun. 2023; 29; 14 (1): 1751. DOI: 10.1038/s41467-023-37221-5.
6. Reynolds I, Healy P, Mcnamara DA. Malignant tumours of the small intestine. Surgeon. 2014; 12 (5): 263–70. DOI: 10.1016/j.surge.2014.02.003.
7. Li T, Wang X, Chen C, et al. Metachronous primary colon and periampullary duodenal cancer: A case report. Medicine (Baltimore). 2021; 22; 100 (3): e24378. DOI: 10.1097/MD.0000000000024378.
8. Li Q, Zhang B, Niu FN, et al. Clinicopathological characteristics, MSI and K-ras gene mutations of double primary malignancies associated with colorectal cancer. Zhonghua Yi Xue Za Zhi. 2020; 4; 100 (4): 301–6. DOI: 10.3760/cma.j.issn.0376-2491.2020.04.012.
9. Kwon JH, Kim H, Lee JK, et al. Incidence and Characteristics of Multiple Primary Cancers: A 20-Year Retrospective Study of a Single Cancer Center in Korea. Cancers (Basel). 2024. 26; 16 (13): 2346. DOI: 10.3390/cancers16132346.